The Earth Technology Corporation®

West Broadway, Suite 5000, Long Beach, CA 90802-4443
Post Office Box 22785, Long Beach, CA 90801-5785
Phone: (213) 495-4449, (714) 821-7062 · Fax: (213) 426-0666

SSCL-SR-1140
GR-81

January 17, 1991

RTK Joint Venture
1800 Harrison Street
Oakland, CA 94623-2321

Attention: Dr. Mack Riddle

Subject: Report on "Laboratory Testing, Samples from Superconducting Super Collider Project", Prototype Installation Facility (PIF) by Professor Olson, University of Texas, Austin
Report No. SSC-GR-81

Dear Mack,

We are herewith transmitting five (5) copies of the above report with Appendix (which contains laboratory test data sheets, plots, and results) and 14 copies without Appendix.

Very truly yours,

THE EARTH TECHNOLOGY CORPORATION

Matthew L. Werner, Ph.D.
Associate - Geosciences

enclosure

werner.a\ssc1

SECTION 1

INTRODUCTION

Contract Provisions

This is the second phase of characterization of the engineering properties of geologic materials present at the proposed site for the Superconducting Super Collider in Ellis County, Texas. This phase will characterize the Eagleford shale for the Prototype Installation Facility (PIF). The contract was divided into three "Task":

Task 1: Laboratory Test Procedures, Data Forms and Instrument Calibrations (QA/QC) and Initiation of Testing.

Task 2: Laboratory Testing.

Task 3: Final Report

This Report satisfies the contract to provide a final report "characterizing the behavior of the geologic materials from the site".

As part of Task 2, the contract provided for the performance of at least eight one-dimensional consolidation tests, eight drained direct shear tests, and fourteen drained triaxial compression tests.

In this report, we will use the expression **Phase 1** to refer to the work performed on the first contract, and **Phase 2** for this contract, and will use the term **Task** to refer to the subsets of the Phase 2 contract.

Previous Reports

Previous reports on the first phase of the contract, their dates, and their general contents, were as follows:

Report	Date	Topics
1	2-20-90	preliminary discussion of apparatus and testing procedures
2	3-6-90	presentation of initial test results, further discussion of preliminary aspects of testing procedures
3	4-24-90	detailed report on experimental procedures for Atterberg limits, specific gravity, moisture content, and density, including data forms
4	4-24-90	detailed report on experimental procedures for one-dimensional consolidation, hydraulic conductivity, drained direct shear, and drained triaxial compression. The data acquisition system was also discussed. Drawings of the apparatus were included. Data forms were presented.
5	6-1-90	presentation of data available at the time the report was submitted. Spreadsheets used in data reduction were presented.
6	7-31-90	final report of phase 1 characterizing the geologic materials at the SSC site.

Previous reports on the PIF phase of the contract, their dates, and their general contents, were as follows:

Report	Date	Topics
1	9-19-90	quality assurance program (QA/QC) for testing of Eagleford shale for the PIF contract.
2	12-10-90	presentation of all data from laboratory tests performed on Eagleford shale for the PIF phase.

Contents of This Report

In this report we will present the most significant experimental data collected on the Eagleford shale on this project, discuss the data for each category of test, and draw such overall conclusions as seem warranted by the program completed. We will also compare the results of the tests on the Eagleford shale of the PIF phase with the most "reliable" data available for the Eagleford shale from Phase 1 in order to assess the homogeneity of the Eagleford shale at the SSC site. Contents of some of the previous reports will be included in this report for completeness.

Finally, we will discuss some of the remaining problems in both measurement techniques and in material characterization and make suggestions as to how these problems can be resolved.

Personnel

Experimental work was performed by R. P. Brouillette, graduate student in Civil Engineering, D. Hodgson, undergraduate student in Civil Engineering at the University of Texas at Austin, and J. Lemke, a former graduate student at the University of Texas at Austin. J. Stewart was involved in construction of the testing equipment.

This report was written by Roy E. Olson and Rickey Brouillette.

SECTION 2

REVIEW OF CORES RECEIVED AND TESTING PROGRAM

Cores Received

A log of the cores received is presented in Table 2.1.

The symbolism used in the column entitled "Test Description" is as follows:

C one-dimensional consolidation/swelling pressure

DS "drained" direct shear tests.

CD "drained" triaxial compression tests

In general, the test numbers were assigned in the sequence the tests were performed but in some instances a test setup failed after assigning a later test. In such cases, the original test number of the failed setup was used for the new setup on the sample from the same boring. Thus, some tests with lower test numbers were started after tests with larger test numbers.

The procedure we followed in handling cores is presented in QA/QC report (Task 1 of the PIF phase). All cores were stored in a moist room during this contract and core weights were recorded initially and at the times that material was removed for testing, to ensure that no measurable weight changes occurred during storage. No weight changes, beyond the accuracy of the measurement, were found.

Testing Program

The testing program is shown in Table 2.2. The tests, their intended purposes, and brief comments on testing procedures, are presented below:

Boring ID	OLSON Sample #	Sample Depth (ft.)	Sample Formation	Test Performed
B1617	36	212.0- 212.5	Eagleford	
	37	212.5-213.55	Eagleford	C14, DS24, CD23
B1597	38	233.85-234.9	Eagleford	C12
	39	234.9-235.5	Eagleford	DS18, CD24
	40	238.4-238.9	Eagleford	
	41	238.9-239.7	Eagleford	
B1637	42	213.2-213.8	Eagleford	
	43	213.8-215.45	Eagleford	DS21
	44	215.45-217.6	Eagleford	C15, CD14, CD18, CD19
B1657	45	160.45-161.15	Eagleford	
	46	161.15-162.85	Eagleford	DS20
	47	170.0-172.15	Eagleford	C18, CD12
B1619	48	178.8-179.45	Eagleford	
	49	180.0-180.9	Eagleford	
	50	180.9-181.75	Eagleford	
	51	182.0-182.8	Eagleford	
	52	183.7-184.4	Eagleford	C13, DS17, CD22
	53	184.4-185.4	Eagleford	
	54	185.4-186.35	Eagleford	
B1697	55	124.0-124.8	Eagleford	
	56	122.3-124.0	Eagleford	C17, DS22, CD15
BC1	57	217.0-218.7	Eagleford	
	58	218.7-220.9	Eagleford	C16, DS19, CD11, CD16, CD17
	59	220.9-221.7	Eagleford	
B1677	60	189.75-191.65	Eagleford	
	61	192.3-192.85	Eagleford	
	62	193.0-195.8	Eagleford	
BF1A	63	168.5-170.6	Eagleford	CD13, CD20, CD21
	64	172.9-175.3	Eagleford	C19, DS23
	65	175.3-176.0	Eagleford	

Table 2.1 Summary of Cores of Eagleford Shale Received and Tests Performed for the PIF Project

Consolidation. The one-dimensional consolidation properties were measured following essentially standard procedures. Samples had nominal dimensions of 1.5 inches in diameter by 0.6 inch high.

The dial indicator used to measure change in thickness was mounted and zeroed under a seating stress of approximately 350 psf. The consolidation samples were subjected to the field overburden effective stress, to help close up any fissures that may have opened during coring, handling, shipping, storage, or trimming. Tap water was added to the cell. The total stress was then adjusted to maintain essentially a constant thickness. When equilibrium was re-established, the applied total stress is considered to be the swelling pressure. The sample was then unloaded in suitable steps to a minimum pressure around 300 psf, then reloaded in increments to a peak pressure of about 178,000 psf, and then unloaded to the minimum pressure in steps. Generally, pressures were doubled for successive steps during loading, and were reduced by a factor of four during unloading.

Properties measured include the swelling pressure, the stress-strain relationship (in the form of void ratio versus log of effective stress) in one-dimensional compression, and the time-rate properties backed out of the data using Terzaghi's theory (coefficients of consolidation and hydraulic conductivity). The fitting operation was based on the square-root-of-time method as a first step, but then the experimental and theoretical curves were compared on a microcomputer screen and adjustments were made to obtain the "best" fit. Hand checks of selected data confirmed the validity of the resulting parameters.

Direct Shear. Direct shear samples were consolidated in one stage with measurement of consolidation properties, and then sheared at essentially a constant rate of deformation up to failure. The nominal sample dimensions were the same as for one-dimensional consolidation.

The interest here was in defining the Coulomb failure envelope both at peak shearing stress and in the immediate post-failure condition. Many of the samples underwent a sudden failure with nearly constant shearing stress after failure. The post-failure condition was here defined as the condition after displacements of the order of 0.2 inch; no cyclic loading tests with stress reversals were performed.

Test ID	Sample No.	Test Type	Formation	Boring	Sample Depth (ft.)
C12	38	1-D Consolidation	Eagleford	B1597	234.8
C13	52	1-D Consolidation	Eagleford	B1619	183.8
C14	37	1-D Consolidation	Eagleford	B1617	212.6
C15	44	1-D Consolidation	Eagleford	B1637	215.7
C16	58	1-D Consolidation	Eagleford	BC1	218.8
C17	56	1-D Consolidation	Eagleford	B1697	122.9
C18	47	1-D Consolidation	Eagleford	B1657	171.4
C19	64	1-D Consolidation	Eagleford	BF1A	175.0
DS17	52	Drained Direct Shear	Eagleford	B1619	183.7
DS18	39	Drained Direct Shear	Eagleford	B1597	235.4
DS19	58	Drained Direct Shear	Eagleford	BC1	219.5
DS20	46	Drained Direct Shear	Eagleford	B1657	161.3
DS21	43	Drained Direct Shear	Eagleford	B1637	215.0
DS22	56	Drained Direct Shear	Eagleford	B1697	122.7
DS23	64	Drained Direct Shear	Eagleford	BF1A	174.8
DS24	37	Drained Direct Shear	Eagleford	B1617	213.1
CD11	58	Drained Triaxial	Eagleford	BC1	219.2
CD12	47	Drained Triaxial	Eagleford	B1657	171.9
CD13	63	Drained Triaxial	Eagleford	BF1A	168.7
CD14	44	Drained Triaxial	Eagleford	B1637	216.7
CD15	56	Drained Triaxial	Eagleford	B1697	122.5
CD16	58	Drained Triaxial	Eagleford	BC1	220.1
CD17	58	Drained Triaxial	Eagleford	BC1	220.5
CD18	44	Drained Triaxial	Eagleford	B1637	216.5
CD19	44	Drained Triaxial	Eagleford	B1637	216.2
CD20	63	Drained Triaxial	Eagleford	BF1A	168.9
CD21	63	Drained Triaxial	Eagleford	BF1A	169.2
CD22	52	Drained Triaxial	Eagleford	B1619	184.1
CD23	37	Drained Triaxial	Eagleford	B1617	213.3
CD24	39	Drained Triaxial	Eagleford	B1597	235.1

Table 2.2 Summary of Testing Program

Triaxial Compression. The triaxial compression tests were performed using samples with nominal dimensions of 1.5 inches in diameter by 3 inches high (actual heights ranged from 2.64 to 3.05 inches). Tests in Phase 1 involved consolidation under several stresses so as to obtain consolidation data, but the consolidation times were too long to allow this practice to continue. The tests

involved establishing equilibrium at 140 psi and then consolidation at the final pressure.

The tests were performed to obtain Mohr-Coulomb failure envelopes for the "drained" condition. In addition, there was an interest in defining stress-strain behavior and in comparing the failure envelopes in triaxial and direct shear.

Index Tests. Index properties measured in our laboratories were mainly Atterberg limits and total unit weight. Atterberg limit tests were generally performed on oven-dried material so the tests could be performed on the same material used for measurement of other engineering properties. Samples were given overnight to hydrate before the final measurements were taken.

Density tests involved measuring the weights and dimensions of carefully trimmed samples.

Data collection. Data for one-dimensional consolidation tests were hand recorded on forms that duplicated spreadsheets included in the QA/QC report. Changes in thickness were measured using dial indicators reading to 0.0001 inch. Loads were applied using Bishop-type loading frames with a mechanical advantage of eleven.

Loads and deformations for the direct shear and triaxial shear tests were recorded using a data acquisition system. The sensors were calibrated at the beginning of each test program and usually several times during each test program. The LVDT's were mechanically calibrated against NIST (National Institute of Standards and Technology) traceable gage blocks that was designed for this purpose. The load cells were calibrated by loading them in in series with a proving ring of NIST traceable stiffness and applying deformations with a loading press.

The volume of water entering or leaving a sample was measured using an external pipet, with the pipet reading evaluated electronically using a pressure transducer at the bottom of the pipet. The calibration of the transducer was verified by hand recording pipet readings periodically.

SECTION 3

INDEX TESTS

Atterberg Limits

Atterberg limit tests were performed in accord with ASTM D4318, "Standard Test Method for Liquid Limit, Plastic Limit, and Plasticity Index of Soils". The samples were oven dried prior to testing and had been used previously for measurement of other properties.

The Atterberg limit data for Eagleford shale are summarized in Table 3.1 and are plotted in a Casagrande plasticity chart in Fig. 3.1. The original data forms were included in the Task 2 report. The points in the plasticity chart plot in a zone that is essentially parallel to the A line, in accord with engineering experience. The Eagleford shale limits for the specimen tested in the PIF phase are within the same range of those for the Phase 1 specimen. The Phase 1 material did have a slightly wider range of Limits. The material is a highly plastic clay when it is disaggregated and mixed with water.

Overnight soaking had no apparent effect on the Atterberg limits, contrary to other experience. The effect of oven drying was to raise the Atterberg limits in comparison with tests started at the natural water content, in accord with limited previous experience.

Unit Weights

The unit weights were determined for each sample used for consolidation, direct shear, and triaxial shear tests. Values of the total, dry, and submerged unit weights for all samples are included in Table 3.2. The total unit weights, for both the PIF phase and Phase 1 Eagleford shale specimens, are plotted against sample depth in Fig. 3.2. The variability of density with depth is essentially the same for the PIF phase and Phase 1 (Eagleford) material.

LL Test No	Sample No.	Boring No.	Depth (ft)	Formation	LL (%)	PL (%)	PI (%)	Engineering Tests
1	38	B1597	234.8	Eagleford	75	32	43	C12
2	52	B1619	183.8	Eagleford	67	30	37	C13
3	37	B1617	212.6	Eagleford	75	31	44	C14
4	44	B1637	215.7	Eagleford	71	33	38	C15
5	58	BC1	218.8	Eagleford	64	30	34	C16
6	56	B1697	122.9	Eagleford	79	30	49	C17
7	47	B1657	171.4	Eagleford	79	28	51	C18
8	64	BF1A	175	Eagleford	79	32	47	C19
9	52	B1619	183.7	Eagleford	66	27	39	DS17
10	39	B1597	235.4	Eagleford	88	34	54	DS18
11	58	BC1	219.5	Eagleford	78	31	47	DS19
12	46	B1657	161.3	Eagleford	82	33	49	DS20
13	43	B1637	215	Eagleford	87	36	51	DS21
14	56	B1697	122.7	Eagleford	82	30	52	DS22
15	64	BF1A	174.8	Eagleford	86	30	56	DS23
16	37	B1617	213.1	Eagleford	89	36	53	DS24
17	58	BC1	219.2	Eagleford	76	32	44	CD11
18	47	B1657	171.9	Eagleford	86	30	56	CD12
19	63	BF1A	168.7	Eagleford	83	30	53	CD13
20	44	B1637	216.7	Eagleford	72	29	43	CD14
21	56	B1697	122.5	Eagleford	80	31	49	CD15
22	58	BC1	220.1	Eagleford	67	29	38	CD16
23	58	BC1	220.5	Eagleford	66	29	37	CD17
24	44	B1637	216.5	Eagleford	77	29	48	CD18
25	44	B1637	216.2	Eagleford	77	30	47	CD19
26	63	BF1A	168.9	Eagleford	84	32	52	CD20
27	63	BF1A	169.2	Eagleford	80	29	51	CD21
28	52	B1619	184.1	Eagleford	68	26	42	CD22
29	37	B1617	213.3	Eagleford	81	27	54	CD23
30	39	B1597	235.1	Eagleford	87	31	56	CD24

Table 3.1 Summary of Atterberg Limits

Test ID	Spl. No.	Formation	Boring	Sample Depth (ft.)	Water Content (%)	Computed Degree of Sat. (%)	Total Unit Weight (pcf)	Subm. Unit Wt. (pcf)	Dry Unit Wt. (pcf)
C12	38	Eagleford	B1597	234.8	16.3	96	137.4	75.0	118.2
C13	52	Eagleford	B1619	183.8	16.0	94	136.4	74.0	117.6
C14	37	Eagleford	B1617	212.6	16.3	100	139.1	76.7	119.6
C15	44	Eagleford	B1637	215.7	15.0	87	134.8	72.4	117.2
C16	58	Eagleford	BC1	218.8	15.9	87	133.6	71.2	115.2
C17	56	Eagleford	B1697	122.9	21.7	109	135.9	73.5	111.7
C18	47	Eagleford	B1657	171.4	20.7	106	135.8	73.4	112.5
C19	64	Eagleford	BF1A	175	16.7	100	138.3	75.9	118.6
DS17	52	Eagleford	B1619	183.7	15.5	97	138.6	76.2	120.0
DS18	39	Eagleford	B1597	235.4	16.8	100	138.2	75.8	118.4
DS19	58	Eagleford	BC1	219.5	14.7	85	134.5	72.1	117.2
DS20	46	Eagleford	B1657	161.3	17.5	98	136.5	74.1	116.1
DS21	43	Eagleford	B1637	215	17.3	98	136.4	74.0	116.3
DS22	56	Eagleford	B1697	122.7	20.4	107	136.4	74.0	113.3
DS23	64	Eagleford	BF1A	174.8	17.2	100	137.7	75.3	117.5
DS24	37	Eagleford	B1617	213.1	17.0	98	136.9	74.5	117.0
CD11	58	Eagleford	BC1	219.2	17.2	98	136.6	74.2	116.5
CD12	47	Eagleford	B1657	171.9	17.4	96	135.7	73.3	115.6
CD13	63	Eagleford	BF1A	168.7	17.3	98	136.4	74.0	116.3
CD14	44	Eagleford	B1637	216.7	16.6	95	136.0	73.6	116.6
CD15	56	Eagleford	B1697	122.5	17.8	95	134.7	72.3	114.3
CD16	58	Eagleford	BC1	220.1	15.9	95	137.3	74.9	118.5
CD17	58	Eagleford	BC1	220.5	15.2	93	137.4	75.0	119.3
CD18	44	Eagleford	B1637	216.5	16.7	94	135.4	73.0	116.0
CD19	44	Eagleford	B1637	216.2	17.0	97	136.4	74.0	116.6
CD20	63	Eagleford	BF1A	168.9	16.9	98	137.0	74.6	117.2
CD21	63	Eagleford	BF1A	169.2	17.1	98	136.7	74.3	116.7
CD22	52	Eagleford	B1619	184.1	14.9	89	136.3	73.9	118.7
CD23	37	Eagleford	B1617	213.3	16.2	99	138.4	76.0	119.1
CD24	39	Eagleford	B1597	235.1	15.8	93	136.6	74.2	118.0

Table 3.2 Densities

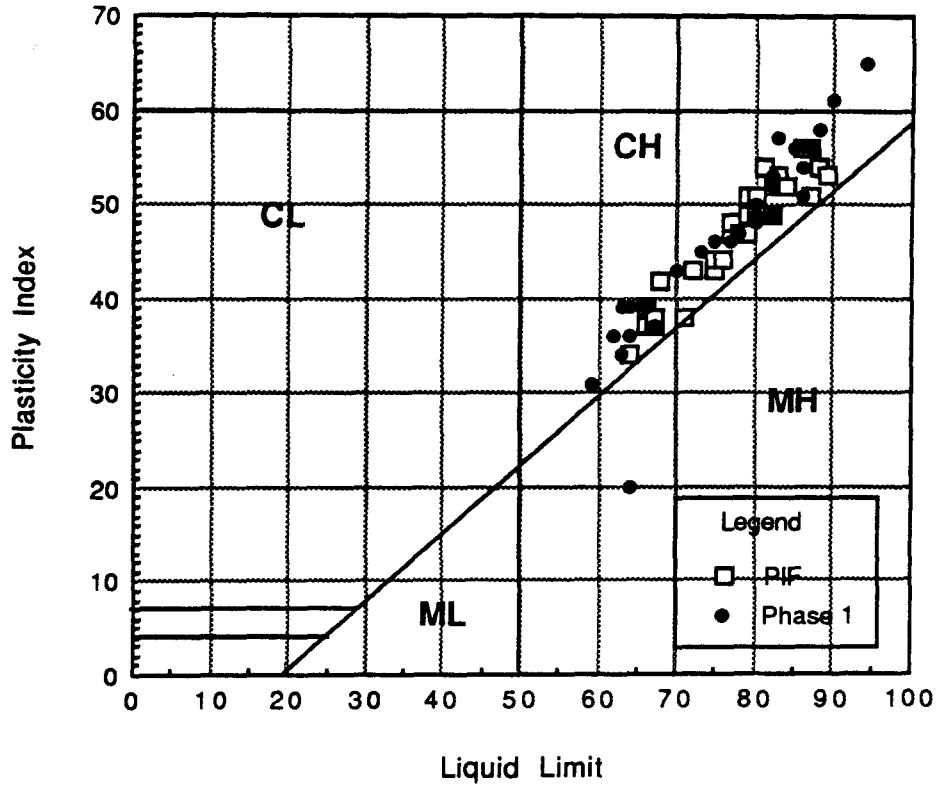

Fig. 3.1 Casagrande Plasticity Chart for Eagleford Shale for PIF and Phase 1

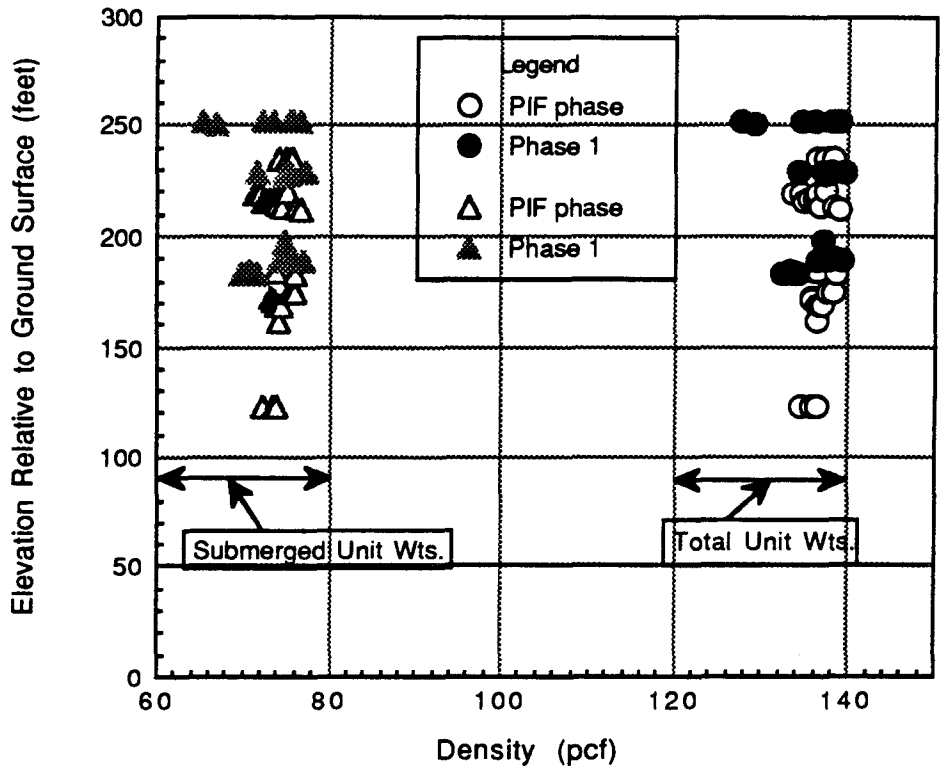

Fig. 3.2 Depth Dependency of Unit Weights for Eagleford Shale

SECTION 4

ONE-DIMENSIONAL CONSOLIDATION

INTRODUCTION

Eight one-dimensional consolidation tests, each from a different boring, were performed on samples of Eagleford shale for the PIF phase of this project. Seven additional tests were performed on samples of Eagleford shale in Phase 1.

The consolidation tests were used to establish the range of expected response for one-dimensional compressibility and consolidation properties of Eagleford shale.

SOURCE DATA

Complete consolidation data were presented in the Task 2 report (PIF phase) and, because of the bulk involved, will not be repeated. The data provided for each test in the Task 2 report included:

1. a spreadsheet showing the boring number, sample depth, name of the formation, sample description, original sample dimensions and weight, relevant index properties, and initials of persons setting up the tests and dates. In addition, the spreadsheet contained summary data each loading stage, including void ratios (e) and strains (ε) at the end of primary consolidation and just prior to the next loading or unloading, coefficients of compressibility (a_v) and consolidation (c_v), coefficient of volume compressibility (m_v), fitted hydraulic conductivity (k), incremental compression indices (C) and

compression ratios (R), and the percentage of the deformation representing initial/primary/secondary compression.

2. stress-strain curves in the form of a plot of void ratio versus log of the vertical effective stress ($\bar{\sigma}$).

3. coefficients of consolidation for the loading phase only (to avoid a confusing number of points) plotted versus log of effective stress, with the e-log($\bar{\sigma}$) relationship included for comparison.

4. all coefficients of volume compressibility plotted versus the log of the effective stress.

5. plots of void ratio versus the log of the hydraulic conductivity calculated from Terzaghi's theory.

6. plots of dial readings versus time, square root of time, and log of time (excluding some initial loadings where sample deformation was only a few ten thousandths of an inch and useful plots could not be prepared)

7. The source readings of the dial indicators and time, with any notes made by persons taking the readings.

GENERAL SUMMARY DATA

General data relating to the consolidation tests performed during the PIF testing phase (numbers C12-C19) are summarized in Tables 4.1 and 4.2.

Data from tests C7 and C10, performed during Phase 1, will be included in some of the figures to represent the average response observed for the Eagleford shale in Phase 1.

Test ID	Sample No.	Formation	Boring No.	Depth (ft.)	Water Content (%)	Liquid Limit (%)	Plastic Limit (%)
C12	38	Eagleford	B1597	234.8	16.3	75	32
C13	52	Eagleford	B1619	183.8	16.0	67	30
C14	37	Eagleford	B1617	212.6	16.3	75	31
C15	44	Eagleford	B1637	215.7	15.0	71	33
C16	58	Eagleford	BC1	218.8	15.9	64	30
C17	56	Eagleford	B1697	122.9	21.7	79	30
C18	47	Eagleford	B1657	171.4	20.7	79	28
C19	64	Eagleford	BF1A	175.0	16.7	79	32

Table 4.1 Summary of Sample Identification Data for One-Dimensional Consolidation Tests

Test ID	Initial Degree of Saturation (%) **	Initial Void Ratio	Field Void Ratio	Field Vertical Effective Stress (psf)	Swelling Pressure (psf)
C12	96	0.469	0.460	18100	17000
C13	94	0.476	0.464	14200	35000
C14	100	0.452	0.442	16400	15000
C15	87	0.481	0.450	16600	11000
C16	88	0.507	0.460	16900	28000
C17	109	0.554	0.547	9600	43000
C18	106	0.543	0.532	13300	28000
C19	100	0.464	na	13500	25000

** used G_s=2.78

Table 4.2 Summary of Calculated Initial Degrees of Saturation, Void Ratios, and Stresses

STRESS-STRAIN PROPERTIES UNDER INCREASING LOADS

Field Condition

Stress-strain curves for loading. The measured stress-strain curves for increasing loads are summarized in Fig. 4.1. Rebound

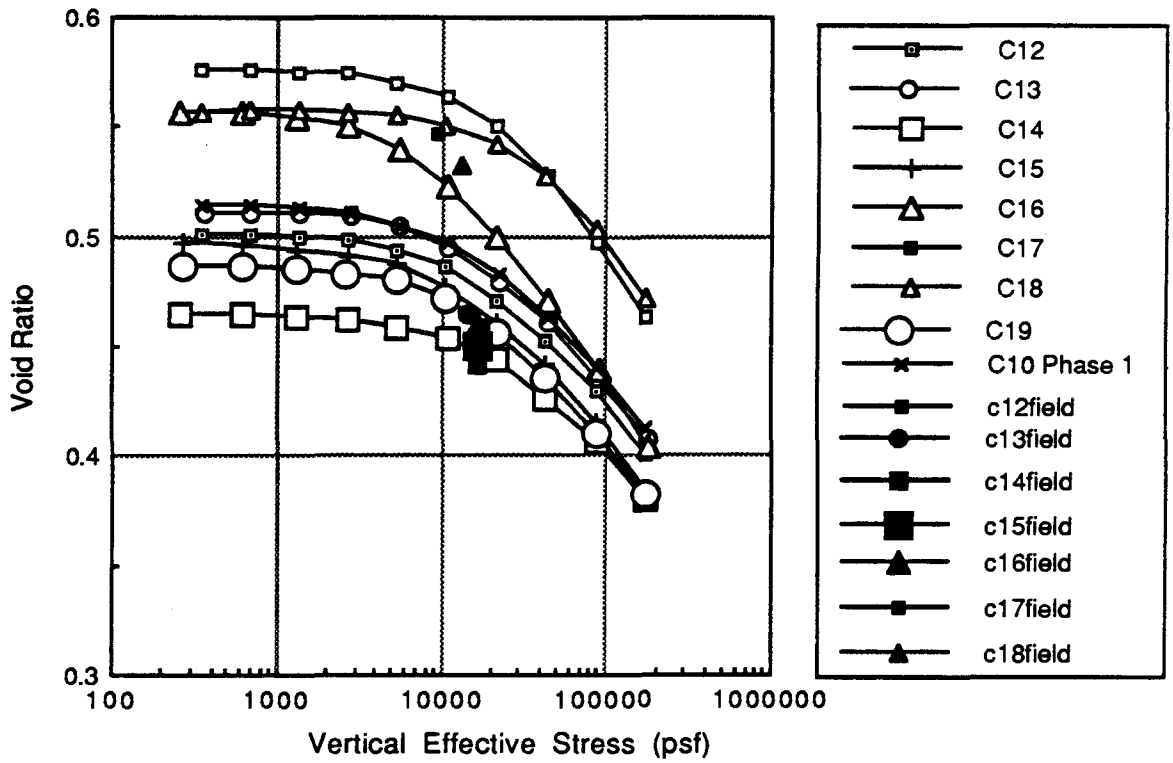

Fig. 4.1 Comparison of Stress-Strain Curves in One-Dimensional Compression for Tests C10 (Phase 1) and C12-C19 on Eagleford Shale in Reloading

stages have been excluded to avoid the presence of a confusing number of lines. The single symbols, identified in the legend using the word "field" represent the estimated void ratio and vertical effective stress in the field.

The stress-strain curves are essentially parallel to each other except for C16. After examining all of the data for C16, compared to data for the other tests, we believe that the sample used for C16 was less cemented than were the other samples.

Estimated field void ratio. We assumed the field void ratio was equal to the laboratory void ratio immediately after application of the field overburden effective stress. In some cases the application of the overburden pressure caused significant reductions in apparent void ratios ("significant" for the greatly expanded void ratio scale used in Fig 4.1), and thus the calculated field void ratio was noticeably smaller than the as-trimmed void ratio.

Immediate compression under load must result from the compression of gas or from seating problems. We found no evidence of seating problems and thus associate the immediate compressions with gas compression. During Phase 1 of this project, we concluded that the immediate compression was probably caused by closing of fissures that opened during some stage in the coring, storage, shipping, and/or trimming operation. The presence of open fissures could not be determined by visual examination. Evidence of the presence of such fissures came from the low initial degrees of saturation in some cases, e.g., 87% for sample C15, and the large amount of immediate compression when the field effective stress was applied, e.g., 209 dial divisions (1 div.=0.0001 inch) for sample C15.

The presence of open fissures was not appreciated until most of the way through the Phase 1 testing, and no measurements were made of the immediate compression that occurred when the field overburden effective stress was applied, so there is a small error in the field void ratios used previously.

Estimated field effective stress. The field effective stress was calculated assuming the water table was at a depth of 5 feet (information from The Earth Technology Corporation) and the soils had a total unit weight of 138 pcf. If the water table was perched, then field pore water pressures would be less than we have assumed, in the depths below the pertched water zone, and the field effective stresses should be larger than the values we calculated, and thus closer to the laboratory void ratio-effective stress curves.

The field e-$\bar{\sigma}$ points are close to the measured reloading stress-strain curves, but generally have slightly lower void ratios. The main reason for the lower void ratios for the field condition is hysteresis associated with the fact that the samples were rebounded back to about 350 psf and then reloaded again.

Maximum Previous Consolidation Pressures

The shapes of the measured compression curves (Fig. 4.1) would suggest a maximum previous consolidation pressure around 15,000 psf. However, for samples with liquid limits of the order of 71%

(64%-79%), the compression index for the virgin consolidation curve, C_c, would be expected to be about:

$$C_c = 0.009(LL-10) = (0.009)(61) = 0.55 \quad (4.1)$$

The measured incremental compression indices (Table 4.3) were all significantly less than 0.55 (see later discussion), indicating that the real maximum previous consolidation pressure must have been in

Pressure (psf)	Test C12	Test C13	Test C14	Test C15	Test C16	Test C17	Test C18	Test C19
11000	0.006							
22000	0.003	0.005				0.020		
44000	0.033	0.023				-		
11000	0.025	0.029				-	0.026	
2700	0.019	0.023				-	-	
350	0.053	0.021	0.014	0.016	0.041	0.013	0.011	
700	0.001	-	-	0.002	0.001	-	-	0.001
1400	0.004	0.002	0.001	0.006	0.008	0.003	0.001	0.002
2700	0.005	0.004	0.005	0.010	0.014	0.005	0.003	0.007
5400	0.014	0.013	0.009	0.015	0.032	0.011	0.006	0.010
11000	0.028	0.032	0.017	0.031	0.057	0.020	0.014	0.027
22000	0.048	0.053	0.035	0.053	0.079	0.044	0.030	0.052
43000	0.058	0.059	0.058	0.067	0.094	0.075	0.049	0.063
87000	0.082	0.083	0.068	0.084	0.105	0.103	0.078	0.087
174000	0.093	0.093	0.085	0.101	0.116	0.114	0.104	0.093
43000	0.055	0.052	0.046	0.055	-	0.069	0.059	0.054
11000	0.051	0.054	0.047	0.055	-	0.070	0.049	0.049
2700	0.039	0.037	0.032	0.043	-	0.036	0.030	0.027
350	0.023	0.022	0.015	0.019	0.034	0.024	0.019	0.016

Table 4.3 Summary of Compression Indices for Eagleford Shale

excess of 200,000 psf. Alternatively, the effects of cementation could have produced a large increase in the apparent maximum previous consolidation pressure.

Swelling Pressures

The laboratory testing procedure involved application of the estimated field effective stress, innundating the sample, and then adjusting the total applied stress to prevent swelling. When

equilibrium was finally established, the void ratio, say e_s, was typically slightly less than the estimated field void ratio, say e_f. The samples were then rebounded back to a small effective stress. The measured slope of this initial rebound curve was then defined as a swelling index, say C, given by:

$$C = \frac{e_2 - e_1}{\log(\frac{\bar{\sigma}_1}{\bar{\sigma}_2})} \tag{4.2}$$

where the subscripts 1 and 2 denote two points on the swelling curve.

If the void ratio and effective stress, when the sample first came to equilibrium, are used as say point 1, and the field void ratio is e_2, then Eq. 4.2 can be used to calculate the swelling pressure as $\bar{\sigma}_2$. The swelling indices were very small (see subsequent discussion) so inevitable uncertainties in estimating the field void ratio lead to substantial uncertainties in the calculated swelling pressure. The major source of uncertainty in the field void ratio is probably associated with the problem of determining when the fissures are closed back to the same state they were in prior to coring in the field.

The calculated swelling pressures (Table 4.1) were larger (two to five times) than the field effective stress for five of the consolidation tests, while two were approximately equal to the field stress.

Compressibility

The stress-strain curves (Fig. 4.1) for the tests on Eagleford shale in the PIF program were essentially identical to the Phase 1 curves, indicating repeatability and possibly homogeneity in response for the sample sizes used for one-dimensional compressibility. However, larger sized samples may represent the field response more closely, since they are likely to contain a statistically more significant number of the macrofabric features that may exist in the field.

Incremental values of the compression indices for various ranges of pressure should generally tend to increase as the liquid limit increases. However, actual data for this study (Fig. 4.2) scatter widely. For the range in liquid limit from 60% to 80%, there is no statistically significant relationship. The one sample with a liquid limit of 88% was more compressible than the other samples.

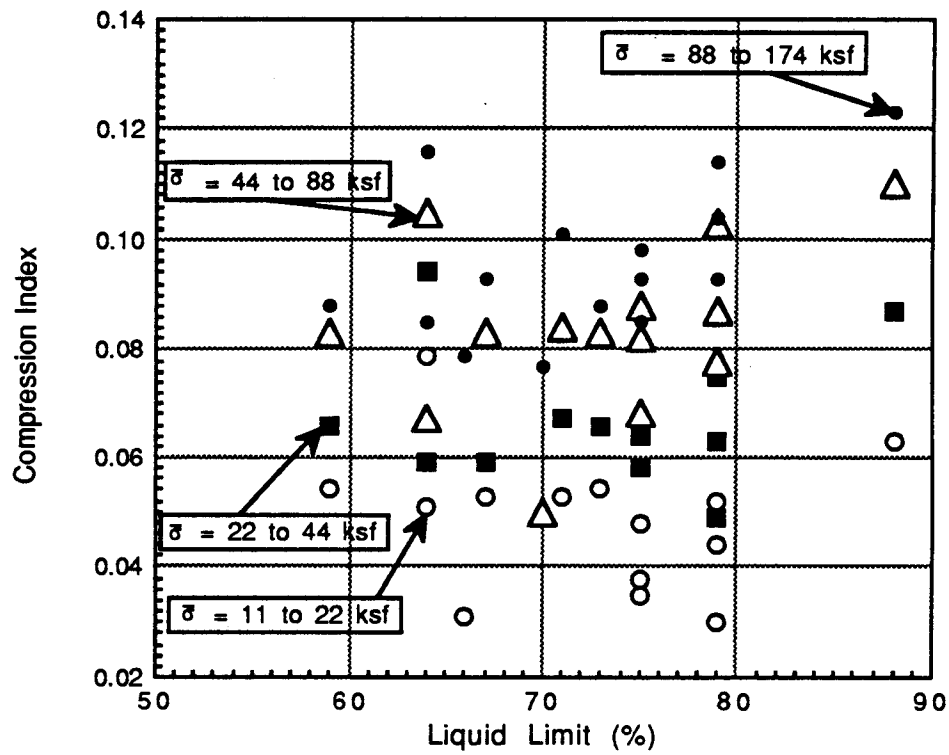

Fig. 4.2 Influence of Liquid Limit on Compression Indices for the Main Loading Curve for Eagleford Shale in the PIF Phase and Phase1

STRESS-STRAIN PROPERTIES DURING REBOUND

Need for These Data

For unloading problems, the properties of the samples during rebound are of major interest. Rebound from the peak pressure leads to better defined properties than for the initial unloading from the

swelling pressure but loading to pressures near 180,000 psf (but less than the apparent maximum previous consolidation pressure) may result in breakage of cement bonds or other changes in properties that would cause departure from current field conditions.

First Rebound

The samples rebounded from significantly different pressures and underwent only very small changes in void ratio. To avoid problems with greatly exaggerated void ratio scales, it is convenient to plot the calculated swelling index (C) versus the mean stress during rebound (Fig. 4.3). The very low values for the swelling index indicate that the material is probably cemented. For highly plastic

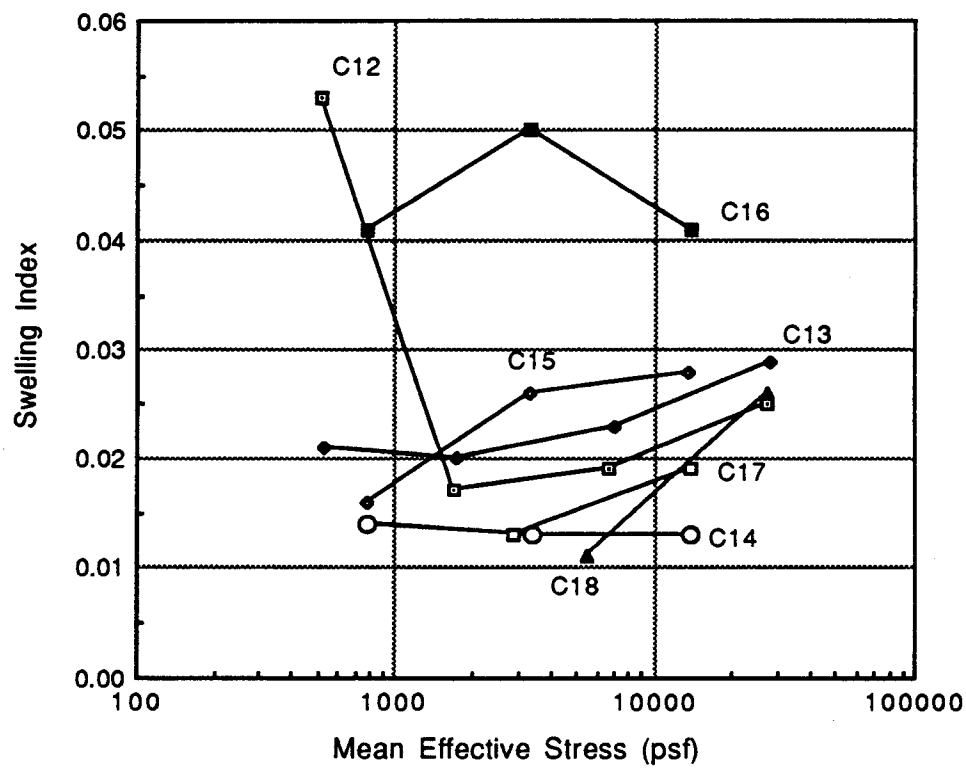

Fig. 4.3 Swelling Indices During First Rebound

materials, the swelling slopes are generally in the range of about 0.3 to 0.9 times the virgin slopes so we might expect swelling slopes of the order of 0.15 to 0.50 for uncemented material.

The measured rebound slopes are in the range of 0.012 to 0.029 except for tests C12 and C16. We believe that for test C12, an incorrect loading weight was placed on the frame. However, the problem was not discoivered until the end of the test when all weights had been removed and thus there was no way to correct the error. For sample C16, the data generally suggest that the sample may not have been cemented as much as were the other samples (or perhaps the cement was partly broken) and thus it was free to swell more than did other samples.

Considering that the changes in void ratio were only about 0.01 for a two times change in applied pressure, significant scatter can result from such problems as small uncertainties in apparatus deflections and variations in the extent of fissuring. Further, at low pressures the amount of ring friction may influence the slope significantly.

Final Rebound

The rebound stress-strain curves for unloading from the highest pressure are compared in Fig. 4.4. A representative rebound curve from the Phase 1 study (C10) is included for comparison. The samples clearly all behaved in a similar manner.

Numerical values of the compression index (C) are summarized in Table 4.3. The indices decrease substantially as the pressure decreases. It is well known that large amounts of ring friction develop in one-dimensional consolidation tests during rebound at small pressures. Thus, we tend to discount the lowest values of the compression (swelling) index. The swelling indices thus range from about 0.03 to 0.07.

Rebound from a pressure of 180,000 psf produced larger indices then for the initial unloading phase, probably because the cement was at least partially broken under the high applied pressures. The swelling indices for final rebound were comparable to the indices for initial swelling for sample C16.

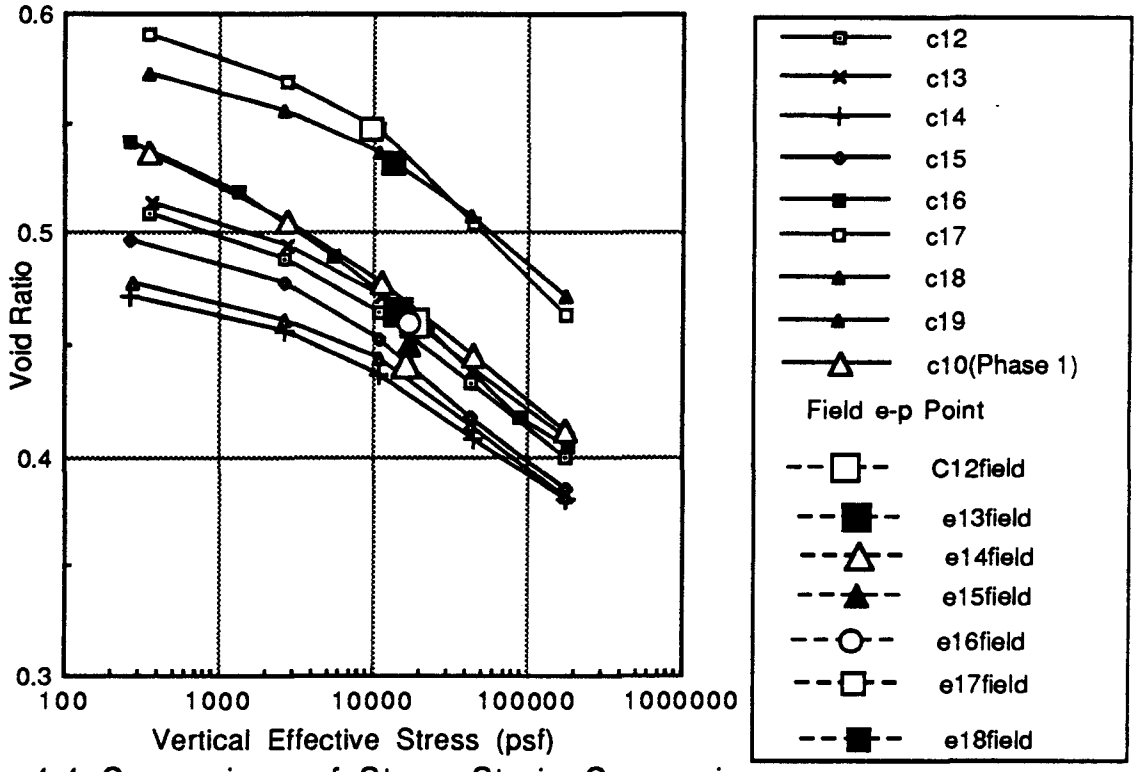

Fig. 4.4 Comparison of Stress-Strain Curves in One-Dimensional Compression for Tests C10 (Phase 1) and C12-C19 on Eagleford Shale in Final Rebound

In the field, the rock will be unloaded and reloaded along stress paths that are more complicated than used in simple one-dimensional consolidation tests. Further study of these materials under generalized stress-strain conditions seems warranted.

Errors associated with apparatus deflections

For the small displacements being measured, uncertainties in the apparatus deflections may introduce significant errors. The problem occurs because we measure apparatus deflections by running a full scale test with the porous stones in contact with each other. If the stones are not perfectly plane, the measured deflections will be larger for stone-on-stone (where the stones may actually bend) than for stone-on-relatively compressible soil or rock (where the stone should deflect less).

If we assume that accuracy in apparatus deflections is of the order of ten dial divisions, i.e., 0.001 inch, that the sample total height is

0.6 inch, the height of solids is 0.4 inch, and loads are doubled or halved each time, then the errors are:

C ± 0.003
R ± 0.002

Errors in a_v and m_v are $\pm 2.5 \times 10^{-5}$ and 1.6×10^{-5} $(psf)^{-1}$ for a stress increase of 100 psf, and decrease linearly as the stress change increases.

Disturbance effects

There is no evidence of large effects of sample disturbance in any test except perhaps C16 and we tentatively conclude that the samples can be treated as being undisturbed. Test C16 was the only test in the PIF phase that had the final rebound curve (see e-log $\bar{\sigma}$ curve, Fig. C16.2 in Task 2 report) parallel to the first unload curve, thus implying that the sample was not cemented during initial rebound, and did not swell back to at least the initial void ratio under the final stress. The cementitious bonds may have been broken or they may never have existed in the field.

COEFFICIENTS OF CONSOLIDATION

Coefficients of consolidation for tests C12-C19 from the PIF phase and C10 from Phase 1 are compared in Fig. 4.5 for the reloading stresses and all values of c_v are presented in Table 4.4. A log-log plot was used in Fig. 4.5 to allow the smaller values of c_v to be viewed on the same plot where much larger values are plotted.

The curves (Fig. 4.5) have the same general shape, indicating a gradual reduction in c_v as the consolidation pressure increases. Some of the scatter can be attributed to the different void ratios and compressibilities of specimen at the same effective stresses.

Loading Curve

Data for test C10 represent the average variation of coefficient of consolidation for Eagleford shale from tests performed in Phase 1.

The data for test C10 fall within the average response for the PIF phase tests for stresses above 5000 psf. The majority of values of cv scatter about ± 5 times about the mean.

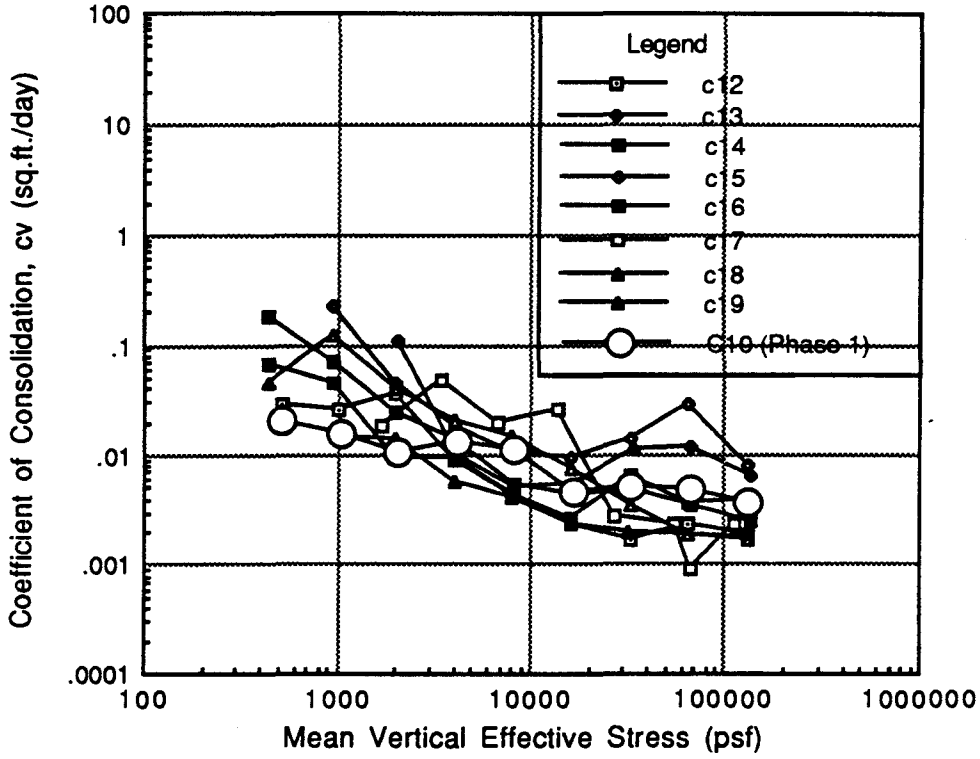

Fig. 4.5 Comparison of Coefficients of Consolidation for the Reloading Curves for Tests C12-C19

For stresses near the field overburden pressures, say 10,000 to 15,000 psf, the values of c_v range from about 0.002 sq.ft./day to 0.01 sq.ft./day with one value of 0.05 sq.ft./day.

Initial Rebound

Values of the coefficient of consolidation for the initial rebound are not likely to be accurate because of the problem of closing up microfissures that we suspect opened in the samples prior to testing. Further, time-displacement plots were not particularly useful because the amount of swell was so small, often only a few dial divisions. The range in values of c_v for the initial unloading range for the tests on Eagleford shale were as follows:

Test	Range in c_v (sq.ft./day)
C12	0.025 - 0.078
C13	0.004 - 0.032
C14	0.001 - 0.004
C15	0.003 - 0.014
C16	0.001
C17	0.004 - 0.006
C18	0.002 - 0.012
C19	0.003

Nominal Pressure psf	Test C12 ft^2/d	Test C13 ft^2/d	Test C14 ft^2/d	Test C15 ft^2/d	Test C16 ft^2/d	Test C17 ft^2/d	Test C18 ft^2/d	Test C19 ft^2/d
11000								
22000						0.0044		
44000	0.0078	0.0322				-	0.0116	
11000	0.0031	0.0067				-	0.0017	
5400	-		0.0039	0.0142	0.0006	0.0049	-	
2700	0.0025	0.0044	-	-	-	-	-	
1300	-	-	0.0006	0.0027	0.0010	-	-	
350	0.0001	-	-	0.0237	0.0014	0.0058	0.0078	0.0003
700	0.0305	-	0.0668	0.2568	0.1838	-	-	0.0456
1400	0.0261	-	0.0451	0.2242	0.0679	0.0188	0.0145	0.1184
2700	0.0365	0.1090	0.0095	0.0436	0.0237	0.0460	0.0140	0.0403
5400	0.0091	0.0102	0.0097	0.0182	0.0140	0.0198	0.0056	0.0210
11000	0.0043	0.0052	0.0043	0.0106	0.0550	0.0252	0.0042	0.0149
22000	0.0023	0.0053	0.0027	0.0094	0.0440	0.0028	0.0023	0.0075
43000	0.0017	0.0114	0.0063	0.0143	0.0049	0.0023	0.0020	0.0034
87000	0.0023	0.0118	0.0037	0.0293	0.0035	0.0023	0.0019	0.0019
174000	0.0019	0.0064	0.0040	0.0078	0.0025	0.0009	0.0018	0.0017
43000	0.0011	0.0018	0.0028	0.0026	-	0.0007	0.0009	0.0010
11000	0.0007	0.0011	0.0013	0.0013	-	0.0003	0.0010	0.0008
2700	0.0003	0.0006	0.0007	0.0008	-	0.0003	0.0004	0.0007
350	0.0002	0.0004	0.0003	0.0006	0.0003	0.0001	0.0001	0.0002

Table 4.3 Summary of Coefficients of Consolidation for Eagleford Shale

Generally, the lower values occurred at the minimum stress of 350 psf and the larger value occurred upon first unloading. Again the range in numerical values is relatively small for samples as widely distributed as the samples tested here.

Final Rebound Curve

For rebound from the peak pressure, the coefficients of consolidation range from about 0.0005 to 0.0030 (again ignoring data at small stresses where effects of ring friction lead to errors of unknown magnitude) and are much lower than for the loading curve. The coefficient of consolidation is given by the equation:

$$c_v = \frac{k\,(1+e)}{a_v \gamma_w} \tag{4.3}$$

where k is the hydraulic conductivity, e is void ratio, av is the coefficient of compressibility, and gw is the unit weight of water. Application of high pressures results in a low void ratio and thus a low value of k. Breakdown of the cement leads to a larger value of av than would otherwise occur. The result is a low value for c_v. Of course, loading in the laboratory may have returned partially open fissile surfaces to a closed condition such as might be anticipated in the field.

For pressures near the field overburden stress, the coefficients of consolidation are around 0.001 sq.ft/day. These values are quite low but are consistent among the various samples of Eagleford shale.

Scatter

The curves of settlement versus $\sqrt{\text{time}}$ were often gently curved during the stage when they should have been linear according to Terzaghi's theory. As a result, a wide range in values of c_v can be obtained for any load depending on what part of the curve is assumed to be linear by the person reducing the data. No benefit can be achieved by using the log(time) fitting method because it utilizes the same assumption for the shape of the early part of the primary curve. We therefore anticipate significant amounts of scatter for any one test and more scatter when data for a group of tests are compared.

Measured and Computed Hydraulic Conductivities

During the Phase 1 study, values of hydraulic conductivity were measured during several of the one-dimensional consolidation tests.

Data for tests on sample C7 are shown in Fig. 4.6. The measured hydraulic conductivities were significantly less than the values backed out of Time-Settlement curves using Terzaghi's theory, indicating that the theory may not be applicable to the Eagleford shale. If Terzaghi's theory does not describe sample behavior properly, then it is not likely to describe field behavior well either and a more basic study of the time-rate parameters for Eagleford shale may be justified.

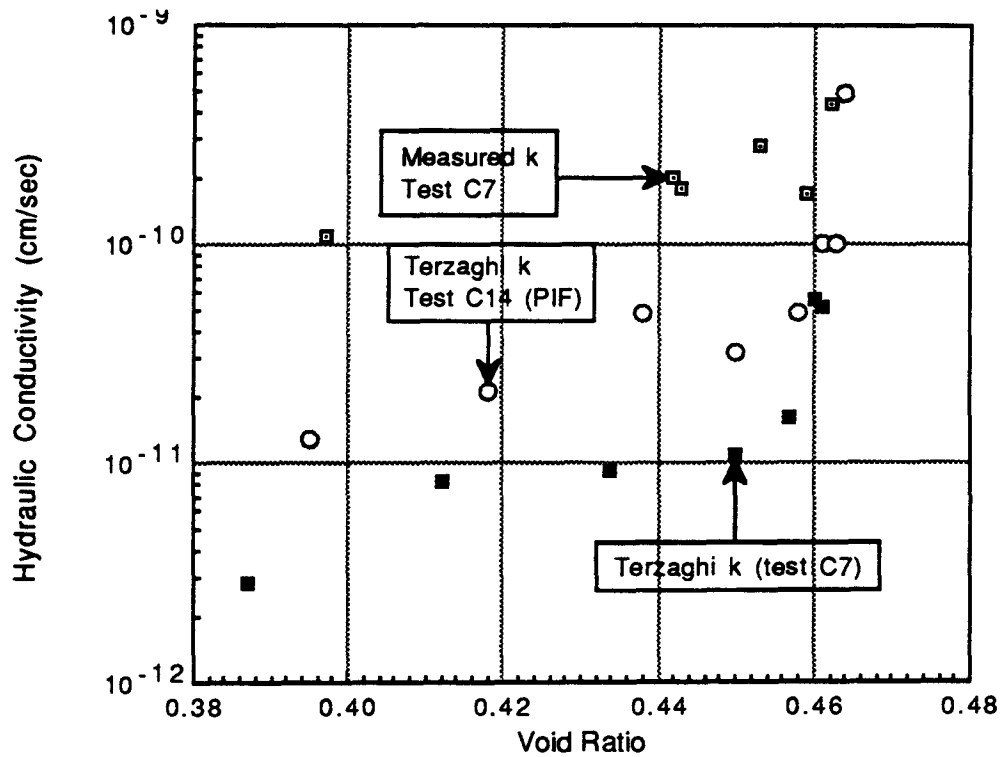

Fig. 4.6 Log Hydraulic Conductivity vs. Void Ratio for One-Dimensional Consolidation Test C7 on Eagleford Shale from Phase 1

SUMMARY AND CONCLUSIONS FOR ONE-DIMENSIONAL CONSOLIDATION TESTS

The following conclusions seem warranted:

1. In general, the consolidation properties of the various samples of Eagleford shale were relatively consistent, at least when

compared with the kinds of scatter we usually encounter for similar tests with soft clays near the surface.

2. The measured swelling pressures were comparable to, or perhaps slightly above, the calculated field overburden effective stress. However, pore water pressures are not known in the field so there is uncertainty in the calculated field effective stresses. In addition, the laboratory stress-strain curves are so flat that small differences in void ratio lead to large differences in apparent swelling pressure. The laboratory void ratios are uncertain, in part, because of the difficulty of dealing with fissured rocks.

3. The stress-strain curves for increasing pressures were generally parallel to each other, with the exception on one sample that may not have been cemented as much as the other samples.

4. The rock is believed to be overconsolidated for stresses below about 200,000 psf.

5. The compression indices during loading ranged from about 0.001 to 0.12, with the low values for reloading at low stresses and the high values at stresses beyond those that are likely to be encountered in field problems. Swelling (rebound) indices for generally between 0.01 and 0.03 for unloading from the swelling pressure and 0.03 to 0.07 for unloading from the peak pressure.

6. For loading, the coefficients of consolidation decreased from about 0.1 sq.ft./day at low stresses to about 0.005 at pressures above those likely to be achieved in a real field problem.

7. The shape of the curves of settlement versus $\sqrt{\text{time}}$ indicate that Terzaghi's theory may not describe the behavior of this rock very well. Further studies in this area seem warrented.

SECTION 5

"DRAINED" DIRECT SHEAR TESTING

INTRODUCTION

Purpose of Investigation

The main purpose of performing the direct shear testing program was to define the effective failure envelope (shearing strength) for Eagleford shale, and in the factors, such as the time to failure, that influence the location of the envelope.

Tests Performed

Eight "drained" direct shear tests (Table 5.1) from different borings were performed on Eagleford shale in the PIF phase. Three tests were performed at effective consolidation pressures of 10 and 100 psi, while two were performed at 50 psi.

In addition, five direct shear tests (3 at 10 psi, 1 each at 50 and 100 psi) on Eagleford shale were added from the Phase 1 study to supplement the PIF-phase data. The Phase 1 tests were chosen because they had shearing times that were considered to be "drained". The liquid limits varied from 63% to 90% for the Phase-1 specimens and 66% to 89% for the PIF-phase specimens. The initial water contents varied by similar amounts for the two series (15%-20% for Phase 1 vs. 14%-18% for PIF).

Test ID	Sample No.	Boring No.	Depth (ft.)	wc (%)	LL (%)	PL (%)	Time to Failure (min.)	Comments
DS9	13	BIR43	182.8	17.5	82	33	2340	PHASE 1
DS10	13	BIR43	182.7	17.1	90	29	7260	PHASE 1
DS11	15	BIR43	251.0	16.7	64	24	2750	PHASE 1
DS12	15	BIR43	252.2	14.0	63	24	2595	PHASE 1
DS13	15	BIR43	251.5	16.0	63	29	2400	PHASE 1
DS17	52	B1619	183.7	15.5	66	27	3270	PIF PHASE Failed during Shear
DS18	39	B1597	235.4	16.8	88	34	5420	PIF PHASE Failed during Shear
DS19	58	BC1	219.5	14.7	78	31	2870	PIF PHASE Failed during Shear
DS20	46	B1657	161.3	17.5	82	33	9230	PIF PHASE,Failed during Shutoff
DS21	43	B1637	215.0	17.3	87	36	2160	PIF PHASE,Failed during Shutoff
DS22	56	B1697	122.7	20.4	82	30	3280	PIF PHASE,Failed during Shutoff
DS23	64	BF1A	174.8	17.2	86	30	1900	PIF PHASE,Failed during Shutoff
DS24	37	B1617	213.1	17.0	89	36	2950	PIF PHASE Failed during Shear

Table 5.1 Summary of General Direct Shear Data on Eagleford Shale with Failure Times Exceeding 1800 Minutes

PRESENTATION OF SOURCE DATA

The original direct shear data were presented in the Task 2 report (PIF phase) and will not be duplicated here Data for each test, in the Task 2 report, included:

1. a spreadsheet that contained sample identification information (boring number, sample depth, formation name, sample description), initials of person setting up the test and checking the data (with dates), data collected at set-up time (sample thickness and weight), relevant index properties, sensor constants, and data for the shearing stage (horizontal

displacement, change in thickness, shearing and normal stresses).

2. plots of shearing stress and vertical deformation versus horizontal displacement.

3. time-displacement readings for the consolidation phase of the test.

4. plots of settlement versus time, log of time, and $\sqrt{time}$ for the consolidation phase.

EXPERIMENTAL PROCEDURES

Consolidation Stage

For optimal results, the samples should have been subjected to a procedure similar to that followed for the one-dimensional consolidation tests, with determination of the swelling pressure first, and then rebound or loading to the desired normal stress with recording of changes in sample thickness with time. In such a way the coefficients of consolidation could have been defined. Such a procedure was not followed because the time period available for these tests was too short.

Instead, the samples were placed in the shear boxes, the loading frame placed, the displacement transducer was "zeroed", and then the specimen was loaded to the final pressure in a single step. Since the final load was applied in one step, the specimen initially compressed for an extended period of time, presumably by closing up fissures, before finally swelling and coming to equilibrium.

Shearing Stage

The coefficient of consolidation was estimated from the adjacent sample tested in one-dimensional consolidation to check the theoretical shearing rate.

However, on the basis of the information obtained from Phase 1, we adopted the following testing procedure (discussed in Report 1 of the PIF phase):

> *To achieve the desired time to failure, shear the samples using the slowest speed on the machines, until the horizontal deformation is 0.002" (in about one hour), then stop the direct shear tests with the load maintained for six hours, and repeat this cycle until failure occurs (a total displacement between 0.01" and 0.02", four to six cycles of shearing in two days).*

REVIEW OF RELEVANT ASPECTS OF DIRECT SHEAR TESTING

Expected behavior

The Eagleford shale did not behave, in all respects, as anticipated. It is convenient to begin the discussion by stating the behavior that was anticipated.

Direct shear tests are almost always performed by allowing samples to consolidate fully under some applied axial stress, and then applying horizontal displacements at some convenient rate to induce failure. For clays it is not economical to use failure times that allow essentially complete dissipation of pore water pressures generated during shear. Thus, the test involves partial drainage and the measured shearing strength lies somewhere between that found for a sample subjected to consolidated-undrained (R) conditions, and that for a sample subjected to consolidated-drained (S) conditions. The R and S failure envelopes for normally consolidated (NC) and simply overconsolidated (OC) typical clays are shown in Fig. 5.1. For the S tests, the failure envelope is usually essentially the same for normally consolidated and overconsolidated samples (sometimes the strengths of overconsolidated samples are slightly higher than for normally consolidated samples). For the R envelope, the envelope for normally consolidated samples typically has a slope about half of that of the S envelope. For R tests on samples that have been rebounded back from some peak pressure (point A), the envelope forms a large loop. For consolidation pressures between those of point A and point B, the S strength exceeds the R strength

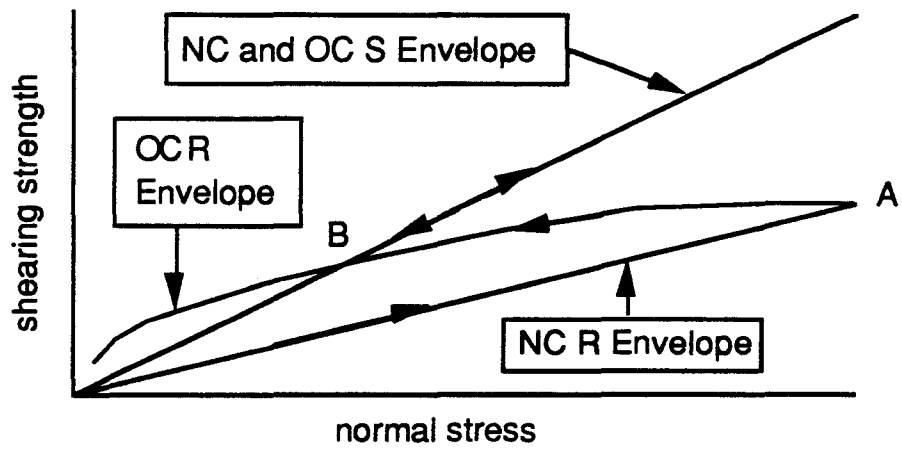

Fig. 5.1 Expected Behavior for Clays under R and S Conditions

and samples tested with increasing times to failure will have gradually increasing strengths. For samples consolidated to the stress at point B, the strength does not depend on the time to failure because the S and R strengths are identical. For samples that are highly overconsolidated, i.e., for consolidation pressures less than that at point B, the R strength exceeds the S strength and consequently the measured shearing strengths decrease as the time to failure increases in tests under partially drained conditions.

Because the Eagleford shale appeared to be highly overconsolidated, we expected that the measured shearing strength of the Eagleford shale would decrease with increasing times to failure. Of course, variations in strength were expected because of inherent variations in the properties of samples of natural materials. Such variations were expected to be important for the Eagleford shale because it is fissured. The strength would therefore be expected to depend on the possible orientation of fissures that would not be visible during trimming.

The presence of horizontal planes of weakness, evident from numerous failures during trimming, made it clear that the Eagleford shale is highly anisotropic. Further, the strength in direct shear

should depend on whether a fissile surface happened to be precisely aligned with the forced failure surface in the shear box, or not.

All direct shear tests were executed with the specimen oriented so that the horizontal planes that exist in the field are horizontal in the shear box. The one-dimensional consolidation tests indicated that the cores and trimming procedures were not introducing significant disturbances (at least not variable).

Estimation of Degree of Consolidation at Failure

The average degree of dissipation of excess pore water pressures at failure (U_f) can be estimated using:

$$U_f = 1 - \frac{H^2}{2c_v t_f} \qquad (5.1)$$

where H is the drainage distance, c_v is the coefficient of consolidation, and t_f is the time to failure. Equation 5.1 is reasonably accurate only if the degree of consolidation at failure is reasonably large, say about 60%. The main uncertainty in ensuring that excess pore pressures do not introduce conditions of variability in the direct shear test results, is in the evaluation of the coefficient of consolidation.

The coefficients of consolidation for the PIF phase direct shear tests were estimated from the one-dimensional consolidation tests on a specimen from the same core. All the uncertainties discussed (closure of fissile surfaces, friction, secondary conditions, etc.) in the one-dimensional consolidation section will apply here too. However, the degrees of consolidation at failure ranged from 98% to 100% (Table 5.2) for most of the direct shear tests whose coefficient of consolidation could be determined from one-dimensional consolidation data. From measurements of hydraulic conductivity in Phase 1, we are reasonably confident that the coefficients of consolidation used to estimate the direct shear specimen degree of consolidation at failure are smaller than those inferred from permeability measurement. As a result, the actual degrees of consolidation are probably larger than those calculated here. Thus, all samples were believed to be adequately "drained".

DS Test	time to failure (min)	Consolidation Test	Coeff. of Consolidation (sq.in./min.)	Degree of Consolidation (%)
DS17	3300	C13	0.001	99
DS18	5420	C12	0.001	99
DS19	2872	C16	0.004	100
DS20	9230	C18	0.001	100
DS21	2160	C15	0.001	98
DS22	3278	C17	0.001	99
DS23	1900	C19	0.001	98
DS24	2950	C14	0.0004	96

Table 5.2 Degrees of Consolidation at Failure for Direct Shear Tests

Size Effects

Although the specimens were large enough in one-dimensional consolidation to obtain repeatable results (they still may not represent the field response), they are probably not large enough to do so in direct shear. The direct shear tests tends to aggravate the problem of discontinuities that may exist in the highly overconsolidated specimen.

Effects of Edge Loading

The goal, in direct shear testing, is to subject the sample to uniform normal and shearing stresses on the opposing flat faces and use the ring only for confinement and development of required complementary stresses. Unfortunately, because of the design of the apparatus, load is applied by the box to the sides of the sample. For soft clays, the shear box presumably makes contact with the loading cap and thereafter there is at least a semblance of shearing applied to the faces.

For stiff, brittle material like the Eagleford shale, the edge stress may cause failure prior to the edge making contact with the loading cap, and thus the sample may be subjected to highly nonuniform shearing stresses.

PRESENTATION OF SHEARING DATA

Summary Data

Summary data for all tests considered in this chapter are presented in **Table 5.3**. Cross sections through the samples tested during the PIF study, showing the shapes of the failure surfaces, are shown in **Figs. 5.2 and 5.3.**

Test ID	Peak Shear Stress (psf)	Peak Eff. Normal Stress (psf)	Failure Horiz. Disp. (in.)	Failure Vert. Disp. (in.)	Resid. Shear Stress (psf)	Resid. Effec. Normal Stress (psf)	Resid. Horiz. Disp. (in.)	Resid. Vert. Disp. (in.)	Smooth Fail. Surf. (?)
DS9	730	1450	0.0084	0.0012	670	1470	0.0199	0.0032	yes
DS10	4560	1460	0.0149	0.0044	1210	1470	0.0276	0.0077	no
DS11	9420	14560	0.0133	0.0000	6970	14830	0.0344	0.0014	no
DS12	1040	1450	0.0102	0.0026	920	1480	0.0303	0.0066	no
DS13	4810	7250	0.0078	0.0006	3370	7400	0.0328	0.0024	no
DS17	2265	1450	0.0057	0.0014	1040	1560	0.0910	0.0217	no
DS18	4090	1460	0.0126	0.0021	1070	1540	0.0707	0.0191	no
DS19	7430	7390	0.0127	0.0008	5160	8020	0.1055	0.0118	yes angled
DS20	3200	1460	0.0173	0.0019	920	1590	0.1104	0.0250	no
DS21	11140	7390	0.0124	0.0021	2890	8120	0.1167	0.0148	rela-tively
DS22	13100	14630	0.0177	0.0006	4560	15800	0.1036	0.0018	yes
DS23	10520	14500	0.0113	0.0006	5190	14500	0.0144	0.0008	rela-tively
DS24	11870	14570	0.0165	0.0010	4470	15700	0.1006	0.0047	yes

Table 5.3 Summary of Direct Shear Tests from Phase 1 and PIF on Eagleford Shale, with Failure Times Exceeding 1800 minutes

Consolidation Pressure at 10 psi

Curves of shearing stress versus horizontal displacement (hereafter referred to as the stress-displacement curves) for the three tests (DS17, DS18, and DS20) performed on the PIF phase, with a consolidation pressure of 10 psi, are shown in Fig. 5.4.

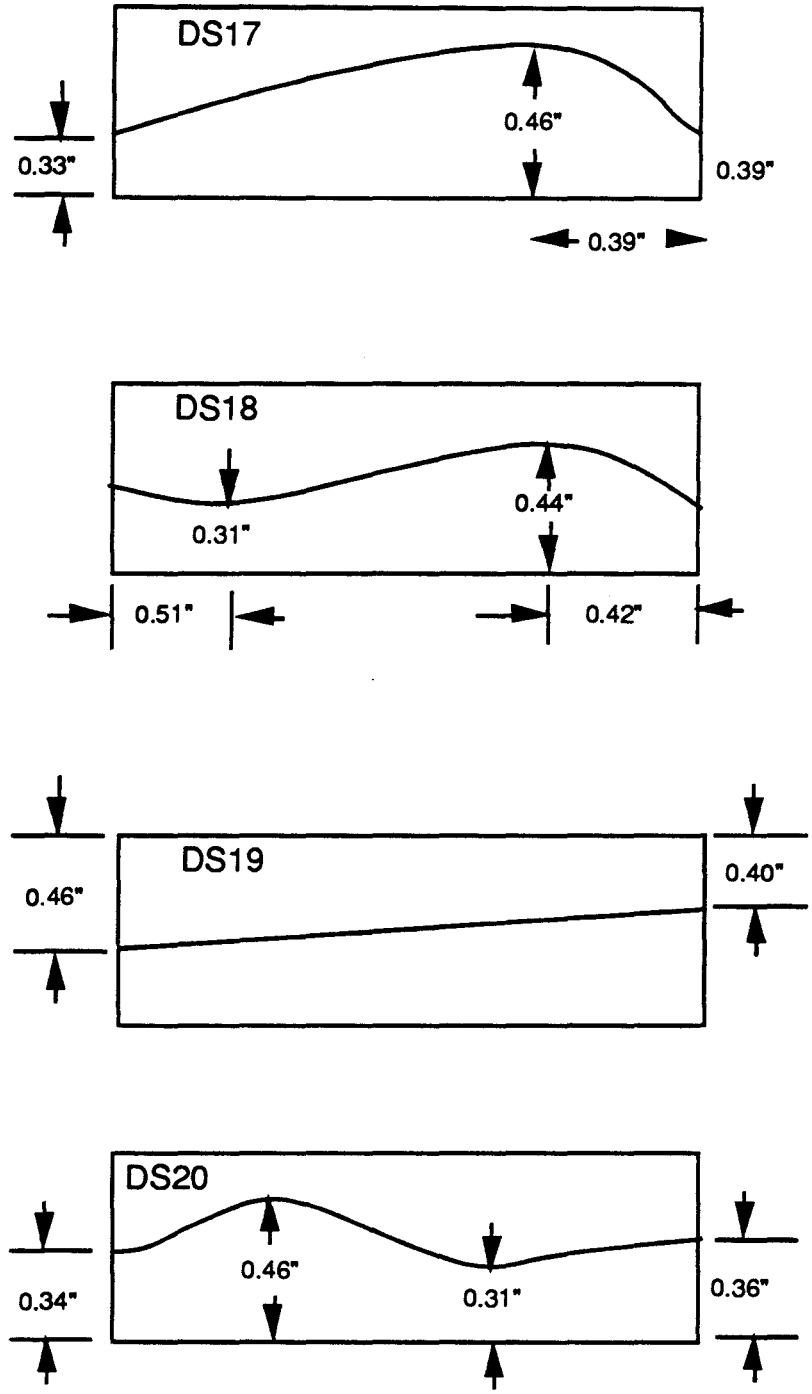

Fig. 5.2 Failure Surfaces in Direct Shear Tests on Eagleford Shale for PIF

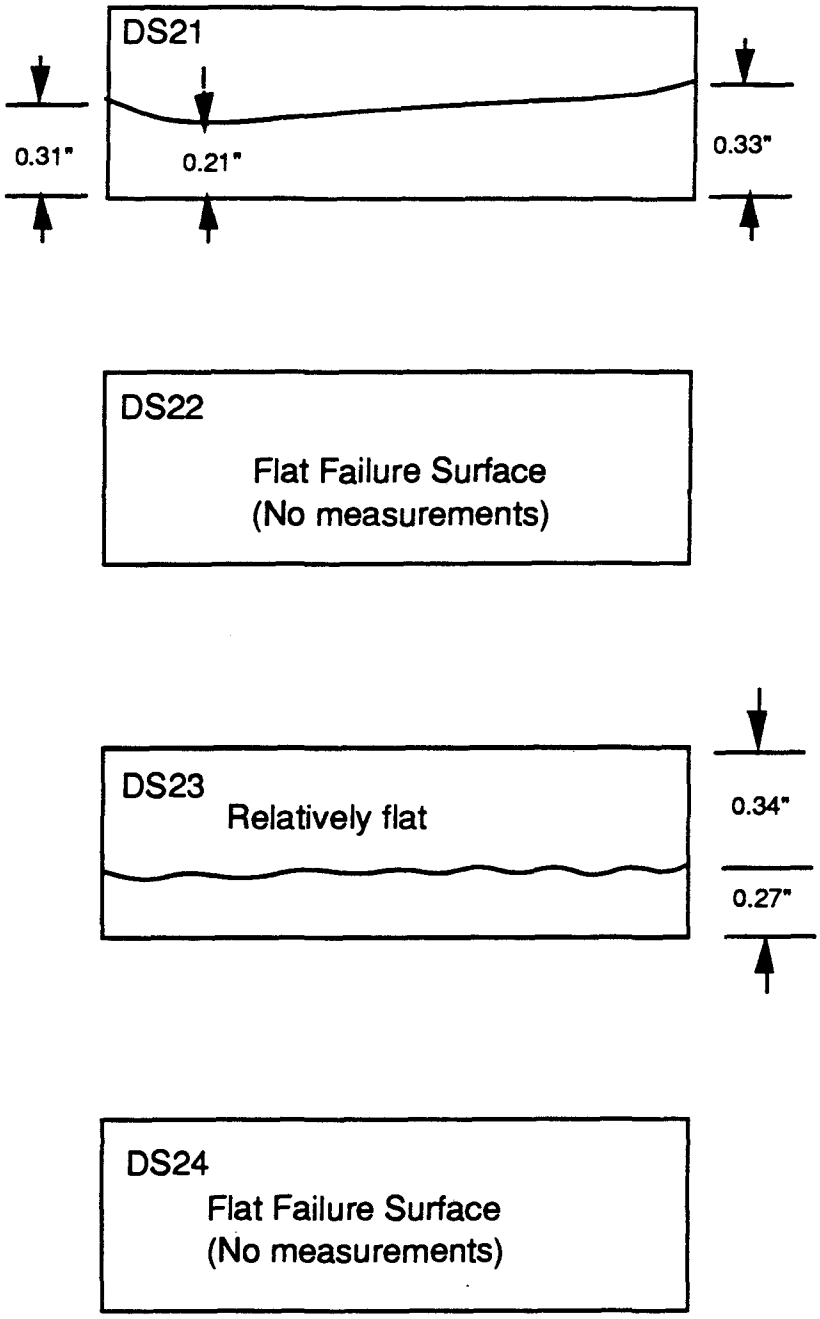

Fig. 5.3 Failure Surfaces in Direct Shear Tests on Eagleford Shale for PIF

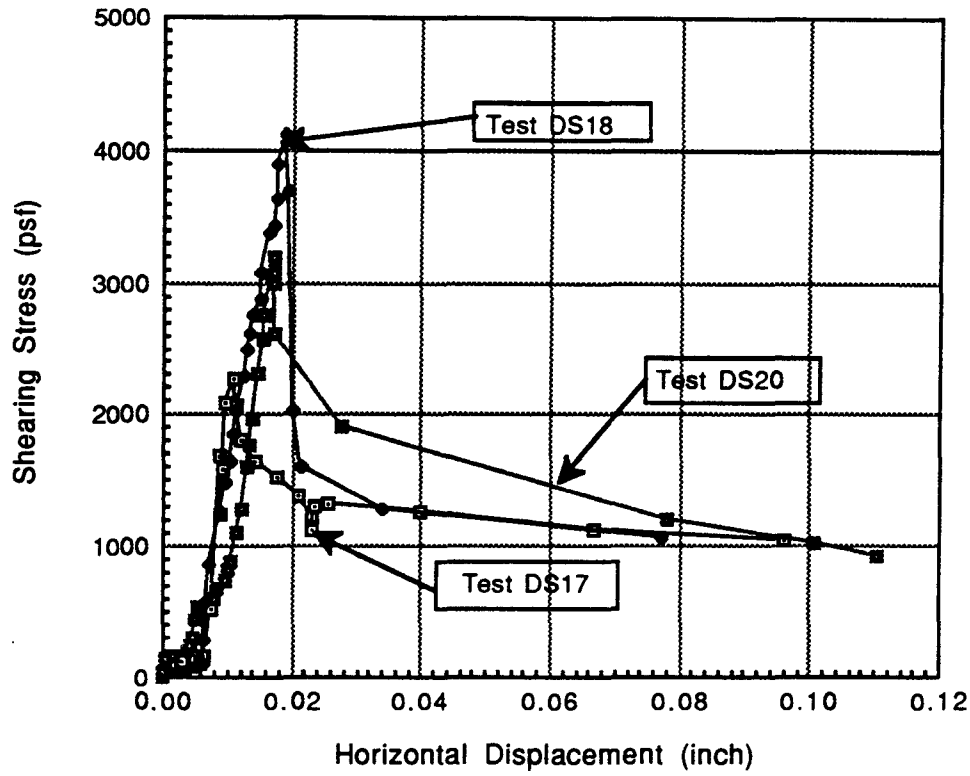

Fig. 5.4 Stress-Deformation Curves for Direct Shear Tests at 1460 psf on Eagleford Shale

The displacements shown in Table 5.3 for DS17 and DS18 were corrected by 0.0050" and 0.0063", respectively, to account for displacements that occurred before firm initial contact between the loading head and shear box were established, but the curves in Fig. 5.4 were not corrected. The corrections had negligible effects on the calculated stresses at both peak or "residual" conditions.

Data from three tests (DS9, DS10, and DS12) from Phase 1 on Eagleford shale, at 10 psi, will be used to broaden the data base. The resulting six tests had liquid limits ranging from 63% to 90%, plastic limits from 24% to 34%, and water contents ranging from 14%-18%. The ranges in the index tests are similar to those seen in one-dimensional consolidation.

Taken collectively, the six tests reached peak shear stress at horizontal displacements ranging from 0.006 inch to 0.017 inch and vertical displacements (expansion) ranging from 0.001 inch to 0.004 inch. The peak shear stress at failure ranged from 730 psf to 4560

psf, while the "residual" shear stress ranged from 670 psf to 1210 psf.

Test DS9 (data in the Phase 1 Report) yielded the lowest peak shearing strength (Table 5.3, Fig. 5.5) and was the only test at 10 psi that produced a flat, relatively smooth failure plane. Further, there was a relatively small reduction in shearing stress from the peak to the residual condition. It seems probable that a weak fissile surface was accidently in alignment with the shear plane of the box.

The times to failure ranged from 2,340 minutes to 9,230 minutes (Fig. 5.5). Contrary to the expected behavior for an overconsolidated material, the strength increased with increasing time to failure.

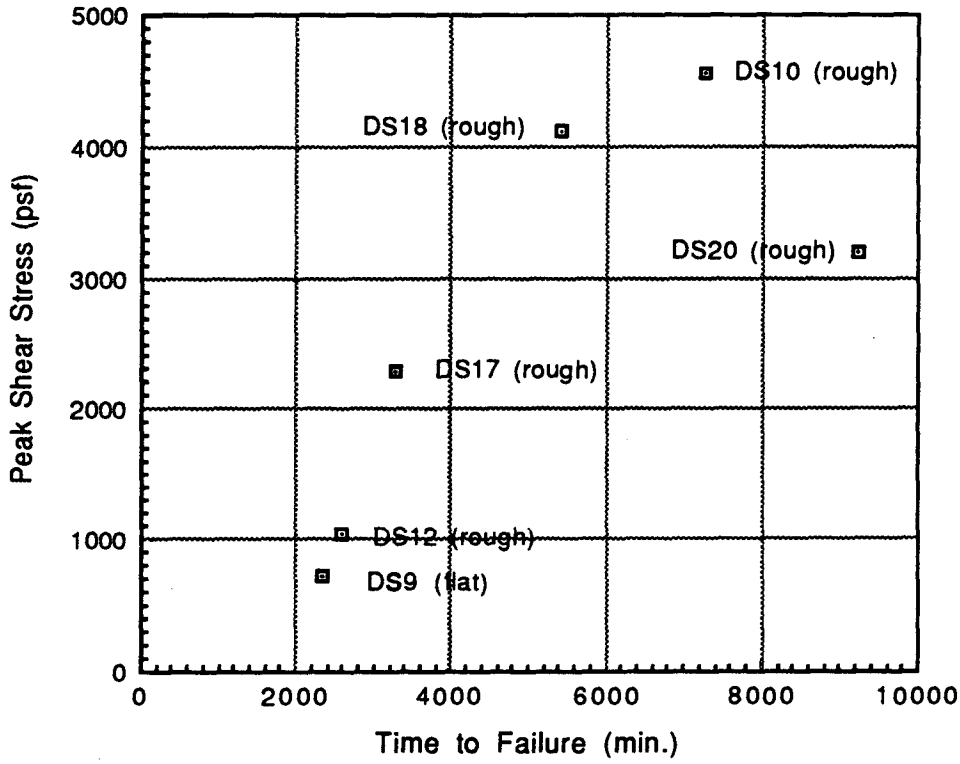

Fig. 5.5 Influence of Shearing Time on Peak Shear Strength at a Normal Stress of 1460 psf on Eagleford Shale

Consolidation Pressure at 50 psi

The stress-displacement curves for the two tests (DS19 and DS21) performed during the PIF phase, with normal stresses of 50 psi, are shown in Fig. 5.6. The displacements for DS21, in Table 5.3, were

corrected by 0.0055" to account for displacements that occurred before firm initial contact between the loading head and shear box was established, but the curves in Fig. 5.6 are uncorrected. The correction had negligible effect on the calculated stresses at both peak or "residual" conditions.

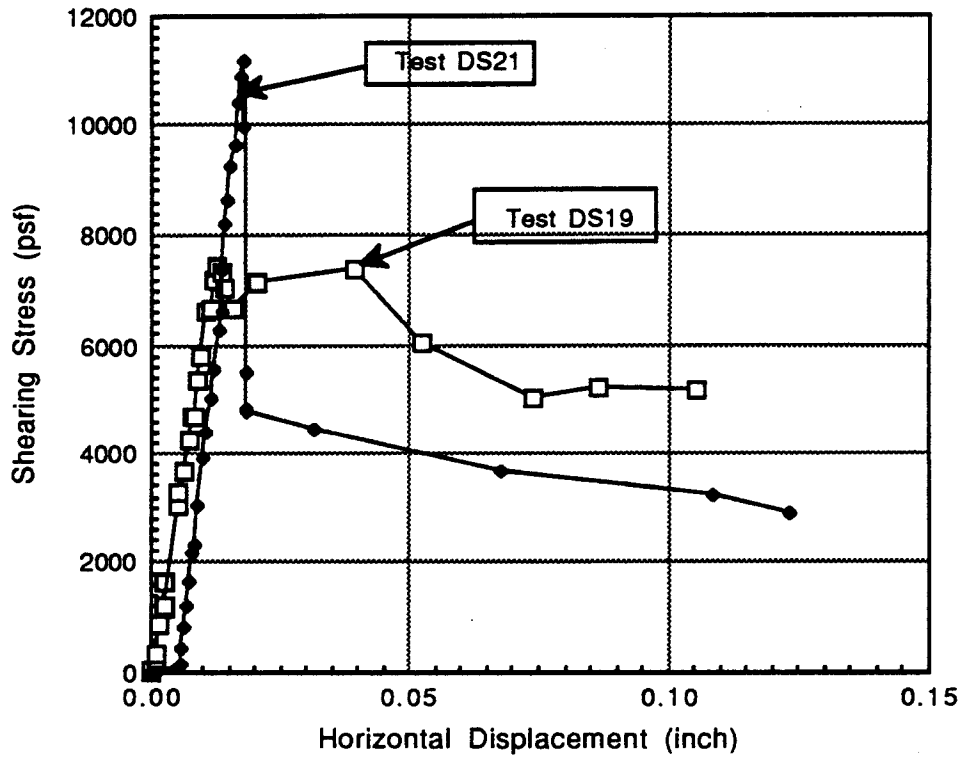

Fig. 5.6 Stress-Deformation Curves for Direct Shear Tests at 7400 psf on Eagleford Shale

Data from the one test (DS13) from Phase 1 on Eagleford shale, at 50 psi, will be used to broaden the data base.

The four tests had liquid limits ranging from 63% to 87%, plastic limits from 29% to 36%, and water contents from 15% to 17%. The ranges in the index tests are similar to those seen in one-dimensional consolidation.

Taken collectively, the four tests reached peak shear stress at horizontal displacements ranging from 0.008 inch to 0.012 inch and vertical displacements (expansion) ranging from 0.001 inch to 0.002

inch. The peak shear stress at failure ranged from 4,810 psf to 11,200 psf, while the "residual" shear stress ranged from 2,910 psf to 5,160 psf.

Test DS13 had the lowest peak shearing strength (Table 5.3) and failed on a rough surface. Tests DS19 and DS21 (Figs. 5.2 and 5.3) failed with smooth failure surfaces, but only DS19 had an angled failure surface. The large and sudden loss in strength for Test DS21 indicates that it was cemented.

The times to failure ranged from 2,160 minutes to 2,870 minutes (Fig. 5.7). The tests do not show any relationship between time to failure and strength. However, the analysis (Table 5.2) indicated that all three samples were fully drained. The large strength of the sample used for test DS21 is apparently the result of it being well cemented (Fig. 5.6). Sample DS19 may have been moderately string because of plane of weakness did not line up with the required failure plane in the shear box. Sample DS13 underwent only a small loss in strength after failure (Fig. 5.09 in Phase 1 Final Report) and was thus apparently less cemented than, for example, the sample for DS21.

Consolidation Pressure at 100 psi

The stress-displacement curves for the three tests (DS22-DS24) performed on the PIF phase are shown in Fig. 5.8. The displacements shown in Table 5.3, for tests DS22-DS24, had to be corrected by 0.0064", 0.0033", and 0.0014", respectively, to account for displacements that occurred before firm initial contact between the loading head and shear box were established. The curves in Fig. 5.8 were not corrected. The correction had negligible effect on the calculated stresses at both peak and "residual" conditions.

Data from the one test (DS11) from Phase 1 on Eagleford shale at 100 psi will be used to broaden the data base. For the four tests, the range in properties was liquid limit 64%-89%, plastic limits 24% - 36%, and water contents 17% - 20%. The ranges in the index tests are similar to those seen in one-dimensional consolidation.

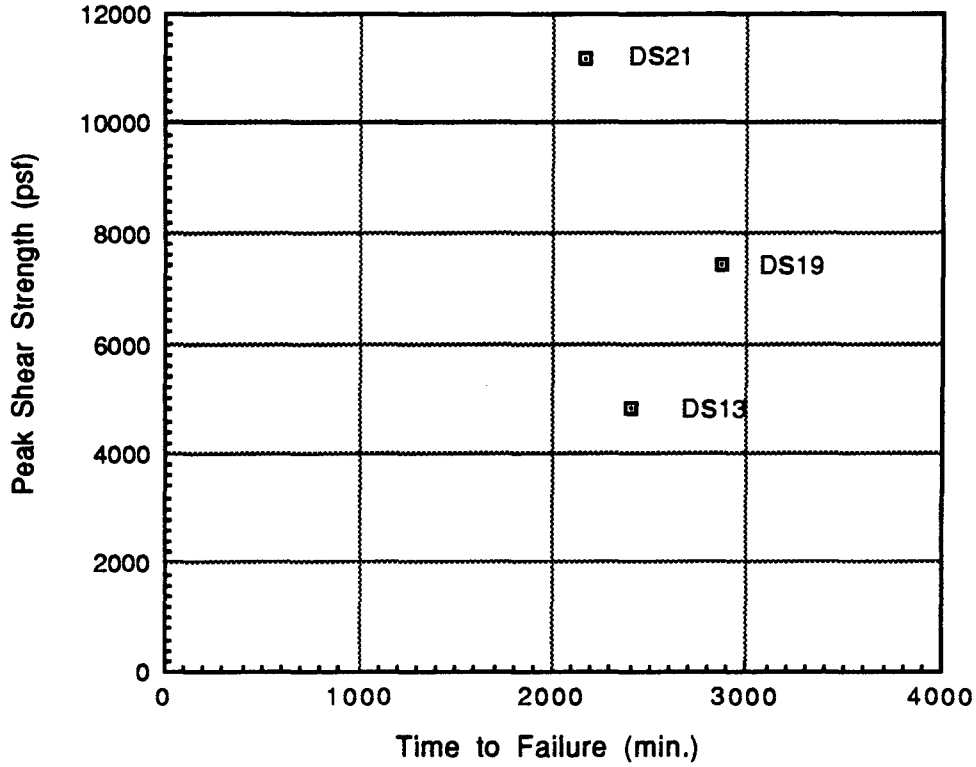

Fig. 5.7 Influence of Shearing Time on Peak Shear Strength at a Normal Stress of 7300 psf on Eagleford Shale

Taken collectively, the four tests reached peak shear stress at horizontal displacements ranging from 0.0133" to 0.0241" and vertical displacements (expansion) ranging from 0.0" to 0.0010". The peak shear stress at failure ranged from 9,420 psf to 13,200 psf, while the "residual" shear stress ranged from 4,470 psf to 6,970 psf. Test DS11 had (Table 5.3) the lowest peak shearing strength, and failed on a rough surface. Tests DS22-DS24 (Table 5.3) failed with smooth failure surfaces. Tests DS22-DS24 exhibited a larger reduction in post peak shear strength, possibly indicating that they were more cemented.

The times to failure ranged from 1,900 minutes to 3,280 minutes (Fig. 5.9). The data seem to suggest that the shearing strength increases with increasing time to failure. However, when samples expand during shear, the shearing strength should decrease with

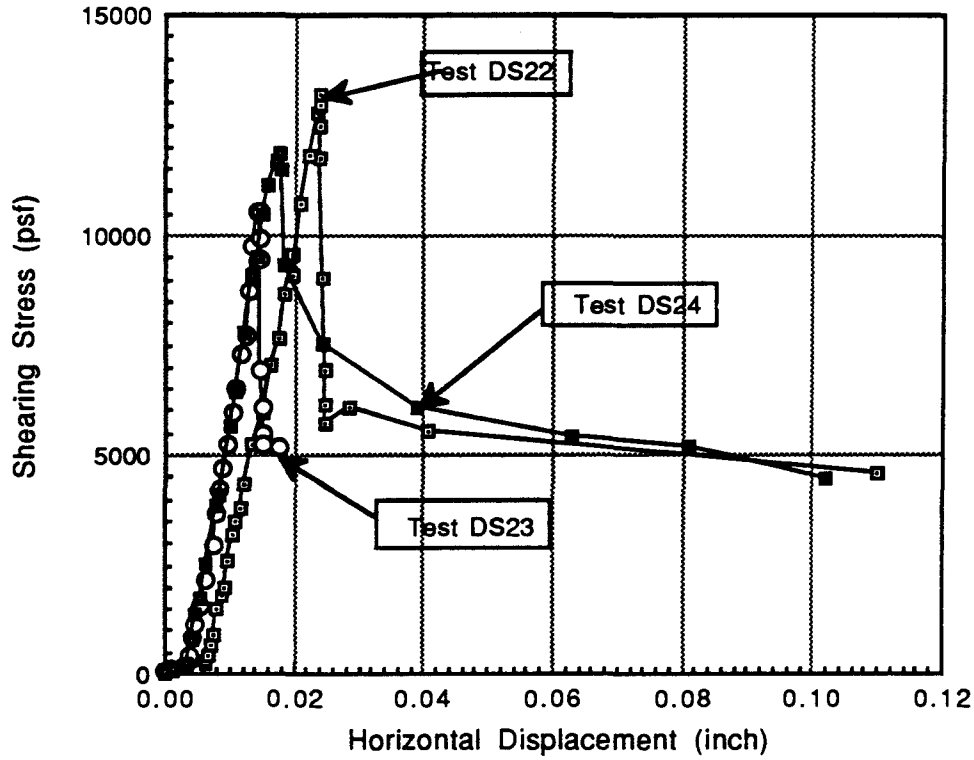

Fig. 5.8 Stress-Deformation Curves for Direct Shear Tests at 14,600 psf on Eagleford Shale

increasing time to failure. The relationship indicated in Fig. 5.9 may just represent scatter associated with varying amounts of cement.

CUMULATIVE SHEAR RESULTS

Displacements at Failure

For samples that failed on relatively smooth, flat failure surfaces (DS9, DS21, DS22, DS23, and DS24), the deformation at failure seems to increase slightly with respect to consolidation pressure. The number of tests is too small to allow a decision to be made as to whether this observation is real or just the result of a small data set and usual scatter. Perhaps the more interesting observation is

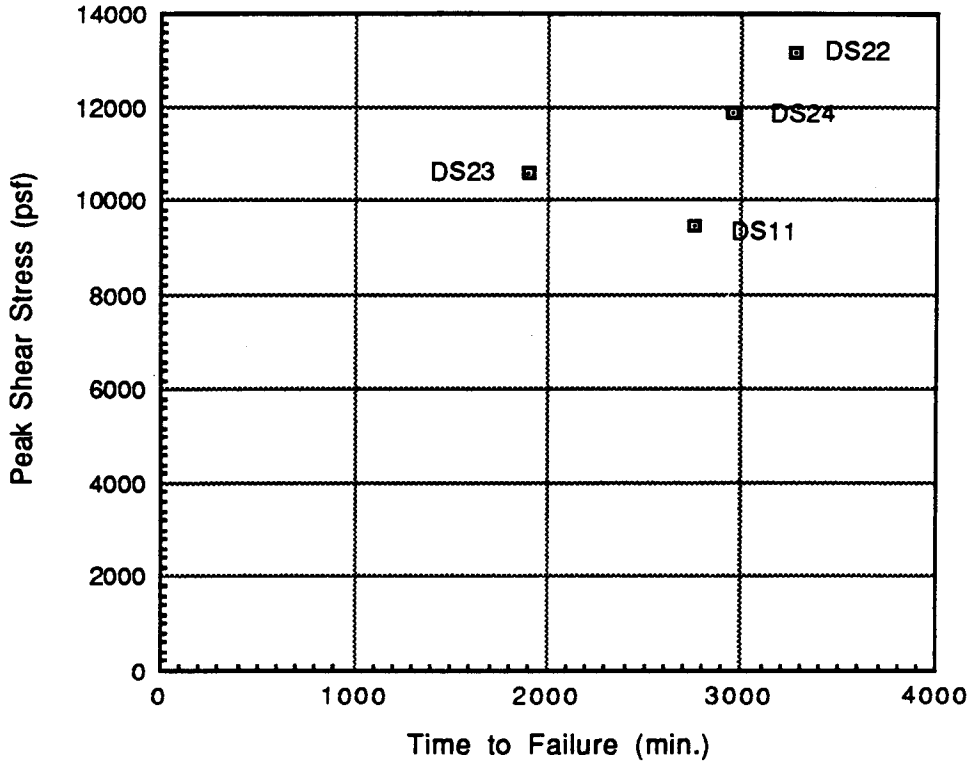

Fig. 5.9 Influence of Shearing Time on Peak Shear Strength at a Normal Stress of 14,600 psf on Eagleford Shale

that the displacements at failure are quite small, of the order of 0.01 inch.

Peak Failure Envelopes

The peak Coulomb envelope (Fig. 5.11) exhibits large amounts of scatter at all effective consolidation pressures when all data is included, probably because of highly variable amounts of cementation. Upper and lower bound failure envelopes, drawn by eye, both have $\bar{\phi}$= 33 degrees. The apparent effective cohesion would be 3200 psf and 130 psf for the upper and lower envelopes.

If only data for tests with relatively smooth, flat, failure surfaces are utilized (Fig. 5.12) the number of data points is too small to provide definitive conclusions. We have reasonable evidence to suggest that DS9 does not represent the peak strength on a horizontal plane at 10 psi. Thus, the "real" peak strength envelope

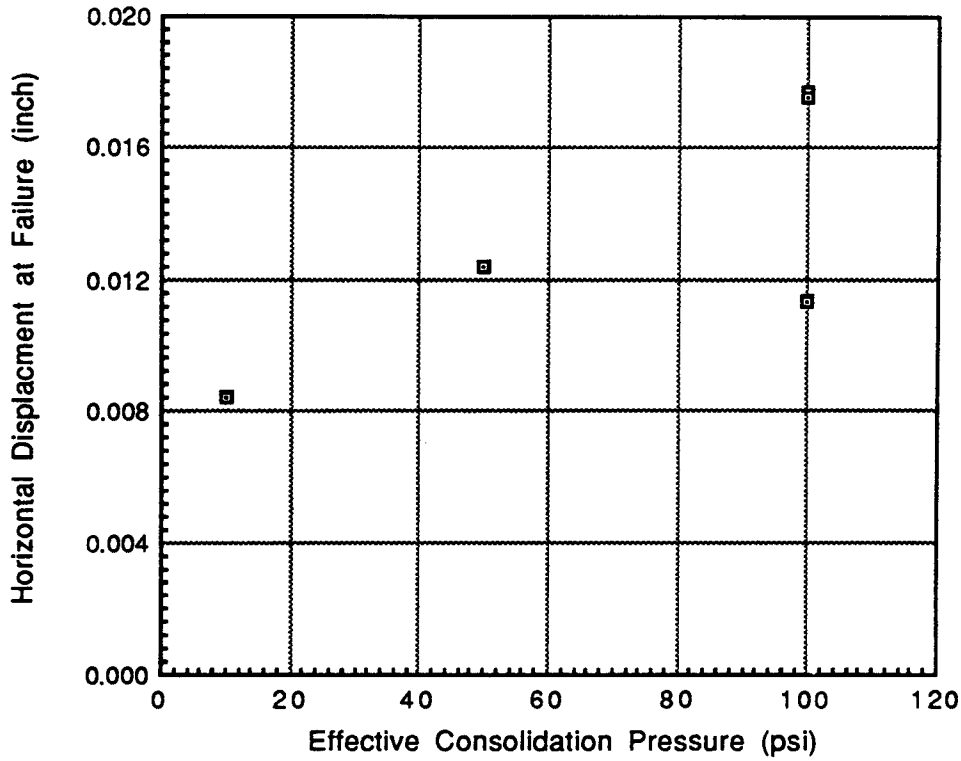

Fig. 5.10 Displacment at Failure vs. Effective Consolidation Pressure for Direct Shear Tests Failing on Smooth, Flat Surfaces

probably curves through the points for DS21-DS24 to some strength above the value measured in DS9. An effective cohesion might be

expected if the cement bonds insitu do not break from unloading, or from mechanical changes that may occur from cyclic wetting and drying. The effects of cyclic wetting and drying was not investigated in this study.

Residual Envelopes

The residual Coulomb envelope (Fig. 5.13) exhibits less scatter than the peak envelope when all data are included. The effective friction angles for upper bound and lower bound failure envelopes are 23 degrees and 15 degrees, respectively. The apparent effective cohesion would be 580 psf and 280 psf for the upper and lower envelopes, respectively. The residual friction angles seem within

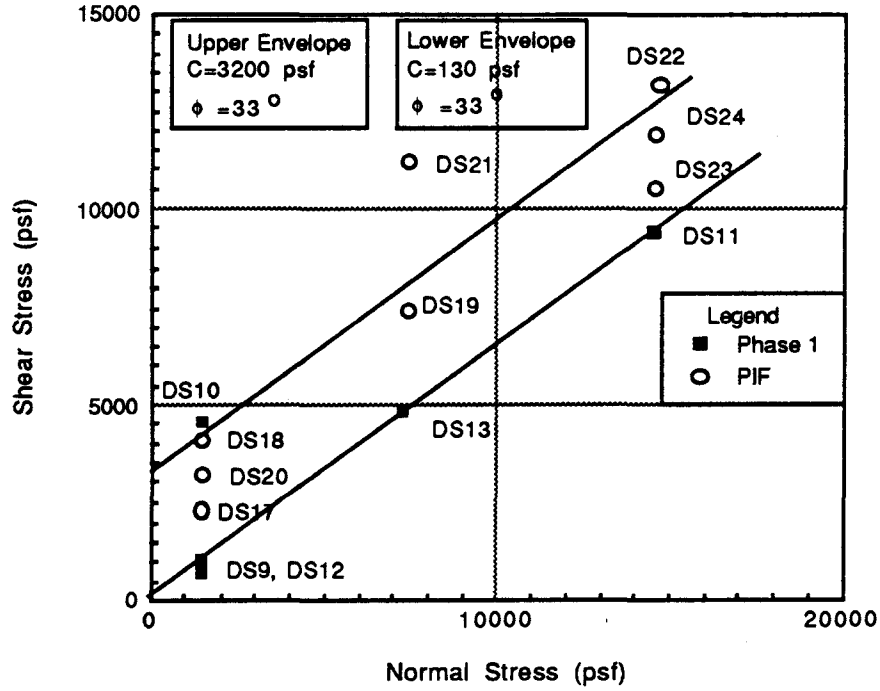

Fig. 5.11 Peak Failure Envelopes for Direct Shear Tests on Eagleford Shale Tested in Phase 1 and PIF (All Data)

the expected range for this plastic material, while the effective cohesion values appear to be high for a residual condition.

If the residual envelope (Fig. 514) were defined with only the results from tests that failed on flat, smooth failure planes the scatter reduces further. If an upper bound and lower bound envelope is drawn the effective friction angles would be approximately 19 degrees and 15 degrees, respectively. The apparent effective cohesion would be 140 psf and 280 psf for the upper and lower envelopes. The residual friction angles seem within the expected range for this plastic material, as do the effective cohesion values.

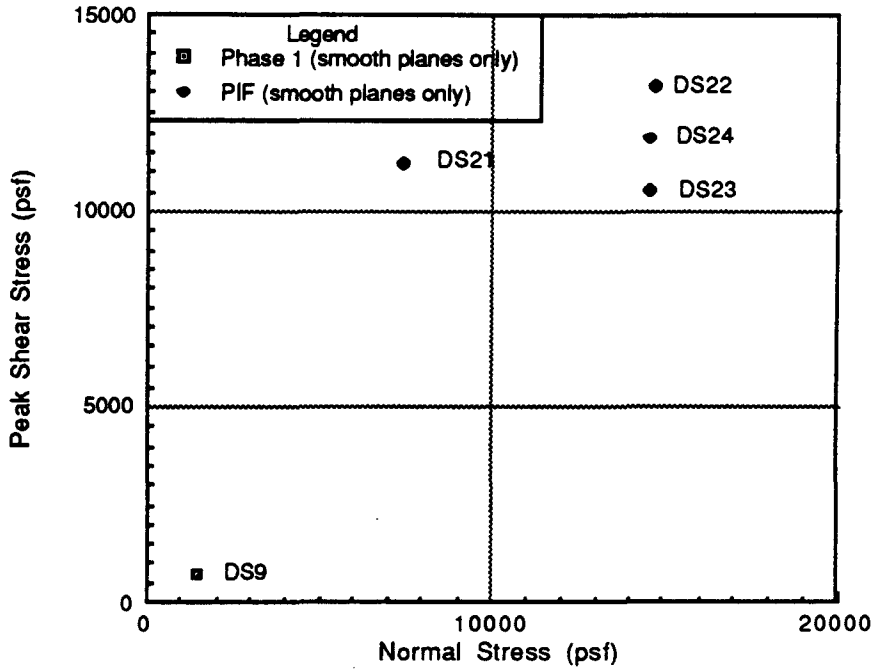

Fig. 5.12 Peak Failure Envelopes for Direct Shear Tests on Eagleford Shale Tested in Phase 1 and PIF (only smooth failure planes)

OPINIONS, CONCLUSIONS, AND RECOMMENDATIONS

The following opinions and conclusions can be made from the study of Eagleford shale

1. These materials are cemented. The amount of cement may vary stratigraphically or may vary locally, with less cement on fissile surfaces.

2. Samples that have smooth failure surfaces probably failed on pre-existing planes of weakness.

3. Samples with highly irregular failure surfaces probably failed, at least in part, through intact material. The failure planes may shift up and down to include fissile surfaces above and below the forced failure plane. These samples seem to lose less strength than those undisturbed samples that fail on flat,

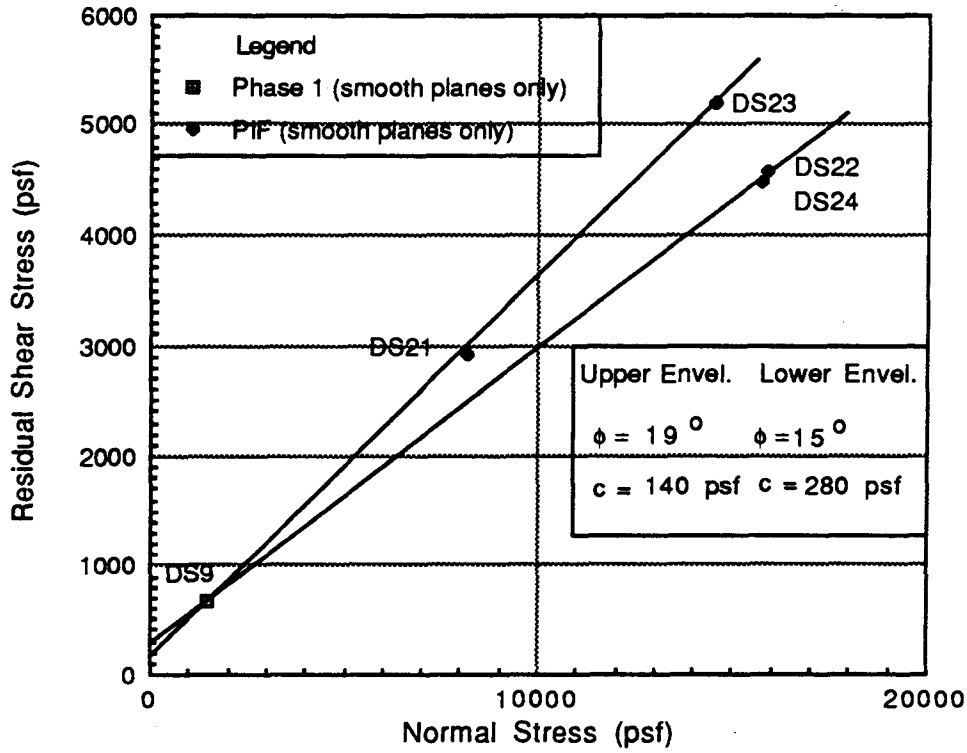

Fig. 5.14 Residual Failure Envelope for Direct Shear Tests on Eagleford Shale Tested in Phase 1 and PIF (smooth failure planes only)

smooth planes, perhaps because of the interlocking on the rough failure surface.

4. These tests suggest that times to failure of about two days will suffice for dissipation of shear-induced excess pore water pressures.

5. The standard direct shear device tends to apply shearing force through opposing edges instead of on the flat faces, for materials as brittle as the Eagleford shale. The result may be progressive failure.

6. Larger sized samples might allow for inclusion of a more statistically significant distribution of fissile surfaces and fissures.

7. Conclusions on the recommended peak and residual envelopes will be delayed until these data are combined with triaxial compression data.

SECTION 6

"DRAINED" TRIAXIAL COMPRESSION TESTING

INTRODUCTION

The main purposes in performing the drained triaxial compression testing program were to determine the effective failure envelope (shearing properties) for Eagleford shale, and the factors that may influence the scatter of the envelope. In addition, evidence of the influence of the testing rates on the shear strength properties was investigated. Factors that influence the measured and predicted consolidation properties, such as coefficient of consolidation and compressibility during shear and isotropic consolidation, were also subsidiary issues that were investigated as the program developed.

Tests Performed

Fourteen "drained" triaxial compression tests (CD11-CD24, Table 6.1) from eight borings were performed on samples of Eagleford shale in the PIF phase. Three sets of tests were performed at effective isotropic consolidation pressures of 10, 50, and 100 psi for samples in three of the cores (9 of the 14 tests). One specimen from each of the remaining five borings was tested (2 at 10 psi, 1 at 50 psi, and 2 at 100 psi).

In addition, triaxial compression tests from Phase 1 (3 at 10 psi, 2 at 100 psi) on Eagleford shale were used to supplement the PIF phase data. The Phase 1 tests were chosen because they were considered to have high degrees of consolidation at failure, either theoretically or due to information obtained subsequent to Phase 1 program. The liquid limits varied from 67% to 83% for the Phase 1 and 66% to 87% for the PIF-phase Eagleford specimens, suggesting

Test ID	Sample No.	Boring	Depth (ft.)	Initial w_c (%)	LL (%)	PL (%)	Project
CD2	14	BIR43	189.2	16.2	80	32	Phase1
CD3	14	BIR43	189.5	16.9	83	26	Phase1
CD5	11	BIR44	227.7	16.7	80	31	Phase1
CD8	11	BIR44	228.9	16.1	77	31	Phase1
CD10	15	BIR43	252	15.8	67	30	Phase1
CD11	58	BC1	219.2	17.2	76	32	PIF
CD12	47	B1657	171.9	17.4	86	30	PIF
CD13	63	BF1A	168.7	17.3	83	30	PIF
CD14	44	B1637	216.7	16.6	72	29	PIF
CD15	56	B1697	122.5	17.8	80	31	PIF
CD16	58	BC1	220.1	15.9	67	29	PIF
CD17	58	BC1	220.5	15.2	66	29	PIF
CD18	44	B1637	216.5	16.7	77	29	PIF
CD19	44	B1637	216.2	17.0	77	30	PIF
CD20	63	BF1A	168.9	16.9	84	32	PIF
CD21	63	BF1A	169.2	17.1	80	29	PIF
CD22	52	B1619	184.1	14.9	68	26	PIF
CD23	37	B1617	213.3	16.2	81	27	PIF
CD24	39	B1597	235.1	15.8	87	31	PIF

Table 6.1 Summary of Sample Data for all PIF Phase and Phase 1 Triaxial Tests with Failure Times Exceeding 1000 minutes or With Degrees of Consolidation at Failure above 50% on Eagleford Shale

similar materials. The initial water contents were 15%-19% and 16%-20% for the for the Phase 1 and PIF phase material, respectively.

Reasons for Using the Triaxial Device

The triaxial device is often preferred over the direct shear because the triaxial apparatus:

1. allows for independent control of two principal stresses.

2. allows measurement of principal strains for isotropic soils.

3. allows control of drainage.

4. allows measurement of pore water pressures.

5. allows samples to fail on planes of weakness provided that those planes are not too close to either the horizontal or the vertical.

However, the triaxial device has problems that increase the cost of the tests and thus lead to a more limited usage than is desirable. For example, in tests to be performed under "drained" conditions, the testing times for samples of a reasonable size, and for cohesive materials, may be quite long.

There are, of course, problems in both devices involving the apparatus itself, and states of stress in the samples. In the case of the triaxial apparatus, these problems include piston friction, membrane leakage, membrane and filter paper drain restraint, end restraint, problems in estimating the proper area of the specimen after a significant axial strain, and tilting of samples which have rotated planes of weakness. Further, while the triaxial device allows for control of two of the principal stresses, it doesn't allow control of all three, nor does it allow for gradual rotation of principal stresses.

In spite of its problems, the triaxial device has been in substantial use in geotechnical engineering since the mid 1940's. Part of the reason for its wide usage is that devices that allow for application of more general states of stress are even more difficult and expensive to use, and have found negligible application.

SOURCE DATA

Triaxial compression shear data were presented in the Task 2 report (PIF phase) and, because of the bulk involved will not be repeated. The data provided for each test in the Task 2 report included :

1. a spreadsheet containing sample identification information (boring number, sample depth, formation name, sample description), data collected at set-up time (sample height and weight, water content, degree of saturation), cell number,

initials of person trimming the sample and date trimmed, initials of person checking the data and the date.

2. a spreadsheet that contains the sample identification information (boring, depth, sample number, formation, test ID), initials and date for person setting up the test and person checking the data sheet, triaxial cell ID, index properties, sample dimensions and weight, deformation rate for the test, constants for the various sensors, and the stress-strain data (date and time of each reading, raw data, axial strain (ε), volumetric strain (υ), stress difference (σ_1-σ_3), Young's modulus (E), Poisson's ratio (μ).

3. spreadsheets containing the dates, times, and pipet readings for the consolidation stages.

4. sketch of the specimen failure plane(s) after breakdown of the test.

5. stress-strain plot for the shearing stage.

6. time-volume change plots for the consolidation phase shown with natural, square root, and log time.

EXPERIMENTAL PROCEDURES

Introduction

The experimental procedures used for the triaxial tests were discussed in detail in the Task 1 report of the PIF phase. The procedures will be summarized here as an aid to the reader of this report.

Trimming

The cores were slightly less than 2 inches in diameter. The outer zone of most of the cores was irregular. Originally the smaller

specimen diameter was chosen because the exterior surfaces of the cores might be softened, presumably by contact with drilling fluid. To form a smooth outside surface and remove disturbed or softened material, the cores were trimmed down to 1.50 inches in diameter for triaxial shear testing.

We planned to use sample lengths of 3.00 inches but the weak horizontal planes caused considerable difficulty in trimming the end surfaces. When parts of the ends flaked off, we trimmed further to obtain smooth uniform end surfaces. As a result, the sample lengths varied between about 2.487 and 3.000 inches.

The trimming process was designed to minimize evaporation by encasing the trimmed material in a plastic membrane and keeping the remaining core encased in wax, except a short distance that was in the process of being trimmed.

Cells

Triaxial cells were of the usual design, with the piston passing through two ball bushings and with a floating O-ring seal.

The first tests in Phase 1 were set up using slotted filter paper (Fig. 6.1) drains and dual prophylactic membranes. In spite of years of previous success with this procedure, we had a high failure rate of the membranes, often after the sample had been under confining pressure for a number of hours and, in one case when the sample was in the shearing stage. We switched to more heavy-duty triaxial membranes (Wykeham-Farrance) and used them for the final two tests of Phase 1 and all tests of the PIF phase, with no failures.

The only other serious problem with the equipment involved failure of the floating bushing on some of the tests. Under low cell pressures, if the tiny O-ring around the piston freezes against the floating bushing, the cell fluid escapes around the bushing and it becomes necessary to tear down the cell, apply grease to the piston, and perhaps replace the O-ring. In two tests (CD16 and CD22) the bushing continued to leak during shear so the test was continued with the bushing leaking slowly. In tests CD16 and CD22 the volumetric strains during shear were estimated from the results of

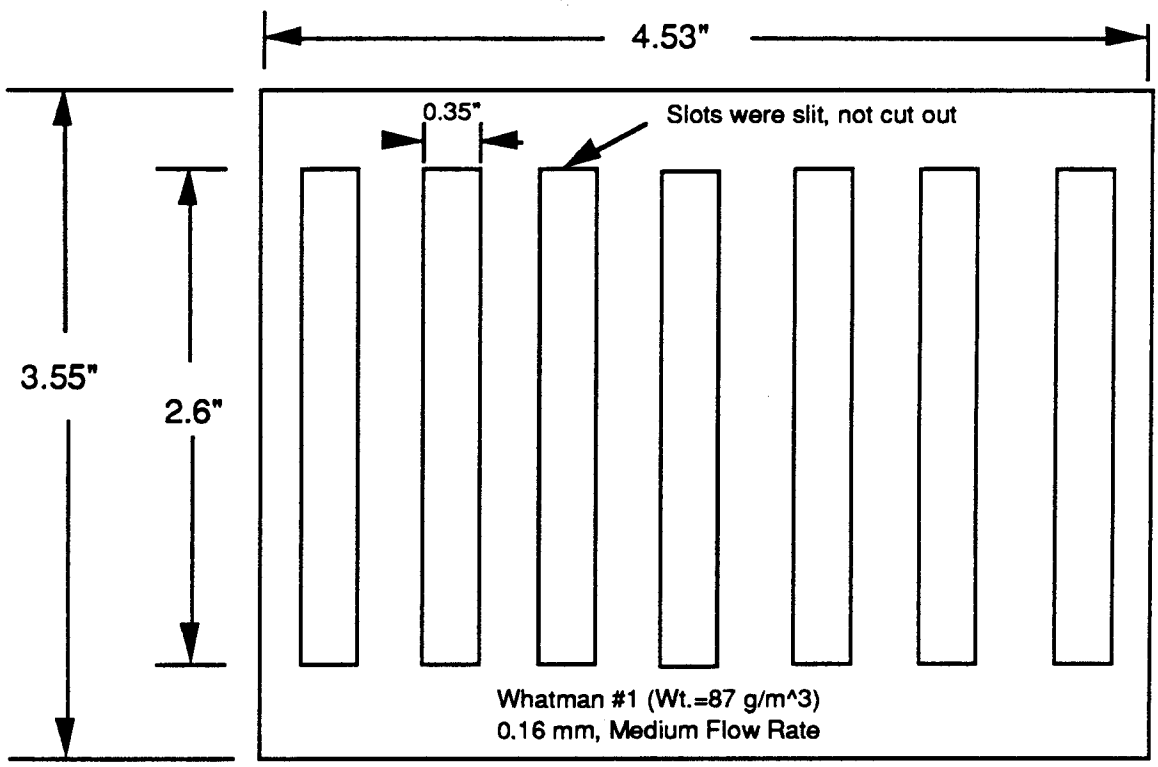

Fig. 6.1 Filter Paper Configuration used to Drain Triaxial Compression Samples

other tests. The resulting uncertainties in volumetric strain will have negligible influence on the calculated failure stress.

Consolidation Stage

The triaxial cell drainage lines, with the pipet/pore pressure transducer arrangement (Fig. 6.2) connected, were saturated prior to sample placement. A saturated porous stone was used on the base. Samples were placed in the triaxial cell with a filter paper drain with slit (Fig. 6.1) sections, filter paper disks on the ends, and a commercial membrane. The membrane was sealed with two O-rings to both the base and top cap. The cell was assembled, and filled with water as quickly as possible to minimize swelling of the sample.

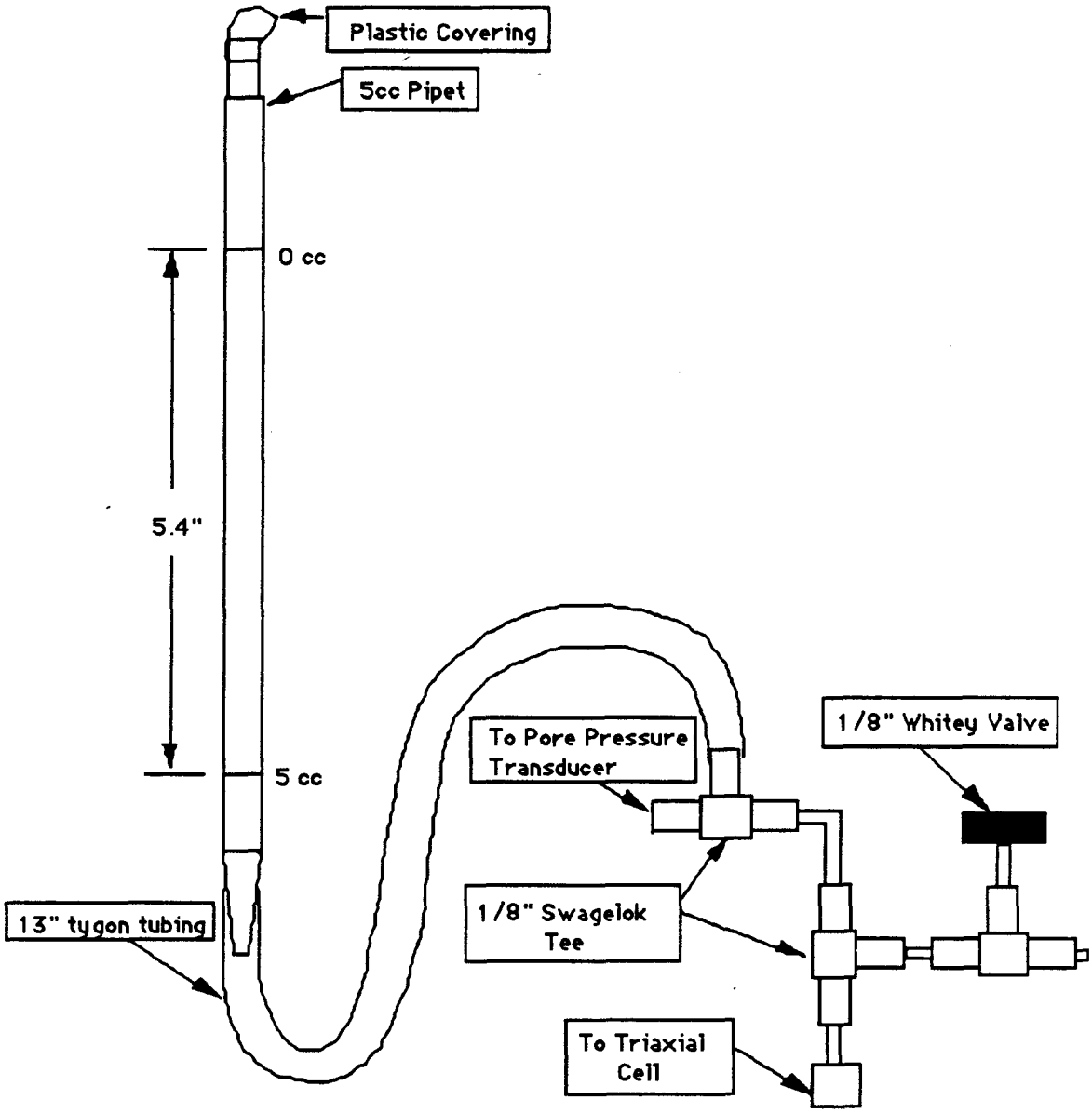

Fig. 6.2 Pipet Arrangement used to Measure Volume Change in Drained Triaxial Compression Tests

A 140-psi cell pressure was applied initially to minimize the swelling of the specimen during the deairing process. Inevitably, air is trapped between the specimen, filter paper, porous stone, and the membrane during test set-up. When the 140 psi cell pressure was applied, some of the air was forced into the porous stone and drainage line. A tygon tubing line, that was previously attached to

the second drainage line, with one end in a 1000 ml flask filled with deaired water, served as a supply of deaired water. The reservoir drainage line and pipet drainage lines were opened simultaneously with the reservoir situated at a larger elevation. The water was allowed to flow through the base, and out the pipet until no more visible air bubbles exited the drainage line. In some cases this procedure took 15 minutes. During this period the pipet could not be used to record the swelling that would occur. The consolidation data at 140 psi suggest that minimal volume changes would have occurred during the deairing period.

Samples were consolidated under an all-around hydrostatic pressure approximately equal to 140 psi, and volume change was measured by recording the amount of water entering or leaving the samples, using glass pipets (Fig. 6.2). Samples typically underwent measurable volume changes for prolonged periods of time. The plots of volume change (ΔV) versus time (t) typically showed little, or no, evidence of the end of consolidation even for times up to a month. In an effort to obtain a reasonable amount of data in the time available, most tests were performed with samples that were still undergoing apparent primary consolidation on ΔV-log(t) plots but where the rate of volume change was very small, e.g., less than 0.03 ml/day.

In a few cases, we had consolidation followed by expansion, under constant confining pressure. The initial consolidation may have been from material on the outside of the specimen that was wetted during the setup and deairing phase, with subsequent expansion from an inner core of unsoftened material. The outer zone may have softened from moisture in the filter drain and trapped under the membrane during test set-up. The apparent expansion may also have resulted from diffusion of gas from the sample through the membrane into deaired water of the cell. The diffusion process usually (not measured on this project) stops within about a week.

Once equilibrium was established at 140 psi, the cell pressure was reduced to the final consolidation pressure in one step. The final pressure was maintained until the apparent swelling was very small. The coefficient of consolidation was calculated from the experimental time-volume change data to estimate the times to failure.

The time to failure should be calculated on the basis of reasonable estimates of the failure strain corrected for machine deformations due to filter paper, base, loading piston, and frame base compressions. The lower bound of the strains at failure measured for all tests would presumably provide a conservative estimate of the strain rate for triaxial compression.

Shearing Stage

The axial deformations were applied using a motor driven loading press. Axial deformations were measured using a DCDT (displacement transducer). Axial forces were measured outside the cell using an electronic load cell. Volume change was recorded using a pipet provided with a pressure transducer at its base, where the head of water in the pipet was calibrated against volume change.

Data were collected by a data acquisition system utilizing an IBM model XT microcomputer. The system allowed for playback of data during a test and for plotting of data on the monitor using engineering units so the data could be checked for reasonableness during the shearing stage. Electronic components were recalibrated several times during each test to ensure that no electrical drift had occurred. The sensors were found to be quite stable.

Comments on Experimental Concerns. The data presented in Phase 1 and the PIF phase (Task 2 report) were not corrected for machine deformations resulting from filter paper, porous stone, and load frame compression. The shear strength, the parameter of primary importance in this study, will be shown to be insensitive to these deformations for the specimen tested in the PIF phase. The subsidiary parameters such as axial strain, incremental stiffness (to a lesser degree the secant value), and Poisson's ratio (secant and incremental values) will be shown to be sensitive to the machine deformations for the sample sizes used in this test program. Increases in the specimen sizes would reduce the relative errors in the stress, strain, moduli values.

The incremental values of stiffness and Poisson's ratio will be shown to be sensitive to the measurement system's resolution (of load, displacement, and volume change). The measurement system's resolution is governed A/D (analog to digital) board resolution, the maximum voltage the A/D board will read, the maximum output

voltage of the sensor after amplifying of the signal, and the noise in the sensor output for a specific load (displacement, volume change), and the accuracy of the calibration standard. Secant values of material parameters are less sensitive to the system resolution because:

1. the parameter is being calculated from data that is always increasing (displacement, load, volume change), so any error becomes less significant as the test proceeds.

2. the "best" fit calibration curve for the sensor reduces the error to essentially one-half the total "noise" error. Since the initial reading has no potential opposite sign error (always beginning with zero load, displacement, and volume change), the potential error is one-half any potential incremental value.

Comments on Shear Strength. The goal was to measure shearing strength under fully drained conditions. The extent of drainage depends on time to failure, soil properties, drainage conditions, and sample dimensions.

The effects of partial drainage should not be confused with viscosity effects. The strain rate recommended for drained triaxial compression tests assume the only time dependent phenomena occurring (affecting the measured shear strength) is dissipation of excess pore water pressures. However, interpretation of data from tests performed at high, intermediate, and low strain rates seem to indicate that viscosity effects may exist for the Eagleford shale.

Post Shearing Measurements

At the end of the shearing stage, the apparatus was dismantled, and the entire sample was weighed. The failure mode was then carefully sketched. Samples often failed in ways that were apparently controlled by fissures and the fissile surfaces. When dominant shear planes formed, the orientation of the planes was measured.

DATA REDUCTION FOR CONSOLIDATION ASPECTS

Introduction

A consolidation theory by Gibson, based on Biot's theory, was used to obtain consolidation properties for the samples involved in this testing program. Secondary rate effects are not accounted for in these analyses.

For an isotropic sample, Bishop and Henkel (1958) recommended that the coefficient of consolidation be estimated by plotting volume change versus the square root of time. They extended the early more-or-less linear part of the curve to the volume change (termed V_{100}) at the last recorded time, terming that time t_{100}. Note that t_{100} is not the time corresponding to 100% primary consolidation; it is actually four times t_{50}. For all-around drainage, the coefficient of consolidation is then calculated using:

$$c = \frac{\pi\left(\frac{L}{2}\right)^2}{4(t_{100})}\left[\frac{1}{\left\{1+\frac{L}{R}\right\}^2}\right] \tag{6.1}$$

where L is the sample length (height), R is the sample radius, both defined during the consolidation stage, and t_{100} was defined previously.

The average degree of consolidation at failure (U_f) during the shearing stage can be calculated using Gibson's equation:

$$U_f = 1 - \frac{(L/2)^2}{\eta c t_f} \tag{6.2}$$

or:

$$t_f = \frac{(L/2)^2}{\eta c(1-U_f)} \tag{6.3}$$

where L is the length (height) of the sample during shear, η is 40 for all-around drainage, c is the coefficient of consolidation, and t_f is the time to failure, provided that the degree of consolidation is

high, say 80% or more. For lower degrees of consolidation, we used the T-U plot in Fig. 4 from Blight (1963).

The samples were subjected to isotropic stress states during consolidation.

Comments. Blight observed that the experimental data (on remolded and normally consolidated soils) indicated faster dissipation of the pore pressures than predicted by the theory. He suggested that the difference was due to the assumption of a rectangular distribution of excess pore pressure, when in fact the pore pressures are approximately parabolic with respect to depth.

Bishop and Henkel had observed no secondary effects during consolidation so the use of V_{100} seemed reasonable. However, their published data, and most of their experience, was with remolded soils which normally have negligible secondary effects even in one-dimensional consolidation. Their method is easy and quick to apply by hand, but it becomes ambiguous when applied to undisturbed materials that may have major secondary effects. Further, the user has no equally simple way of determining how well the theoretical and experimental ΔV-t curves compare.

We concluded, on the basis of the strain rate study in Phase 1, that regardless of the predicted times to failure, reasonable estimates of the "drained" shear strength would be obtained for triaxial compression for shear times on the order of 1-2 days for samples consolidated at 10 psi and 2-3 days for samples consolidated at 100 psi.

For the tests (this phase) with no problems (no end failure, reasonable testing times, and failure angles that seem logical) the axial strains at peak stress difference were about 2%. If a minimum height of 2.5 inches is used, the minimum failure deformation would be expected to be 0.045 inches. As a result, the strain rate of loading should proceed at a rate of 0.0006 inch/hr. The slowest setting for the loading presses that we had was 0.0017 inch/hr., which is approximately three times faster than the desired rate for tests at 100 psi. For most of the tests at 10 psi, we set the press at the slowest rate, and let the specimens shear until peak stress difference was reached. For tests at 50 psi and 100 psi, we generally sheared the sample for several hours, and then turned the press off at convenient times to allow for dissipation of excess pore

water pressures. In mosts cases, the dissipation of excess pore pressures were accompanied by volume change ranging from 0.01 cc to 0.04 cc during the shut off period. The small volume changes may indicated a high degree of consolidation during the shearing.

It should be noted that these recommendations are for triaxial compression tests only. The recommended strain rate for tests with different stress paths would require further experimental and numerical study.

DATA REDUCTION FOR SHEARING STAGE

Sample Area

During the shearing stage, the horizontal area of the sample (A_ε) at any axial strain (ε) was calculated assuming the sample deformed as a right circular cylinder:

$$A_\varepsilon = A_o \frac{1+v}{1-\varepsilon} \tag{6.4}$$

where A_o is the area at the beginning of shear, v is the volumetric strain (positive for expansion), and ε is the axial strain (positive for compression).

The area at the beginning of shear was calculated by dividing the volume of the specimen by its length. The volume was determined as the initial volume of the sample corrected for measured volume changes during consolidation. The initial volume was determined from measurements of the height and diameter. The sample length at the beginning of shear was measured using a cathetometer.

Secant Young's Modulus and Poisson's Ratio

Shearing data were reduced using a spreadsheet (see Task 2 report). For each set of readings, the secant value of Young's modulus was calculated as:

$$E = \frac{\sigma_1 - \sigma_3}{\varepsilon} \tag{6.5}$$

where $\sigma_1 - \sigma_3$ is the stress difference and ε is axial strain. A value of Poisson's ratio (μ) was also defined using:

$$\mu = -\frac{\varepsilon_{lateral}}{\varepsilon_{vertical}} = \frac{1}{2}\left(\frac{v}{\varepsilon} + 1\right) \tag{6.6}$$

We used μ for Poisson's ratio to avoid confusion with the standard use of v to represent volumetric strains. As defined in this report, volumetric strains are positive for swelling (expansion), while axial strains are positive for compression (shortening). The secant value of Poisson's ratio includes plastic axial and volumetric strains even for stress differences below the peak stress difference.

Mohr-Coulomb Failure Envelopes

Historically, failure envelopes were defined using Mohr's circles. However, the circles are awkward to plot and cause severe difficulties when there are many tests or when data from several types of tests are to be plotted in the same diagram.

Accordingly, since about 1960, failure envelopes have usually been plotted using modified Mohr-Coulomb diagrams in which the axes have been transformed to allow a single point to be used to represent the entire Mohr circle. The slope and intercept of the resulting failure envelope are then transformed to give the usual Coulomb parameters. Because we performed multiple tests at identical consolidation pressures, it is convenient to plot the compressive stresses, $(\sigma_1 - \sigma_3)$, on the y axis, and the confining pressure, $\bar{\sigma}_3$, as the x axis. If the slope of the failure envelope in the modified diagram is ψ and the cohesion intercept is d, then the usual shearing properties are obtained from the equations:

$$\phi = \sin^{-1}\left(\frac{\tan\psi}{2+\tan\psi}\right) \tag{6.7}$$

and

$$c = d\left(\frac{1-\sin(\phi)}{2\cos(\phi)}\right) \tag{6.8}$$

The usual interpretation of Mohr-Coulomb failure envelopes for triaxial compression involves the assumption that the planes of maximum deformation are oriented at an angle of $45+\frac{\bar{\phi}}{2}$ from the horizontal. It is clear that the failure planes actually ranged widely in slope but did not, in general, coincide with the Mohr-Coulomb planes. An alternative interpretation of the data is to calculate the normal and shearing stresses on the actual failure planes using the standard equations:

$$\sigma = \frac{1}{2}(\sigma_1+\sigma_3) + \frac{1}{2}(\sigma_1-\sigma_3)\cos(2\alpha) \tag{6.9}$$

$$\tau = \frac{1}{2}(\sigma_1-\sigma_3)\sin(2\alpha) \tag{6.10}$$

where α is the angle between the failure plane and the plane upon which σ_1 acts, i.e., the angle between the failure plane and the horizontal. The state of stress on the failure planes probably cannot be calculated when the shear plane passes through one end of the specimen because the distribution of stresses on the end of the sample is unknown.

PRESENTATION OF RESULTS

Introduction

Data to be included from the Phase 1 program were chosen on the following basis :

1. The samples had reasonable degrees of consolidation at failure, based on either direct computation of the degree of consolidation or because the shearing times exceeding 1000 minutes (test CD5). Samples that were subjected to large consolidation times probably had errors associated with membrane/pipet/gas leakage that affected the measured time volume response. In most cases the leakage would produce a predicted coefficient of consolidation that was too low and as result would predict low degrees of consolidation at failure.

2. failure angles did not pass through the ends

The displacements (included in the Task 2 report) for Tests CD19, CD20, and CD21 in the PIF phase were corrected for seating load errors by 0.0052", 0.0094", and 0.0034", respectively, for calculations of the moduli.

Summary Data

General information on samples, including the sequence of consolidation pressures, is presented in Table 6.2. Times to failure, fitted coefficients of consolidation, theoretical degrees of consolidation at failure, and stresses and strains at failure, are summarized in Tables 6.3 and 6.4, and modulii in Table 6.5. Consolidation data are summarized in Table 6.6.

Test ID	Measure Final w_c (%)	Calc. Final w_c (%)	Initial Height (in.)	Cal. Initial Sat. (G_S=2.78)	Field Vertical Effective Stress (psf)	Initial Void Ratio	Consol. Stress History (psi)
CD2	17.1	-	2.804	103	15000	0.420	100,50,10
CD3	15.5	-	2.743	99	15000	0.475	100
CD5	18.6	-	2.88	98	18000	0.470	100,120, 140,50,10
CD8	19.2	-	2.82	96	18100	0.464	10
CD10	15.2	-	2.802	99	19900	0.444	140;100
		-					
CD11	19.7	20.6	2.667	98	16900	0.490	140,10
CD12	19.5	19.9	3.000	96	13300	0.502	140,10.9
CD13	19.4	19.3	2.804	98	13100	0.492	140,10
CD14	19.1	leak	2.659	95	16700	0.487	141,10
CD15	19.8	20.1	2.995	95	9600	0.518	140,10.9
CD16	16.3	leak	2.879	95	17000	0.464	141,50
CD17	16.9	15.8	2.808	93	17000	0.454	140;100
CD18	18.2	17.8	2.717	94	16700	0.496	140,50
CD19	17.0	16.0	2.881	97	16700	0.489	140;100
CD20	17.4	17.2	2.736	98	13100	0.481	140,50
CD21	17.1	16.4	2.528	98	13100	0.488	140;100
CD22	16.2	leak	2.993	89	14200	0.462	140,50
CD23	16.2	16.0	2.487	99	16400	0.458	140;100
CD24	17.0	15.8	2.603	93	18100	0.471	140;100

Table 6.2 Summary of Specimen's and Test's Initial Conditions and Details for all PIF Phase (and those Included From Phase 1) Triaxial Tests

Test ID	Actual Time to Failure (min.)	Final Cell Pres. (psi)	Final Coeff. of Consol., c_v (ft^2/day)	Uncorr. Axial Failure Strain, ε_f (%)	Corr. Axial Failure Strain, ε_f (%)	Fail. Vol. Strain υ_f (%)	Uncorr. Peak Stress Diff., $(\sigma_1-\sigma_3)_f$ (psi)	Corr. Peak Stress Diff., $(\sigma_1-\sigma_3)_f$ (psi)
CD2	490	10	0.002500	4.6	-	-2.2	180	-
CD3	785	100	0.001400	4.3	-	-3.2	601	-
CD5	1140	10	0.000100	4.0	-	-2.5	336	-
CD8	2340	10	0.002500	3.3	-	0.2	231	-
CD10	4318	100	0.003000	2.5	-	-1.8	400	-
CD11	3596	10	0.002100	3.1	2.7	-1.2	194	194
CD12	6210	10.9	0.000287	2.0	1.8	-2.3	148	148
CD13	3528	10	0.000395	2.8	2.5	-2.6	188	188
CD14	3844	10	0.001090	3.3	3.1	-1.1	139	139
CD15	4814	10.9	0.002780	2.4	2.1	-1.2	192	192
CD16	3688	50	0.001040	2.8	2.3	-1.2	343	344
CD17	3964	100	0.000770	2.4	1.8	-1.7	415	416
CD18	10678	50	0.000633	2.8	2.4	-1.6	292	291
CD19	3967	100	0.001210	2.4	1.9	-2.2	412	413
CD20	8925	50	0.000429	1.9	1.6	-1.6	183	183
CD21	1967	100	0.000732	1.1	0.8	-1.0	171	170
CD22	8638	50	0.001050	2.6	2.1	-1.3	326	326
CD23	7534	100	0.001370	3.3	2.6	-2.4	472	471
CD24	7882	100	0.000744	2.2	1.8	-1.4	275	275

Table 6.3 Summary of General Consolidation and Shear Data for Triaxial Compression Tests on Eagleford Shale

Test ID	Degree of Consol. at Failure(%)	Fail. Plane Angle to Horiz. (Deg.)	Normal Stress on Failure Plane (psi)	Shear Stress on Failure Plane (psi)
CD2	60	22	165	63
CD3	52	36	498	284
CD5	20	42	198	167
CD8	91	62	62	97
CD10	96	37	355	192
CD11	93	35	140	91
CD12	70	thru end	na	na
CD13	65	thru end	na	na
CD14	87	thru end	na	na
CD15	95	50	90	95
CD16	86	thru end	na	na
CD17	80	41	337	206
CD18	90	43	206	145
CD19	87	40	343	204
CD20	86	thru end	na	na
CD21	75	20	250	55
CD22	92	59	137	144
CD23	96	39	385	230
CD24	90	thru end	na	na

Table 6.4 Conditions at Failure for Triaxial Compression Tests on Eagleford Shale

Test ID	$^1/_2(\sigma_1 - \sigma_3)_f$ or (0.5 PSDF) (psi)	Cor. $\varepsilon_{vertical}$ at $^1/_2(\sigma_1 - \sigma_3)_f$ (%)	$E_{uncor.}$ at 0.5 PSDF (psi)	$E_{corr.}$ at 0.5 PSDF (psi)	Uncorr. Poisson's Ratio at 0.5 PSDF	Corr. Poisson's Ratio at 0.5 PSDF	Mean Eff. Stress at 0.5 PSDF (psi)
CD11	98.9	1.38	6400	7200	0.075	0.02	43
CD12	73.7	0.78	8200	9400	-0.123	-0.22	36
CD13	88.5	1.21	6500	7300	-0.007	-0.07	40
CD14	73.4	1.23	5400	6000	0.034	-0.02	35
CD15	101.4	0.77	10800	13100	-0.079	-0.2	45
CD16	163.2	1.00	13000	16400	0.053	-0.06	104
CD17	203.2	0.68	20200	29700	0.018	-0.21	168
CD18	155.4	0.98	12600	15900	0.007	-0.13	102
CD19	203.1	0.65	21100	31600	-0.065	-0.34	168
CD20	84.1	0.41	15100	20500	-0.076	-0.28	78
CD21	84.8	0.21	23000	24600	-0.138	-0.62	128
CD22	163.3	0.89	14300	18300	0.035	-0.09	104
CD23	255.5	1.16	15900	22100	0.060	-0.11	185
CD24	140.7	0.60	16600	23500	0.044	-0.14	147

Table 6.5 Summary of Secant Moduli

Test ID	Field Effect. Stress (psi)	Initial Void Ratio	Consol. Press. No. 1 (psi)	Corrected Void Ratio at Consol. Press. No. 1	Consol. Press. No. 2 (psi)	Corrected Void Ratio at Consol. Press. No. 2	Compression Index
CD11	117	0.490	140	0.500	10	0.540	0.0349
CD12	92	0.502	140	0.504	10.9	0.559	0.0496
CD13	91	0.492	140	0.496	10	0.545	0.0428
CD14	116	0.487	141	0.499	10	0.529	0.0261
CD15	67	0.518	140	0.517	10.9	0.550	0.0298
CD16	118	0.464	141	0.478	50	0.493	0.0333
CD17	118	0.454	140	0.470	100	0.476	0.0411
CD18	116	0.496	140	0.503	50	0.521	0.0403
CD19	116	0.489	140	0.484	100	0.482	na
CD20	91	0.481	140	0.482	50	0.501	0.0425
CD21	91	0.488	140	0.479	100	0.483	0.0274
CD22	99	0.462	140	0.464	50	0.476	0.0268
CD23	114	0.458	140	0.463	100	0.466	0.0205
CD24	126	0.471	140	0.479	100	0.483	0.0274

Table 6.6 Summary of Consolidation Stress-Strain Data

Tests at 10 psi Cell Pressure

Introduction. Five triaxial compression tests (CD11, CD12, CD13, CD14, CD15) on Eagleford shale were conducted at a cell pressure of 10 psi in the PIF phase. In addition to these tests, three tests (CD2, CD5, and CD8) performed in Phase 1 will be used to supplement the results.

Data. The maximum and minimum values of various parameters, measured during the Phase 1 and PIF studies, are summarized below. The intents involved in presenting this table are: (1) to show the approximate values of the different parameters, (2) to show the total range in values encountered, and (3) to compare ranges from the two studies.

Property	Phase 1, Min. Value	Phase 1 Max. Value	PIF Min. Value	PIF Max. Value
Depth (ft.)	189	229	122	219
Water Content (%)	16	17	17	18
Liquid Limit (%)	77	80	72	86
Plastic Limit (%)	31	32	29	31
Consolidation Time (min.)	1200	65,000	12,000	27,000
Coeff. of Consol., (sq.ft./day)	0.0001	0.003	0.0003	0.0028
Compression Index (C)				
$(\sigma_1-\sigma_3)_f$ (psi)	180	340	140	190
Degree of Consolidation at Failure (%)	20	91	65	95
Slope of Failure Planes (not through ends) (deg.)	22	62	35	50
Shearing Time to Failure (min.)	500	2300	3500	6200
Uncorr. Axial Strain at Failure (%)	3.3	4.6	2.0	3.3
Corr. Axial Strain at Failure (%)	N.A.	N.A.	1.8	3.1
Vol. Strain at Failure (%)	-2.5	0.2	-1.1	2.6
Secant Poisson's ratio	-0.02	0.45	-0.12	0.08
Secant Young's modulus (psi)	4100	9000	5400	10,800

The samples with low coefficients of consolidation (CD5, CD12, CD13, CD14) were those tests where the final consolidation pressure was held for the longest time. Future discussions will suggest that some of this effect is due to leakage problems, and possibly secondary effects.

The secant Poisson's Ratio for the PIF phase, after correction for machine deformations, ranged from -0.22 to +0.02. Only PIF phase materials were corrected for machine deformations. .

The negative Poisson's ratio implies (Eq. 6.6) compressive lateral strains. Such a situation seems unlikely for this rock. The tests (CD11, CD13, CD14) with larger axial strains at $^1/_2$ $(\sigma_1-\sigma_3)_f$ tended

to have values of Poisson's ratio approaching zero, indicating a more logical zero lateral strain condition. The negative values of Poisson's ratio may be an indication of an error in volume change or displacement during the shearing stage. However, a sensitivity analysis of a typical test in which Poisson's ratio was negative did not explain the anomaly. Additional "corrections" to the volume change and displacements that were all chosen to "make the Poisson's ratio approach zero" for typical tests were:

1. correction to axial strain due to an error in machine deformation due to resolution of measurement sensor (0.0004" is a reasonable error estimate)

2. error in measured deformation during shear (also 0.0004")

3. compression (water into pipet) from the end filter disk (0.01cc at 144 lb.) and compression of the lateral filter (0.01 cc for 0.024" displacement) to be applied to the volumetric strain

4. membrane/pipet/fittings leakage during shearing (0.03cc for three days of shearing)

Even after correcting the volume change and displacements the value of Poisson's ratio is still negative for the typical test. The anomaly of the negative Poisson's ratio needs further study to determine if there is real material justification or if it is a test specific artifact.

The low values of secant modulus were associated with the specimens that failed at a small angle (CD2), or through the ends (CD13, CD14). The corrected secant moduli for the PIF phase specimens at one-half the peak stress difference ranged from 5400 to 11,000 psi, while the compression index ranged from 0.026 to 0.050 (generally increasing with liquid limit).

The stress-strain curves are presented in Fig. 6.3.

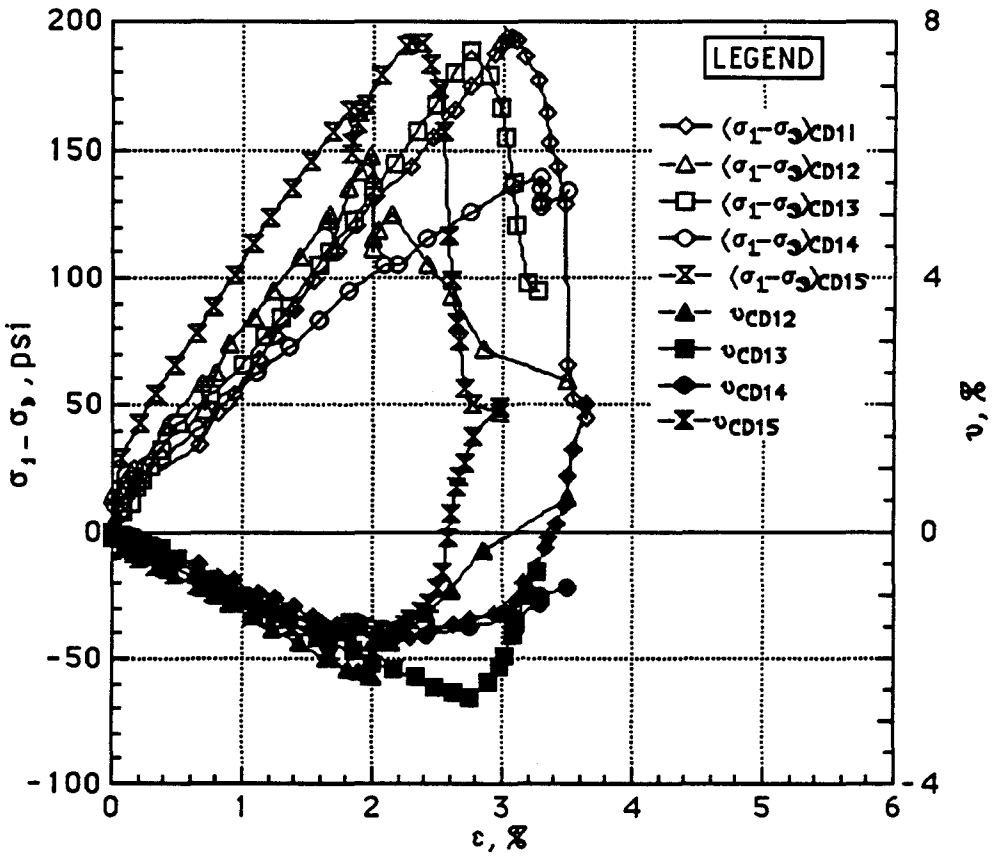

Fig. 6.3 Stress-Strain-Volumetric Strain Curves for Triaxial Tests CD11-CD15 for Eagleford Shale at 10 psi

Tests at 50 psi Cell Pressure

Introduction. Four triaxial compression tests (CD16, CD18, CD20, CD22) were conducted at a cell pressure of 50 psi in the PIF phase.

Data. The maximum and minimum values of various parameters, measured during the PIF studies, are summarized below.

Property	Phase 1, Min. Value	Phase 1 Max. Value	PIF Min. Value	PIF Max. Value
Depth (ft.)			169	220
Water Content (%)			15	17
Liquid Limit (%)			67	84
Plastic Limit (%)			26	32
Consolidation Time (min.)			8300	59,000
Coeff. of Consol., (sq.ft./day)			0.0004	0.0011
Compression Index (C)			0.027	0.043
$(\sigma_1-\sigma_3)_f$ (psi)			180	330
Degree of Consolidation at Failure (%)			86	92
Slope of Failure Planes (not through ends) (deg.)			43	59
Shearing Time to Failure (min.)			3700	11,000
Uncorr. Axial Strain at Failure (%)			1.9	2.8
Corr. Axial Strain at Failure (%)			1.6	2.4
Vol. Strain at Failure (%)			-1.6	-1.2
Secant Poisson's ratio			-0.08	0.05
Secant Young's modulus (psi)			12,600	15,100

The samples with low coefficients of consolidation (CD18, CD20) were those tests where the final consolidation pressure was held for the longest time. The stress-strain curves are presented in Fig. 6.4.

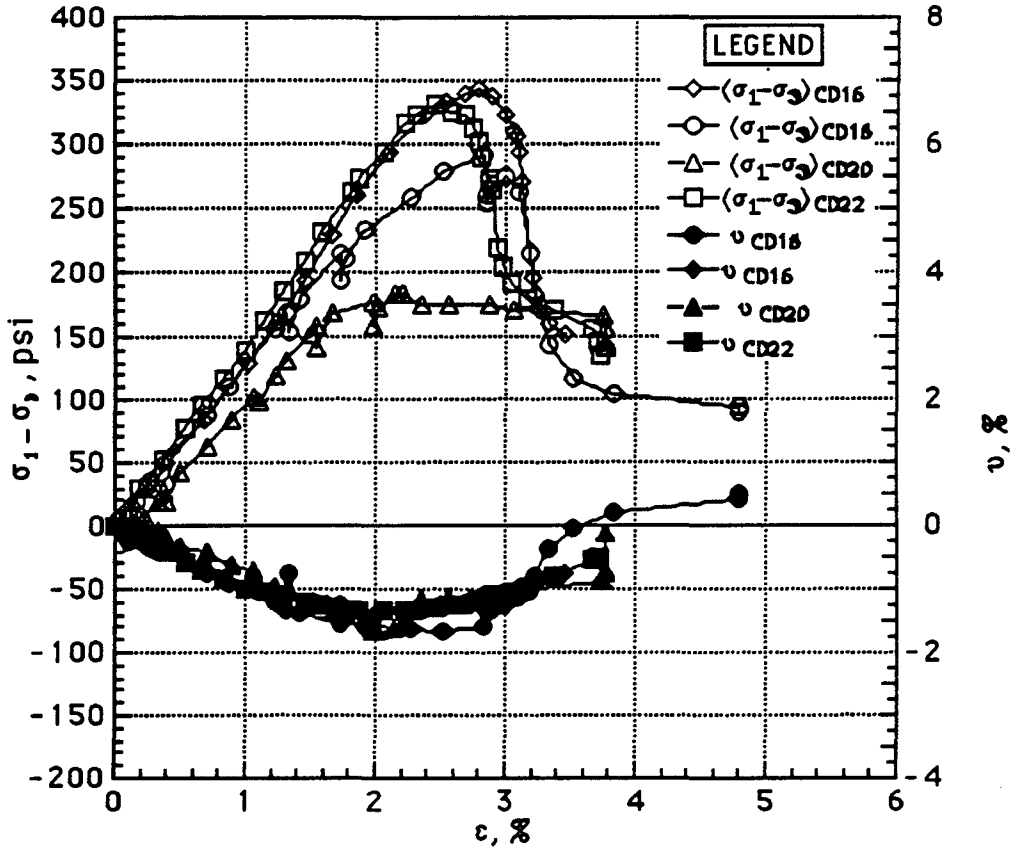

Fig. 6.4 Stress-Strain-Volumetric Strain Curves for Triaxial Tests CD16, CD18, CD20, CD22 for Eagleford Shale at 50 psi

For the samples that failed at reasonable angles (CD18, CD22), the value of the corrected Poisson's ratio ranged from -0.09 to -0.13.

Tests at 100 psi Cell Pressure

Introduction. Five triaxial compression tests (CD17, CD19, CD21, CD23, CD24) were conducted at a cell pressure of 100 psi in the PIF phase. In addition to these tests, two tests (CD3, CD10) from Phase 1 will be included.

General Data. The maximum and minimum values of various parameters, measured during the Phase 1 and PIF studies, are summarized below. The intents involved in presenting this table are: (1) to show the approximate values of the different parameters, (2)

to show the total range in values encountered, and (3) to compare ranges from the two studies.

Property	Phase 1, Min. Value	Phase 1 Max. Value	PIF Min. Value	PIF Max. Value
Depth (ft.)	190	252	169	235
Water Content (%)	15	17	15	17
Liquid Limit (%)	67	83	67	87
Plastic Limit (%)	26	30	27	31
Consolidation Time (min.)	2700	17,000	7200	20,000
Coeff. of Consol., (sq.ft./day)	0.0014	0.0030	0.0007	0.0014
Compression Index (C)			0.027	0.043
$(\sigma_1-\sigma_3)_f$ (psi)	400	600	170	470
Degree of Consolidation at Failure (%)	52	96	75	96
Slope of Failure Planes (not through ends) (deg.)	36	37	39	41
Shearing Time to Failure (min.)	780	4300	1200	7900
Uncorr. Axial Strain at Failure (%)	2.5	4.3	1.1	3.3
Corr. Axial Strain at Failure (%)			1.8	2.6
Vol. Strain at Failure (%)	-3.2	-1.8	-1.0	2.4
Secant Poisson's ratio	0.06	0.15	-0.14	0.02
Secant Young's modulus (psi)	16,600	18,000	15,900	23,000

The samples with low coefficients of consolidation tended to be those tests where the final consolidation pressure was held for the longest time.

The secant Poisson's ratio, corrected for apparatus deflection, for the PIF phase ranged from -0.62 to -0.11. For the samples that failed at reasonable angles (CD17, CD19, CD23) the values of "corrected" Poisson's ratio ranged from -0.34 to -0.11.

The variation in compression index was inconsistent with liquid limit, apparently due to small volume changes of the specimens, and uncertainties (discussed later) in volume change corrections.

The stress-strain curves are presented in Fig. 6.5.

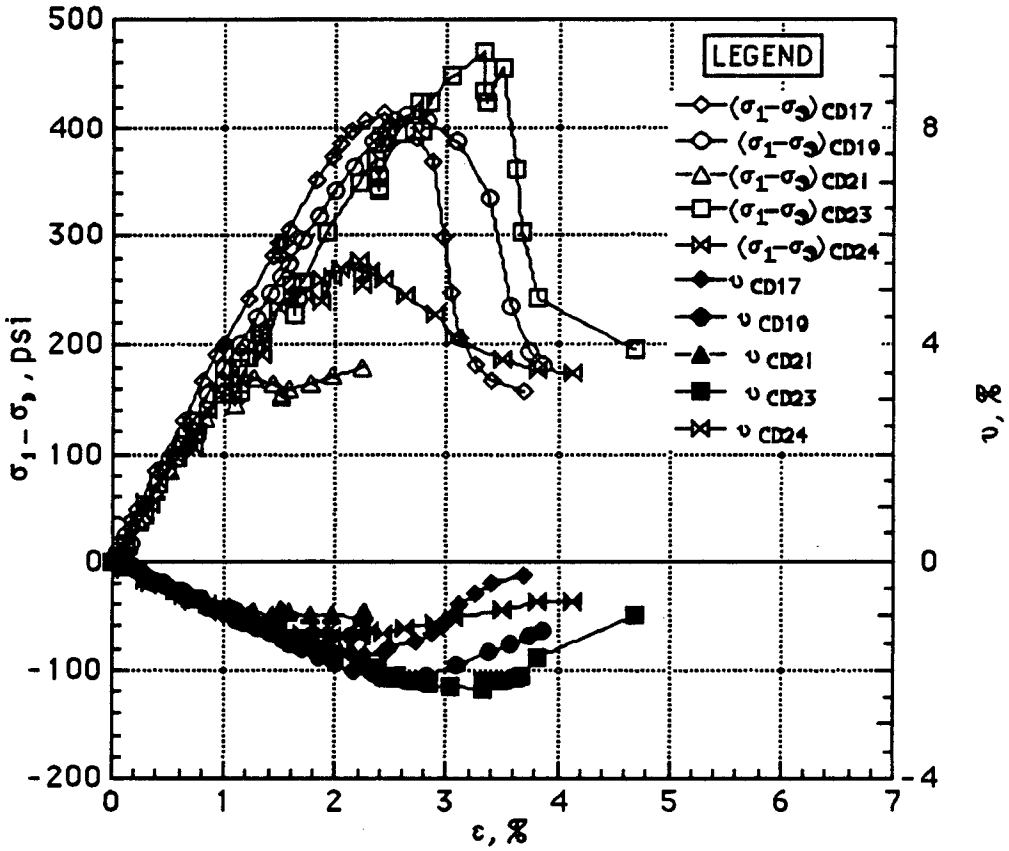

Fig. 6.5 Stress-Strain-Volumetric Strain Curves for Triaxial Tests CD17, CD19, CD 21, CD23, CD24 for Eagleford Shale at 100 psi

Failure Envelopes

The contract provided for three sets of tests to be performed, using the consolidation pressures of 10 psi, 50 psi, and 100 psi, for samples in each set. Three different cores were used and the hope was to compare failure envelopes. The first failure envelope was to be defined using tests CD11, CD16, and CD17, the second using tests CD14, CD18, and CD19, and the third using tests CD13, CD20, and CD21. The associated stress-strain curves are presented in Fig.s 6.6 through 6.8.

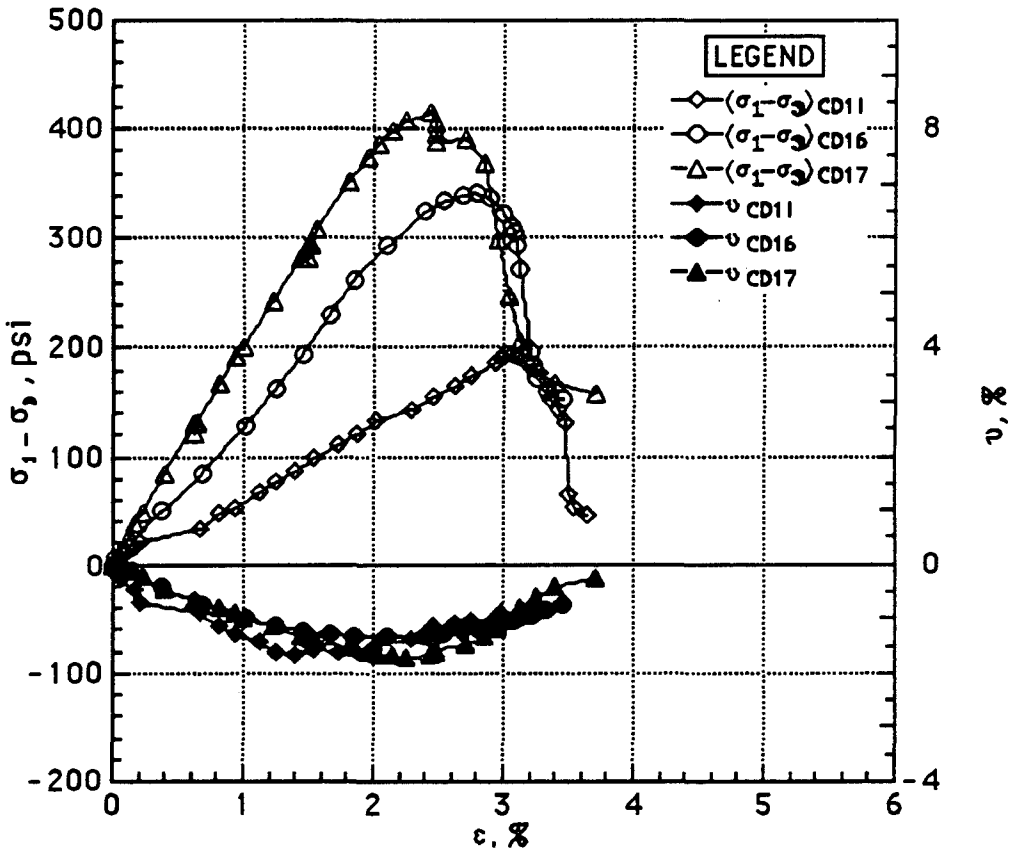

Fig. 6.6 Stress-Strain-Volumetric Strain Curves for Triaxial Tests on Sample No. 58 (CD11, CD16, & CD17) for Eagleford Shale

Tests CD13, CD14, CD16, and CD20 had end failures. Test CD21 failed at trimming time at an angle of 20 deg. We set up test CD21 anyway, because of a shortage of core, and in hoping that the failure plane would form elsewhere. As a result, none of the cores yielded data to define "ideal" envelopes. As a result, we will treat all of the triaxial data as part of a single set of data. The samples had similar index properties and response in one-consolidation tests.

The Modified Mohr-Coulomb diagram, including the data from the PIF phase triaxial compression tests and the "good" tests from Phase 1, is shown in Fig. 6.9. We did not attempt to draw any conclusions from this data base, since tests with end failures are included.

The Modified Mohr-Coulomb diagram for all tests without end failures is shown in Fig. 6.10. Significant scatter exists in the

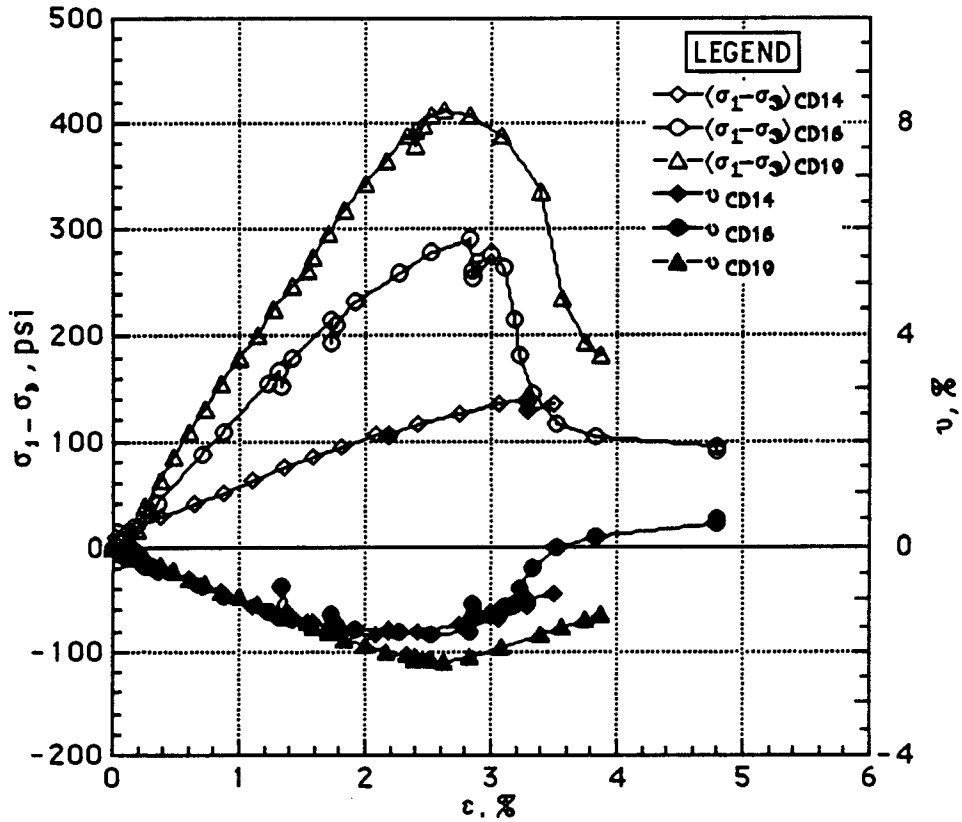

Fig. 6.7 Stress-Strain-Volumetric Strain Curves for Triaxial Tests on Sample No. 44 (CD14, CD18, & CD19) for Eagleford Shale

results. However, there may be evidence (to be discussed later) to justify removing CD3 and CD5 from the data base, significantly reducing the scatter. The values of the friction angle and cohesion would be 37 deg. and 77 psi (11,100 psf) for the upper bound envelope, and 34 deg. and 42 psi (6,000 psf) for the lower bound envelope. The friction angles seem to be high for a highly plastic material but, of course, the Atterberg limits are performed using disaggregated material whereas the rock is apparently cemented in the field.

The Coulomb diagram for all tests with no end failures is shown in Fig. 6.11. The sample used in test CD2 failed on a plane at a small angle (22 deg.), but the stress-strain curve (Phase 1 report) did not indicate failure on a previously existing plane. However, CD 2 had a relatively short testing time, so significant pore pressures may have existed at failure. The scatter for the Coulomb diagram

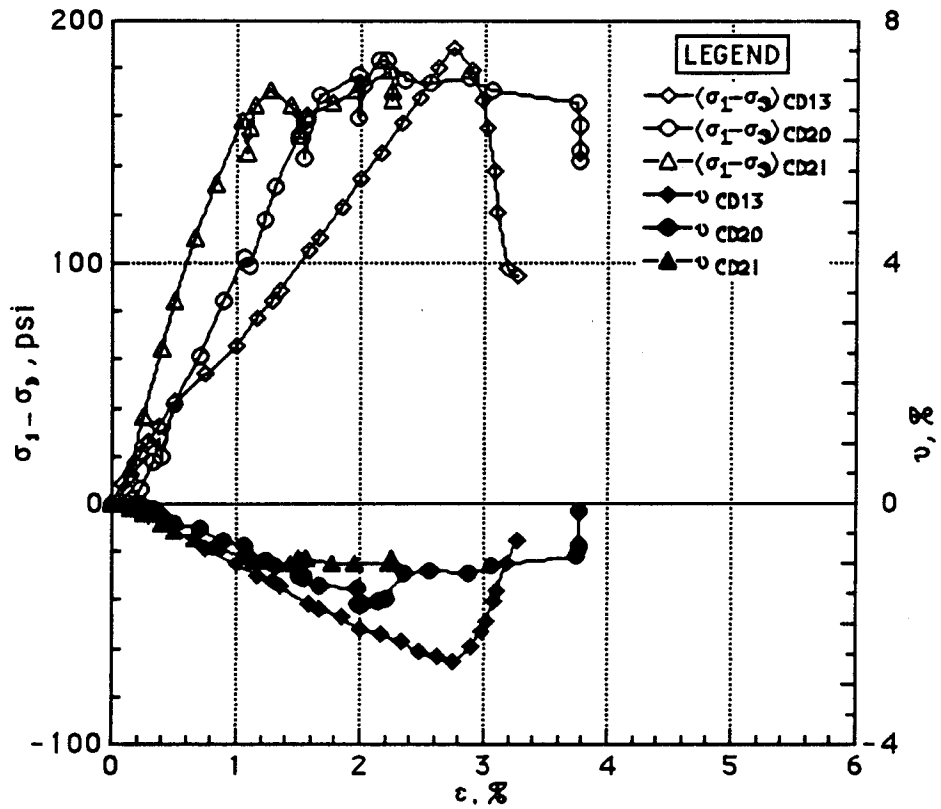

Fig. 6.8 Stress-Strain-Volumetric Strain Curves for Triaxial Tests on Sample No. 63 (CD13, CD20, & CD21) for Eagleford Shale

(excluding CD2 and CD21) is relatively small, considering the variety of borings, depths, and liquid limits that the samples had. If CD3 and CD 5 data were removed the scatter would be reduced for normal stresses above 200 psi. The values of the friction angle and cohesion would be 21 deg. and 90 psi (13,000 psf) for the upper bound envelope, and 25 deg. and 25 psi (3,600 psf) for the lower bound envelope.

The fact that the scatter in the peak Coulomb diagram is relatively small seems to indicate that the peak shear strength on failure planes of several orientations (35 deg. to 62 deg.), relative to the presumed cross-anisotropic anisotropy, is reasonably homogeneous.

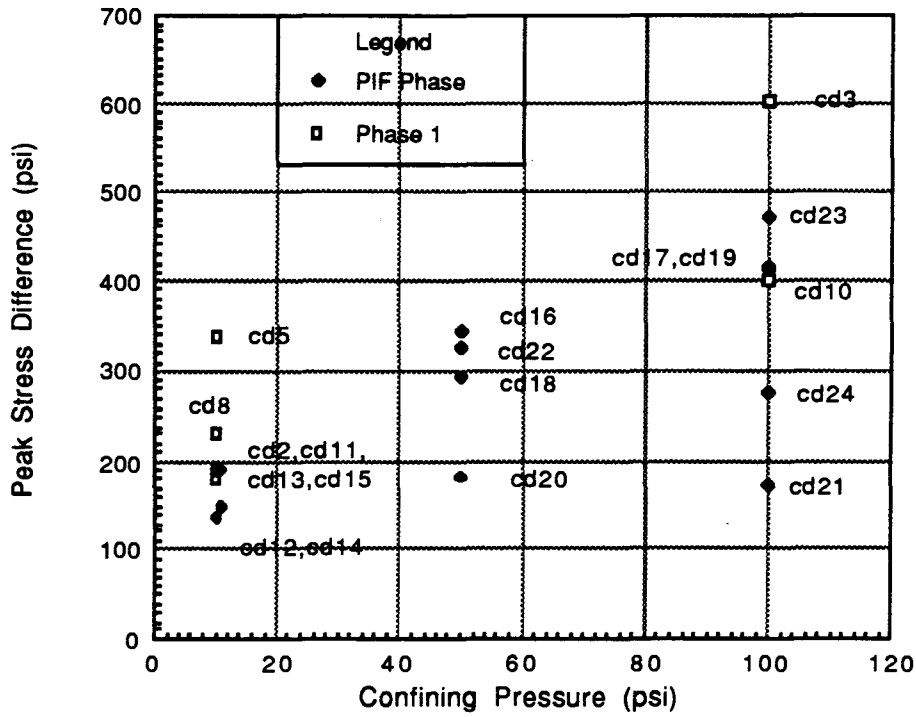

Fig. 6.9 Modified Mohr-Coulomb Diagram for all Triaxial Compression Tests on Eagleford Shale

Times to Failure

There may be a time rate effect (Figs. 6.12-6.14) in the drained shear strength when we consider only the specimens that did not fail through the ends or at small angles (CD2 and CD21). All of the specimens underwent a decrease in volume during shear in spite of the fact that the material appear to be highly overconsolidated. The large axial stiffness, results in an increase in mean stress and compressive volumetric strains. The mean-stress induced volumetric strains apparently dominate the dilative volumetric strains due to shearing stresses. However, an apparent anomaly exists, since the shear strength appears to be larger at the smaller testing times, in particular CD5 (Fig. 6.12) and CD3 (Fig. 6.14) tests.

In order to develop a working hypothesis, other data (CD4 and CD9) from Phase 1 will be introduced here. The tests (all failure angles between 35 deg. and 47 deg.) that will be used are presented below:

Test ID	LL (%)	t_f (min.)	(ε_f)uncor. (%)	υ_f (%)	$(\sigma_1 - \sigma_3)_f$ (psi)	Degree Consol. (%)	Cell Pres. (psi)	Angle (deg.)
CD5	80	1140	4.0	-2.5	335	20	10	42
CD11	76	3600	3.1	-1.2	190	93	10	35
CD4	82	635	3.4	-2.4	460	15	50	39
CD18	77	10680	2.8	-1.6	290	90	50	43
CD3	88	785	4.3	-3.2	600	52	100	36
CD10	67	4320	2.5	-1.8	400	96	100	37
CD9	64	22	2.7	-0.95	320	20	100	47

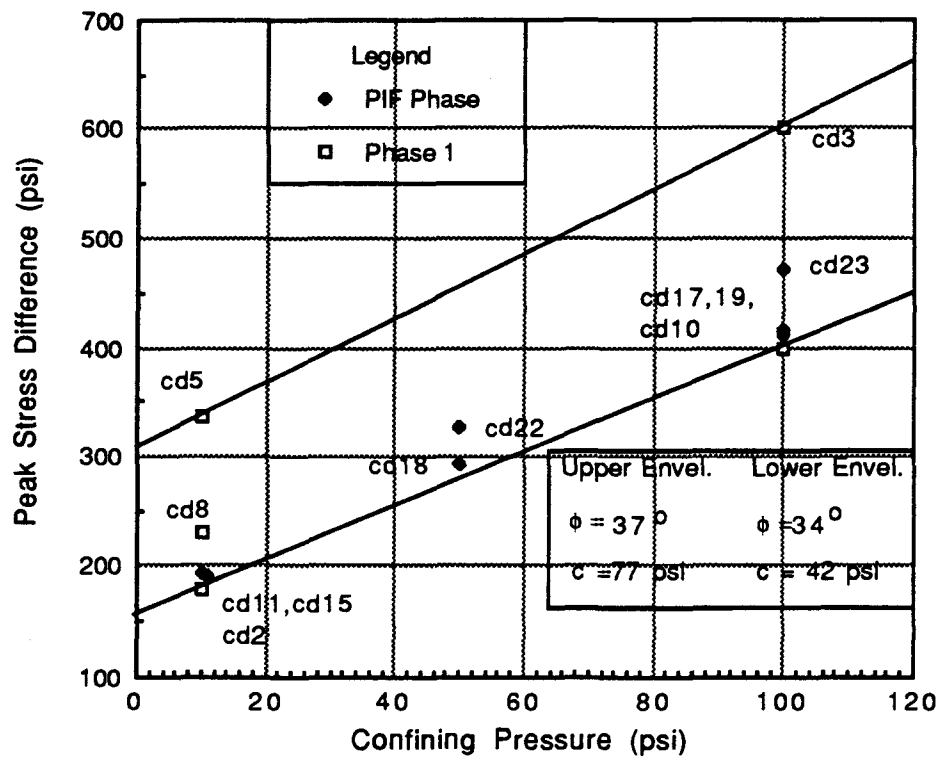

Fig. 6.10 Modified Mohr-Coulomb Diagram for all "Good" Triaxial Compression Tests on Eagleford Shale

The tests with relatively low degrees of consolidation (CD5, CD4, and CD3) exhibited larger strengths than their counterparts at the same consolidation pressure (but had shorter shearing times). Also, the magnitude of both the uncorrected axial strain (used for convenient comparison between phases) and volumetric strains are larger for the tests with short shearing times, possibly indicating a

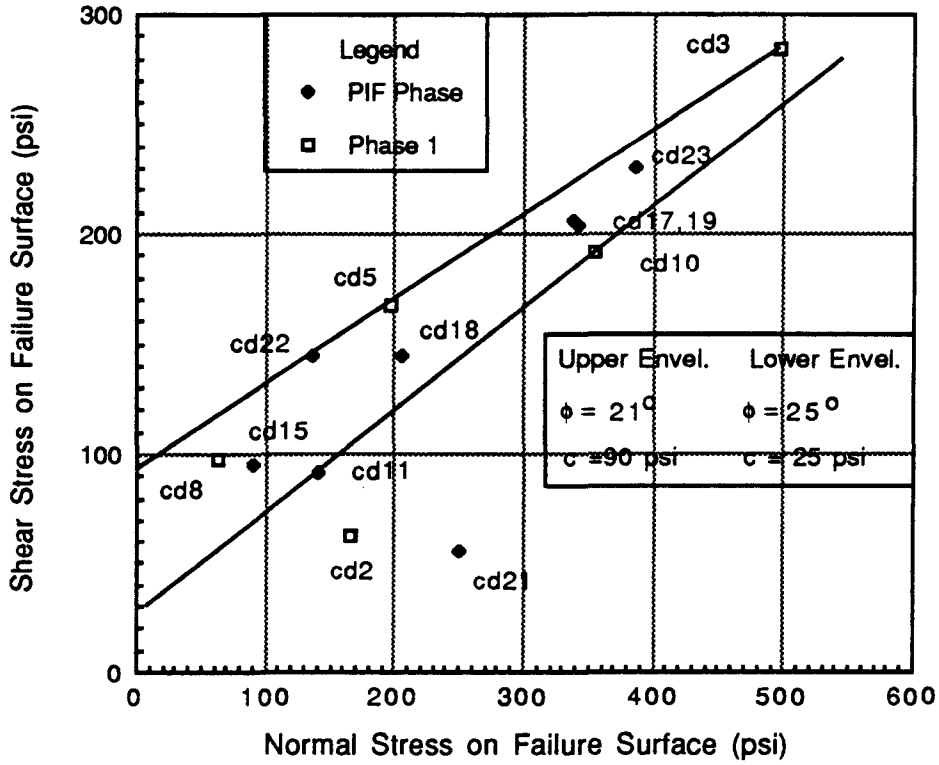

Fig. 6.11 Coulomb Diagram for all Triaxial Compression Tests on Eagleford Shale

component of strain due to creep. One possible explanation for the anomaly in the strength-time relationship might be strain rate effects associated with partially drained creep. Apparently, the increase in shear strength due to the creep dominates any strength decrease due to positive excess pore water pressures that are generated during the shearing stage.

Test CD9 was sheared in 22 minutes, and yet has a lower shear strength than either C3 and CD10. Apparently, since CD9 had a short shearing time, failure occurred under relatively undrained conditions (small volumetric strain). As a result, the strength reduction due to positive excess pore water pressures dominated the creep effects.

Most of the available literature suggest stain rates should cause 10% increases in the undrained shear strength for a 10-fold increase in strain rate. The strain rates used in this study varied by a factor of about 17 times. Thus, we'd expect, at most, a 20% increase in undrained strength. However, these tests indicate increases from

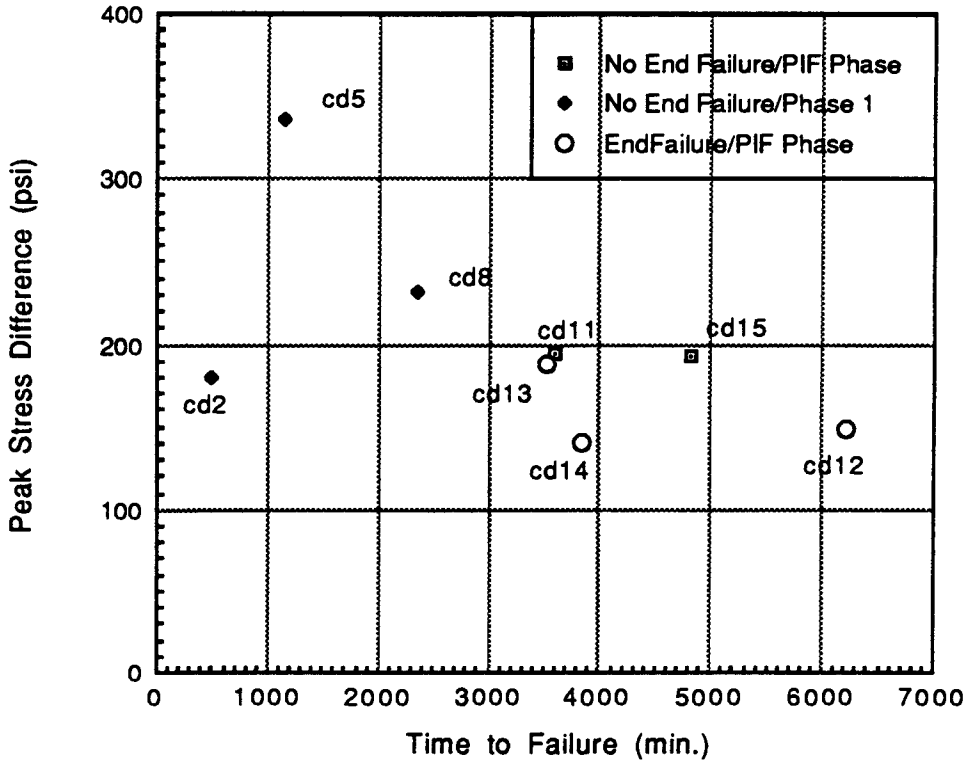

Fig. 6.12 Effect of Time to Failure on Peak Stress Difference at 10 psi Cell Pressure

50% to 76% (over the "drained" strength) in partially drained strength. Further study is required to determine the consequences of this possible material response.

GENERAL REMARKS ON TRIAXIAL COMPRESSION TESTS

Time-Dependent Chemical Changes

The existence of pyrite in the cores indicates that the material is in a reducing environment in the field. The laboratory environment is an oxidizing one so chemical changes are anticipated when samples are exposed to the laboratory environment for prolonged periods of time. The only obvious change that we detected was the presence of

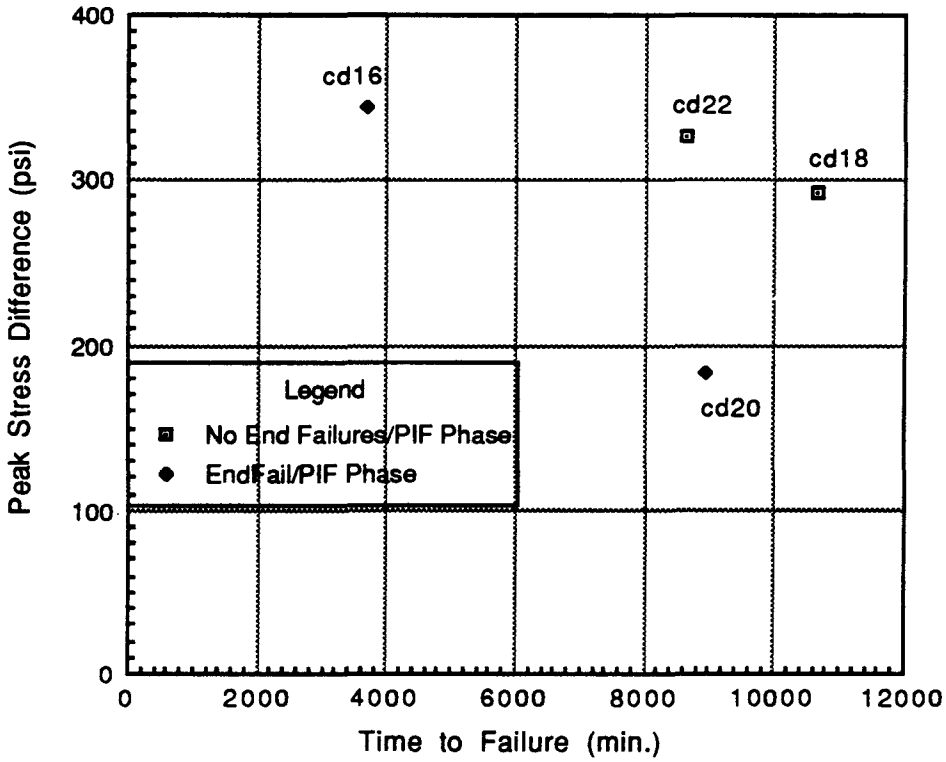

Fig. 6.13 Effect of Time to Failure on Peak Stress Difference at 50 psi Cell Pressure

a strong odor from triaxial samples when they were being dismantled. The source of the odor was not determined. Chemical changes may have occurred in direct shear and consolidation samples as well but any gases generated in the process could easily escape during the test.

Secondary Effects

In the absence of any measurements of pore water pressures, it is not possible to decide when primary effects have damped out and secondary effects have become dominant. The shapes of the ΔV-log(t) curves (see Task 2 report) often indicate that primary effects are not governing volume change behavior. Further, the measured values of hydraulic conductivity in the one-dimensional consolidation tests were substantially higher than the values of hydraulic conductivity obtained by fitting Terzaghi's theory to measured time-settlement curves, indicating important secondary effects.

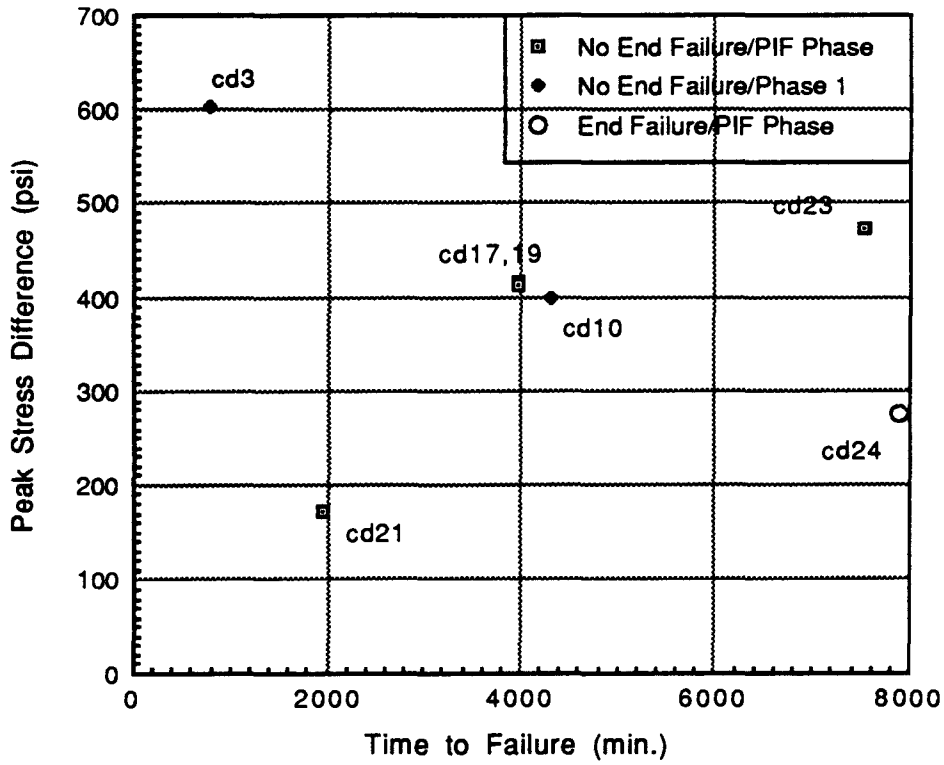

Fig. 6.14 Effect of Failure Time on Peak Stress Difference at 100 psi Cell Pressure

With respect to shear, secondary effects are of interest in trying to estimate shearing times that will result in a reasonable dissipation of excess pore water pressures generated during the shearing stage.

One way to estimate the influence of secondary effects during primary consolidation would be to use measured values of hydraulic conductivity (k) from one-dimensional consolidation tests, and measured volumetric strains in the triaxial tests to estimate coefficients of consolidation. It is recognized that drainage is mainly in the horizontal direction in the triaxial specimen, while it is restricted to the vertical direction in the one-dimensional test, and that the soil is probably highly anisotropic with respect to hydraulic conductivity.

Shearing stress-strain behavior. Specimens with no end failures or small failure angles exhibit the brittle behavior (Figs. 6.1-6.6)

expected of highly overconsolidated materials. However, the samples all decreased in volume up until failure.

In direct shear, the specimens of Eagleford shale expanded during shear. In direct shear tests there should be only a small increase in mean normal stress so the predominant influence is the shear. In the case of triaxial compression tests, the specimens compressed up to failure indicating the preponderant influence of the mean normal stress.

Failure mode. The samples failed on distinct shear planes that did not coincide with the planes of maximum obliquity, but were apparently controlled by fissures and horizontal planes of weakness and the consolidation pressure.

In the tests where the operator was able to view the sample when the peak stress difference developed, a failure plane did not become noticeable until the stress difference started to decrease.

After the failure plane develops, the strains are highly localized so the interpretation of the test can no longer be based on the assumption of uniform stresses and strains. The stress-strain curves are extended beyond their intended usefulness (after the failure plane develops) for qualitative purposes only.

Samples that fail through the ends probably do so because of the presence of planes of weakness, particularly fissures. It is possible that problems with trimming the ends could cause some of the end failures. However, end trimming was performed carefully. At one stage we considered using a capping compound on the ends, to ensure good contact, but such a compound would prevent drainage through the ends and was thus abandoned.

Our laboratory contains perhaps one hundred end caps, all of which were believed to be the same size. A few were checked during the Phase 1 study and were found to have a diameter of 1.500 inches. As part of the study of end effects, a number of end caps were measured and some were found to be somewhat smaller. The tests during the PIF study

After several end failures in the PIF phase, we noticed that some of the specimen's endcaps were smaller (as low as 1.475") than the specimen (1.504") diameter. As a result, from that time on we

ensured that all top caps were at least 1.491". Apparently, in Phase 1 we used only one or two triaxial cells and used a limited number of top caps, all of which were probably approximately 1.500". When the problem was discovered, some samples were still being sheared, or the caps were still associated with the cells, and the caps could be measured. The measured cap diameters were:

Cap Test ID	Diam (in.)	End Fail. (?)	Cell Pressure (psi)
CD18	1.491	no	50
CD19	1.475	no	100
CD20	1.475	yes	50
CD21	1.503	no	100
CD22	1.504	no	50
CD23	1.507	no	100
CD24	1.504	yes	100

The effect of fissures is to increase scatter substantially for samples that are relatively small. If the samples are large, compared to fissure spacing, the fissures should be randomly distributed in all samples and the scatter would be reduced.

We thought that the effects of fissures might diminish as the consolidation pressure increased. There is a limited amount of evidence in support of this view, based on orientation of failure planes (Fig. 6.15). However, the planes for samples at 100 psi are flatter than they should be, based on Mohr-Coulomb, indicating the influence of the fissile surfaces.

SUBSIDIARY TOPICS

Machine Deformations

Compression of filter paper drainage disks on the specimen ends, the lateral filter drain, porous stone, cell base, and loading frame can be significant when testing relatively stiff materials. A steel 1.5" cylindrical specimen was used as a dummy in place of a rock sample.

The testing procedure duplicated that used with rock samples in that the dummy was subjected to a cell pressure of 140 psi initially and

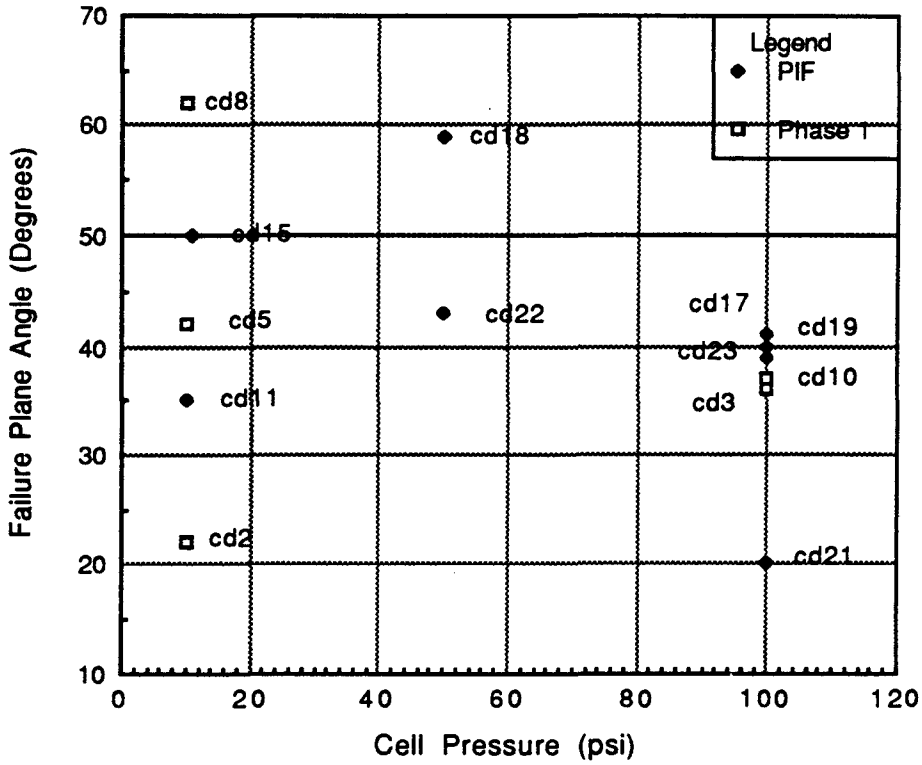

Fig. 6.15 Effect of Cell Pressure on Failure Plane Orientation

then the pressure was backed off to one of the consolidation pressures used for other tests (10 psi, 50 psi, and 100 psi). The results of the measured displacements are shown in Fig. 6.16 and tabulated in Table 6.5.

The curves have inflection points that more or less account for the fact that the paper was prestressed at 140 psi, but the inflection may also just represent a non-linear response of the system. The correction for machine displacements reduces the axial strain by up to 0.7% (Table 6.3) but has a negligible effect on stress difference.

The errors in the secant modulus at one-half the peak stress difference (Table 6.5) ranged from 1% to 18%, 21% to 26%, and 7% to 33% for the PIF phase tests executed at 10 psi, 50 psi, and 100 psi, respectively. The error in calculated stress difference associated with the machine deformations increases with stress difference up until failure (Fig. 6.17).

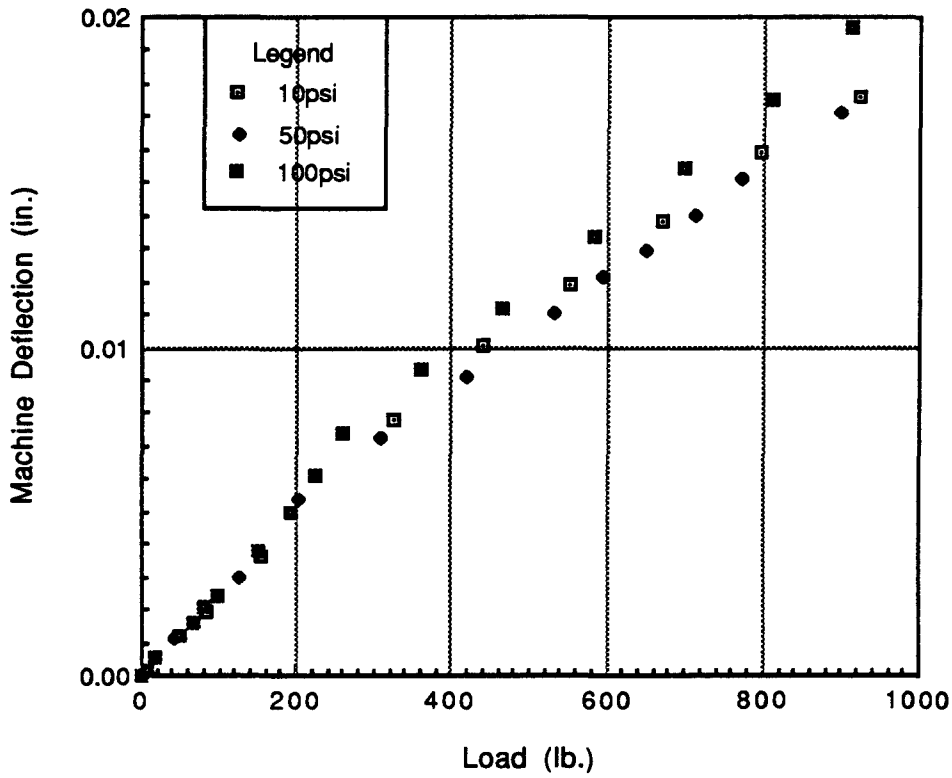

Fig. 6.16 Machine Deflection for Triaxial Compression

The corrected and uncorrected secant moduli at one-half the peak stress difference indicate (Fig. 6.18) a strong tendency to increase with mean "effective" stress.

Errors in the secant Poisson's ratio (due to errors in displacements associated with machine deformation) ranged from 40% to 280%, 70% to 190%, and 80% to 160% for the PIF phase tests executed at 10 psi, 50 psi, and 100 psi, respectively.

Incremental Moduli. The secant value of moduli incorporates some amount of plastic strain for stress levels significantly below the peak stress difference, as evidenced by the fact that strains are not fully recovered upon loading, and straining continues if we stop a test and maintain a constant stress difference. Experience shows that the modulii obtained by unloading and reloading a sample, through a small range of stress, is more than the tangent or secant modulii. We did not perform specific tests to study such effects. However, we did turn off the press and let the samples creep, and

thus unload. We calculated the incremental modulii for reloading, for several of these tests. The increments in displacement were 0.0006" to 0.0058", and the associated increments of strain were 0.022% to 0.192%, and stress difference 7.8 psi to 57.5 psi for the tests performed in the PIF phase, respectively.

100 psi Cell Pressure Axial Load(lb.)	100 psi Machine Displ. (in.)	50 psi Cell Pressure Axial Load (lb.)	50 psi Machine Disp. (in.)	10 psi Cell Pressure Axial Load (lb.)	10 psi Machine Displ. (in.)
0	0.0000	0	0.0000	0	0.0000
1.4	0.0000	43	0.0011	86	0.0019
8	0.0002	124	0.0030	152	0.0036
19	0.0006	203	0.0054	223	0.0061
49	0.0012	307	0.0072	326	0.0078
66	0.0016	419	0.0091	441	0.0100
80	0.0021	532	0.0110	554	0.0119
99	0.0024	593	0.0121	671	0.0138
150	0.0038	649	0.0129	798	0.0159
193	0.0050	715	0.0140	922	0.0176
225	0.0061	772	0.0151		
258	0.0074	900	0.0171		
361	0.0093	1027	0.0193		
466	0.0112				
583	0.0133				
701	0.0154				
810	0.0175				
912	0.0197				
1010	0.0216				
1110	0.0235				
1204	0.0250				
1301	0.0269				
1393	0.0288				

Table 6.7 Machine Deformation Data at 100 psi, 50 psi, and 10 psi Cell Pressure Using a 1.5" Steel Specimen

The incremental moduli for tests with no end failures (Fig. 6.19) are significantly larger than the secant value at one-half the failure stress difference. Of course, even for the small increments of strain, some plastic strains still probably occur. Further, for our tests, the samples undoubtedly consolidated during the "quiet" period, thus increasing sample stiffness. The incremental moduli

tend to decrease as the shear stress approaches the value of the peak stress difference (CD23).

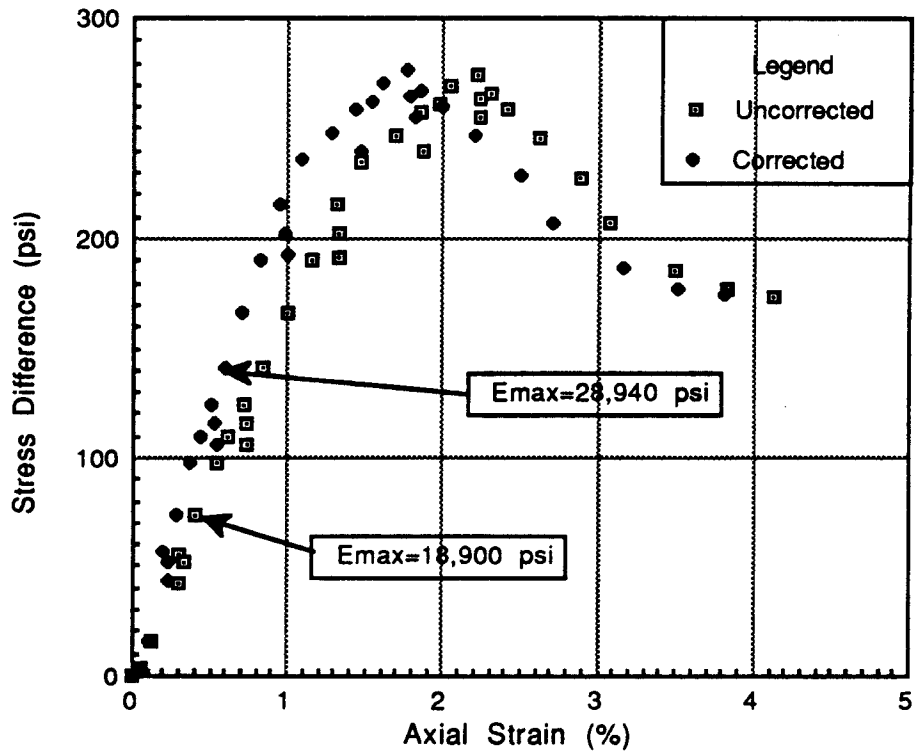

Fig. 6.17 Comparison of Stress-Strain Curves (Corrected and Uncorrected) for Machine Deformation for Test CD24

Errors Associated with Sensor Sensitivity

The data acquisition system used has an inherent minimum error in measurement of load, displacement, and volume change. The A/D card converts the analog sensor output to a digital output with 12 bit resolution (2^2= 4096 bits) at 10 volts for a resolution of 10v/4096 bits = 0.00244 v/bit. The 0.5" DCDT's used for triaxial compression output 3 volts at 0.5" displacement. The 2000 lb. load cell outputs approximately 10 volts at 2000 lb. The pore pressure transducer outputs approximately 4 volts in the 0-5 cc pipet reading range. Thus, the maximum resolution of the measurement system (before calibration to the standard, noise and best fit errors) for displacement, load, and volume change is :

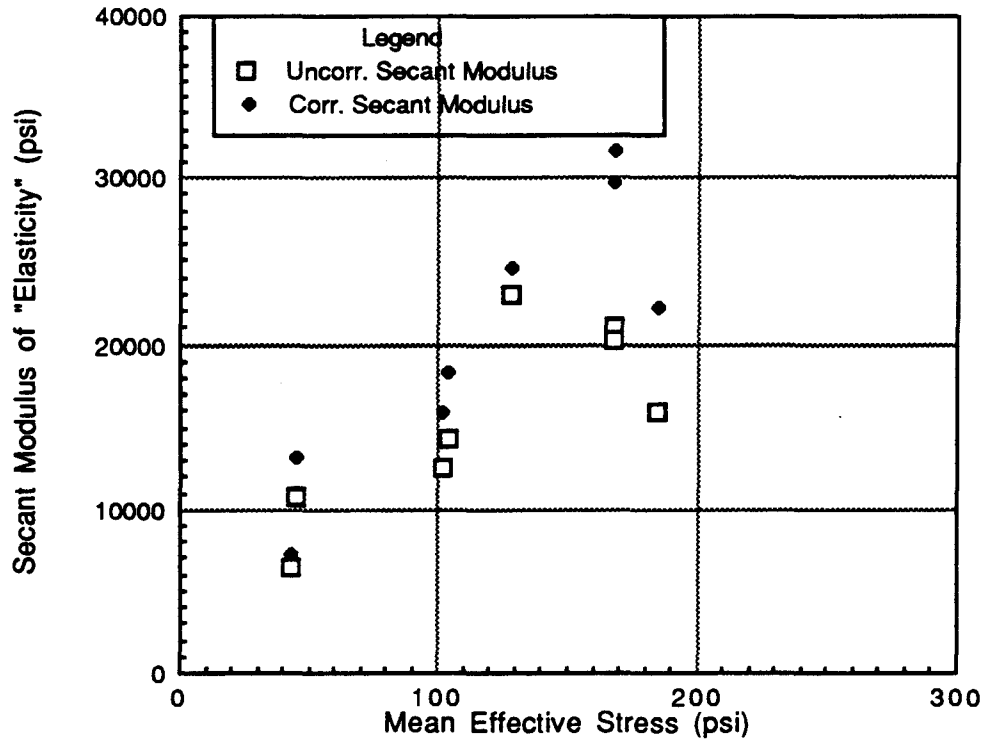

Fig. 6.18 Secant Modulus of Elasticity (Corrected and Uncorrected for Machine Deformations) vs Mean Effective Stress for Triaxial Tests with No End Failures

Displacement Resolution= 0.5"/((3v/10v)*4096 bits)
= 0.0004 "/bit

Load Resolution= 2000 lb. /((10v/10v)*4096 bits)
= 0.49 lb./bit

Pipet Reading Resolution= 5 cc /((4v/10v)*4096 bits)
= 0.003 cc/bit

We have found the noise in the load cells and (DCDT) to be minimal for the 12 bit A/D card resolution. However, if a A/D card with a larger bit capacity is used, eventually the resolution of the card would exceed the sensor sensitivity.

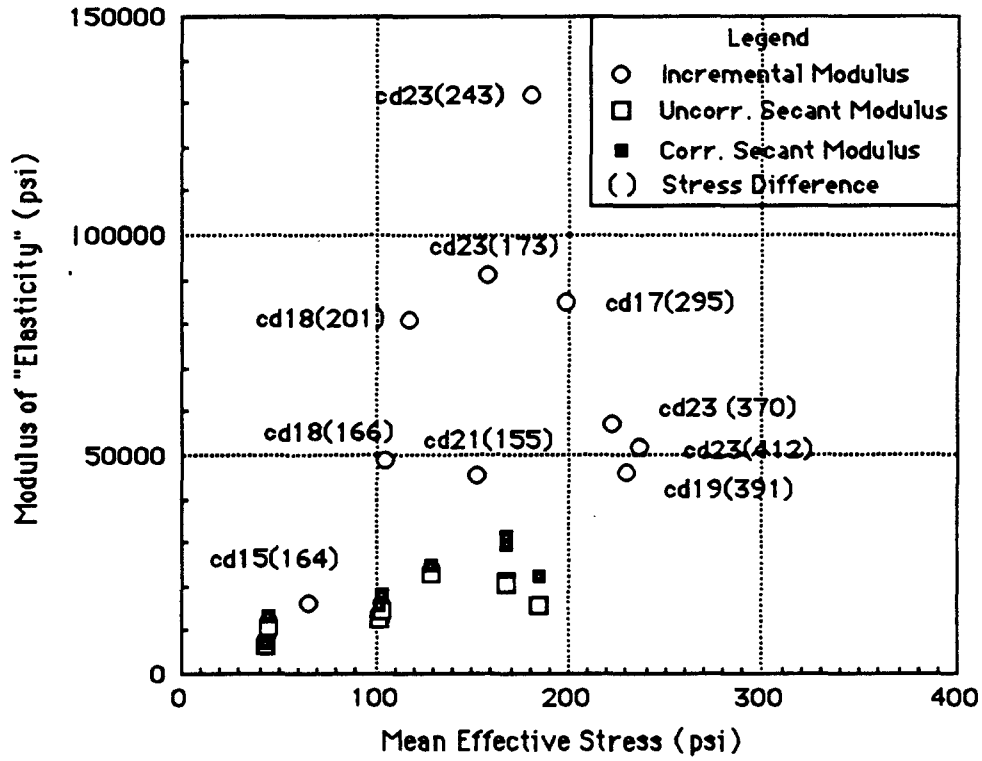

Fig. 6.19 Secant and Incremental Modulus of Elasticity vs Mean Effective Stress for Triaxial Tests with No End Failures

The noise in the pore pressure transducers (pipet) was significant, up to ± 0.030 volt in some cases. The ± 0.030 volt noise would be equivalent to 12 bits of noise (0.03v/(0.0244v/bit)), an error of 0.04 cc (12 bits * 0.003 cc/bit) for secant values of volume change. The noise is apparently due to the noise generated in the modulator/demodulator box, and vibrational noise. A water hammer of sufficient magnitude is generated in the pipet from accelerations induced by the motor of the loading press. The pore pressure transducer (1.25 psi) is sensitive enough to measure this water hammer.

Presumably, the calibration standard used would be more accurate than needed. However, repeatability of the method of calibration would probably be the factor that controls the calibration error. In general, the sensors should be chosen to match the range of likely displacements (load, volume change) to maximize the sensor sensitivity. After the sensor is calibrated against the standard, and repeatability is assured, the "best" fit calibration (be it linear,

interpolated, quadratic, or other) should be checked against the standard. Modifications in the measurement system will be necessary, if the differences between the best fit sensor reading and standard are unacceptable.

Effects of Sensor Sensitivity on Incremental Moduli. The potential errors in measurement of secant values of modulus and Poisson's ratio will be large at the beginning of the tests (when total displacement, load, and volume change are small), and should decrease as the strain increases. The measurement of incremental moduli and Poisson's ratio would represent the quantities most sensitive to these errors. A crude estimate of the errors can be obtained by assuming the exact values of sensor readings are known, and varying the "noisy" sensor reading.

Consider a specimen with the following "exact" conditions at the beginning of shear:

Initial Area= 1.83 in^2
Initial Length= 3.060 in.
Initial Volume= 5.600 in^3

Consider the typical values of deformation, load, and volume change for Eagleford shale at two times, one associated with the beginning of reloading after test stoppage, the other at the end of the linear portion of the reload stress-strain curve:

Vertical displacement 1 = 0.0057 in.
Load 1 = 33 lb.
Volume Change 1 = -0.27 cc

Vertical displacement 2 = 0.0070 in.
Load 2 = 47 lb.
Volume Change 2 = -0.33 cc

The "exact" values of incremental modulus and incremental Poisson's ratio would be 18,040 psi and -0.2695.

The errors in the calculated incremental modulus and incremental Poisson's ratio associated with an error in displacement of +0.0004 in. for point 1 would be -45% and -126%, respectively. The errors in the calculated incremental modulus and incremental Poisson's ratio

associated with an error in displacement of +0.0004 in. for point 2 would be 24% and 67%, respectively.

The errors in the calculated incremental modulus and incremental Poisson's ratio associated with an error in load (other factors assumed to remain "exact") of 2.0 lbs. for point 1 would be -14% and and less than 1%, respectively. The error would be the same for variation in load 2.

The errors in the calculated incremental modulus and incremental Poisson's ratio associated with an error in volume change (other factors assumed to remain "exact") of 0.08 cc for point 1 would be less than 1 % and -380 %, respectively. The error would be the same for variation in the volume change for point 2.

The error in the displacement will control the magnitude of the error (potentially 50%) in incremental modulus. The error in the volume change measurement, and to a lesser extent in displacement, will control the error (potentially 400%) in the incremental Poisson's ratio. The errors should decrease as sample size increases since the displacements and volume changes will increase for the same strains. The errors in secant values will be somewhat smaller than incremental values at larger strains.

Errors in Coefficient of Consolidation

Introduction. There does not appear to be much data available to support the applicability of a rate independent consolidation theory to predict shearing rates for stiff shales. We would like to determine if the coefficients of consolidation derived from isotropic swell increments are providing reasonable estimates of the degrees of consolidation at failure. In addition, we are interested in what might be the causes for the apparent incomplete "primary" consolidation phase.

The range in coefficients of consolidation for the triaxial compression tests varied by a factor of up to 25 (9, if the test associated with the factor of 25 is removed). The mean value of the coefficients of consolidation for the 19 tests is approximately 0.001 $ft.^2$/day. There does appear to be a slight reduction (at a given cell pressure) in the coefficient of consolidation (Fig. 6.20) as the liquid limit increases. We would expect decreases in hydraulic

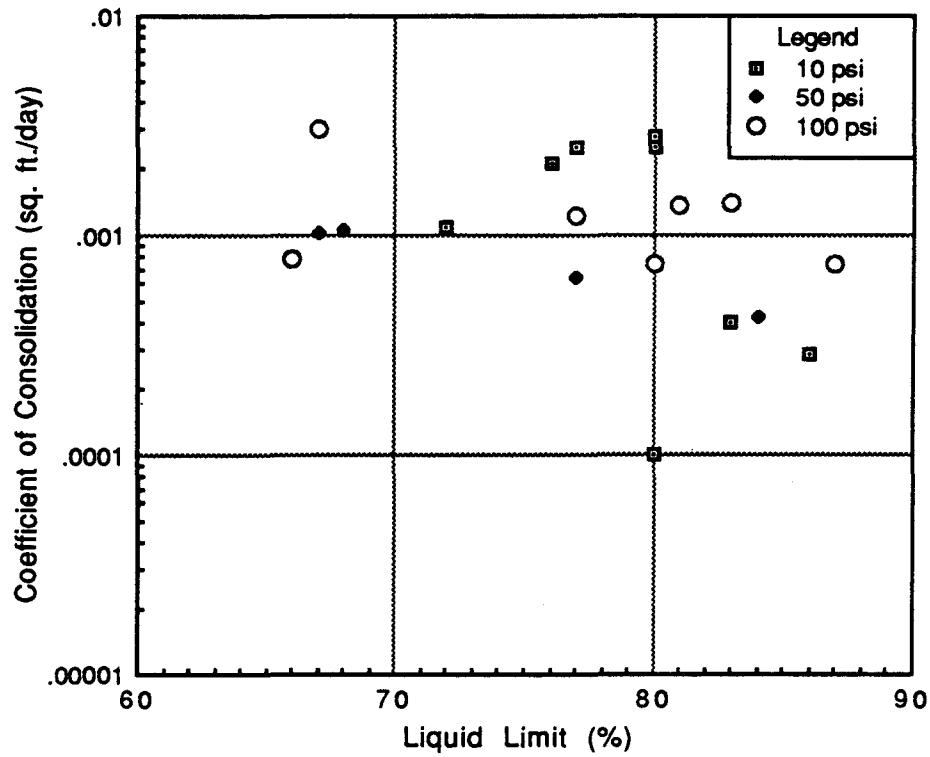

Fig. 6.20 Coefficient of Consolidation vs Liquid Limit for Triaxial Compression Tests on Eagleford Shale

conductivity and increases in compressibility for increased liquid limits, both leading to reductions in coefficient of consolidation. The range in all coefficients of consolidation at any particular liquid limit (excluding the one extreme value) was approximately four. Of course, the liquid limit is determined using a disaggregated sample and the Eagleford shale appears to be cemented so any such correlation may be fortuitous.

We would normally expect the secondary consolidation effects that are significant under one-dimensional consolidation to be smaller in isotropic consolidation. The time-volume data for isotropic swell in the triaxial tests exhibited either incomplete primary, apparent secondary effects, or both. If the apparent incomplete portion of primary consolidation is due to secondary effects the predicted coefficients of consolidation will be too small.

Leakage Effects. The effects of membrane/pipet/fitting leakage, gas diffusion, and osmotic leakage introduce significant apparent volume changes that are recorded by the pipet. The small

sample volumes, low load decrement ratios, and relatively incompressible nature of the material magnify the problem associated with measuring the small volume changes. Experimental evidence (Fig. 6.21) suggest that the coefficient of consolidation is

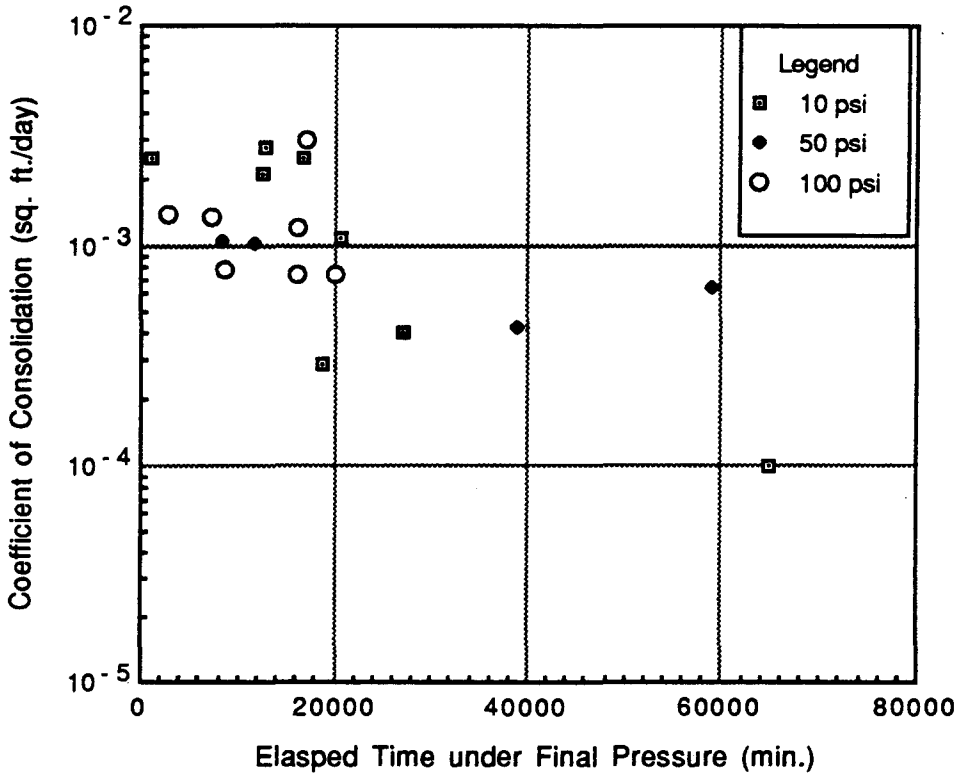

Fig. 6.21 Effect of Length of Consolidation Period on Coefficient of Consolidation

significantly affected by the length of the consolidation period under the final total stress. Notice that the test (CD 5 from Phase 1 with a different membrane/pipet arrangement) with the longest consolidation period has the lowest coefficient of consolidation.

(Osmotic Leakage): The study of the effects of osmotic leakage due to electrolyte differences in cell water and sample pore water was beyond the scope of the current contract. The flow of water would be from the cell into the sample, producing an apparent consolidation volume change.

(Gas Diffusion): The study of gas diffusion from the gas in the sample, and trapped between the sample and membrane was also not studied. However, an estimate of the effects of the gas diffusion can be made. The cell water was originally stored in a chamber

under a partial vacuum. Thus, gas associated with the specimens would diffuse into the cell water, producing an apparent swell volume change. An estimate of the magnitude of gas diffusion can be obtained if we compare the expected volume of gas in the samples based on the knowledge of the specific gravity.

The triaxial specimens had volumes of free gas (as opposed to dissolved gas) at the "as trimmed" volume ranging from 0.56 cc to 1.85 cc (one had 2.91 cc). The average gas diffusion rate would vary from 0.01 cc/day to 0.13 cc/day. Application of the 140 psi setup pressure should close some of the fissile surfaces and might force some of the gas down into the porous stone. Some of this gas would be removed during the deairing process.

(Filter Paper Volume Change): The effects of the filter paper swell was investigated by setting up a dummy triaxial test with a solid steel specimen surrounded by the filter paper, set up in the same procedure as used in testing the rock specimens. The results of the volume change for four tests (8 load) are presented in Tables 6.8 and 6.9. All consolidation stages in the PIF phase started from 140 psi, and reached the final effective stress in one increment. The filter paper swelled 0.54 cc, 0.16 cc, and 0.04 cc under 10 psi, 50 psi, and 100 psi, respectively. Quite surprisingly, the filter paper often took several minutes (Tables 6.8 and 6.9) before swelling was complete.

(Tubing/Fitting Leakage): We also investigated (Fig. 6.22 and Table 6.11) the pipet/tygon tubing/fitting leakage effects by setting up a "dummy" pipet on a triaxial cell with the drainage line closed, and recording the pipet reading with time.

The combined effects of the pipet/tygon tubing/fitting leakage and membrane leakage (no osmotic or gas diffusion component) were also investigated by using a saturated porous stone. The porous stone was saturated by boiling it in tap water and allowing the mixture to cool. We used boiled tap water to fill the air panel reservoir, since the reservoir partial vacuum could not remove all gas from the water. All lines to the triaxial cell were bled with the deaired tap water. A top cap with a Swagelok fitting was used to attach a drainage line from the top cap to a secondary drainage line inside the triaxial cell. All drainage lines were bled with deaired tap water prior to placing the saturated porous stone.

Test 1 Load1 (140-10 psi) Time (min.)	Test1 Load1 Vol. Change (cc)	Test1 Load2 (10-50 psi) Time (min.)	Test1 Load2 Vol. Change (cc)	Test1 Load3 (50-100 psi) Time (min.)	Test1 Load3 Vol. Change (cc)	Test1 Load4 (100-140 psi) Time (min.)	Test1 Load4 Vol. Change (cc)	Test1 Load45 (140-50 psi) Time (min.)	Test1 Load5 Vol. Change (cc)
0	0	0	0	0	0	0	0	0	0
0.1	0.13	0.1	-0.16	0.1	-0.05	0.1	-0.02	0.1	0.06
0.25	0.21	0.25	-0.19	0.25	-0.07	0.25	-0.03	0.25	0.07
0.5	0.26	0.5	-0.2	0.5	-0.09	0.5	-0.04	0.5	0.1
1	0.33	1	-0.21	1	-0.1	1	-0.04	1	0.11
2	0.38	2	-0.22	2	-0.11	2	-0.05	2	0.12
4	0.42	4	-0.23	4	-0.12	4	-0.05	4	0.13
8	0.43	8	-0.24	8	-0.13	8	-0.06	8	0.14
26	0.47	15	-0.25	18	-0.14	15	-0.06	16	0.15
71	0.48	93	-0.26	34	-0.15			47	0.15
120	0.5			49	-0.15			64	0.15
198	0.52							726	0.17
565	0.54								

Table 6.9 Filter Paper Volume Change Data (Test 1)

Test 2 Load1 (140-100 psi) Time (min.)	Test2 Load1 Vol. Change (cc)	Test3 Load1 (140-50 psi) Time (min.)	Test3 Load1 Vol. Change (cc)	Test4 Load1 (140-10 psi) Time (min.)	Test4 Load1 Vol. Change (cc)
0	0	0	0	0	0
0.1	0	0.1	0.04	0.1	0.15
0.25	0	0.25	0.05	0.25	0.23
0.5	0.01	0.5	0.06	0.5	0.3
1	0.01	1	0.08	1	0.37
2	0.01	2	0.09	2	0.44
20	0.04	3	0.1	4	0.48
		7	0.13	6	0.49
		9	0.14	13	0.54
		17	0.16	15	0.55

Table 6.10 Filter Paper Volume Change Data (Test 2-Test 4)

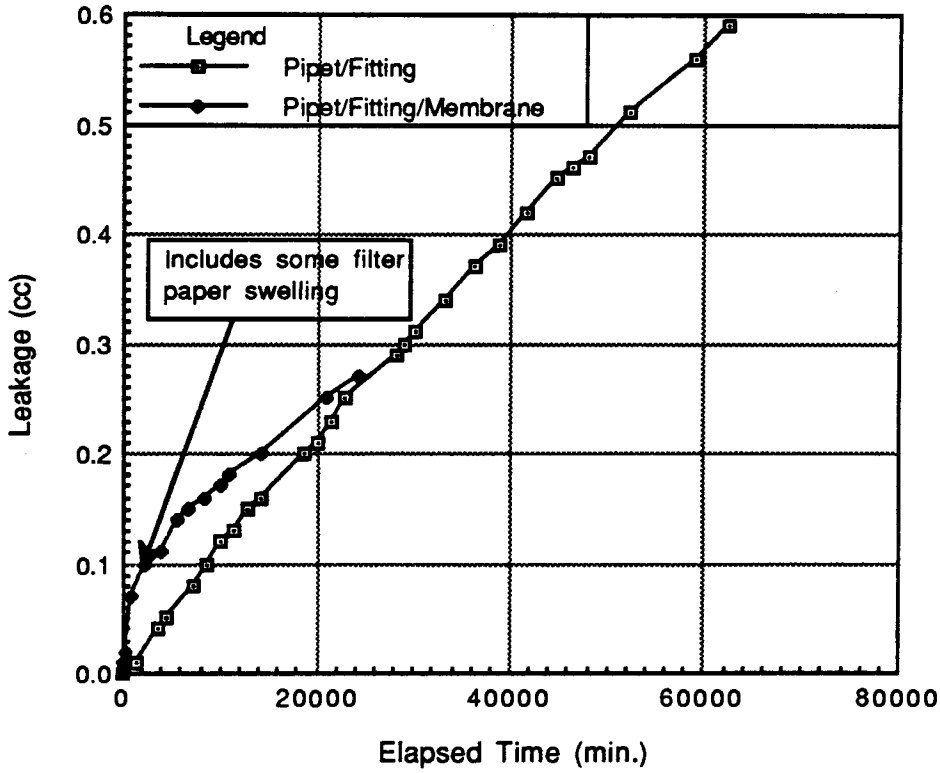

Fig. 6.22 Pipet/Fitting Leakage and Pipet/Fitting/Membrane (at 100 psi) Leakage with Time

The porous stone/filter paper was set up in the triaxial cell in the same manner used for the specimens. Another reservoir with deaired tap water served as a source for the base drainage line. A vacuum was applied to the end of the pipet. Both drainage lines were opened and deaired tap water flowed from the reservoir through the base, up through the porous stone, and out the second drainage line attached to the top cap leading to the pipet under a vacuum. The deairing process was continued until no air bubbles exited the porous stone, and all visible air bubbles adhering to the tubing dissolved into the deaired water.

A 100 psi cell pressure was maintained to measure the largest leakage rates expected for the PIF phase tests. Steady state was not reached until after approximately 12 hours (Fig. 6.22), apparently due to some remaining trapped gas and filter paper creep.

Pipet/Fitting Leakage Study	Pipet/Fitting Leakage Study	Pipet/Fitting/ Membrane Leakage Study	Pipet/Fitting/ Membrane Leakage Study
Elapsed Time (min.)	Volume Change (cc)	Elapsed Time (min.)	Volume Change (cc)
0	0.00	0	0.00
1387	0.01	0.1	0.00
3690	0.04	0.25	0.00
4340	0.05	6	0.00
7379	0.08	61	0.01
8598	0.10	219	0.02
10050	0.12	870	0.07
11472	0.13	2258	0.10
12899	0.15	3779	0.11
14369	0.16	5517	0.14
18729	0.20	6787	0.15
20028	0.21	8321	0.16
21653	0.23	10156	0.17
23037	0.25	11018	0.18
28140	0.29	14168	0.20
29112	0.30	20967	0.25
30276	0.31	24292	0.27
33213	0.34		
36389	0.37		
38904	0.39		
41813	0.42		
44760	0.45		
46352	0.46		
48127	0.47		
52201	0.51		
58998	0.56		
62323	0.59		

The membrane leakage is offset by the pipet/tygon tubing/fitting leakage. The combined (Fig. 6.22) steady state leakage rate is approximately 0.01 cc/day of apparent swell.

Volume Change Corrections The tests at 10 psi and 50 psi were subjected to some of the longest consolidation periods. The tests at 10 psi should have exhibited the largest filter paper swell. A relatively crude approach to estimate the leakage was used to account for these effects. The volume change data from test CD13 (Fig. 6.23) was corrected for the steady state pipet/tubing/fitting leakage. The effects do not become apparent until the later stages of

the swelling period, and the leakage may explain the apparent secondary swelling.

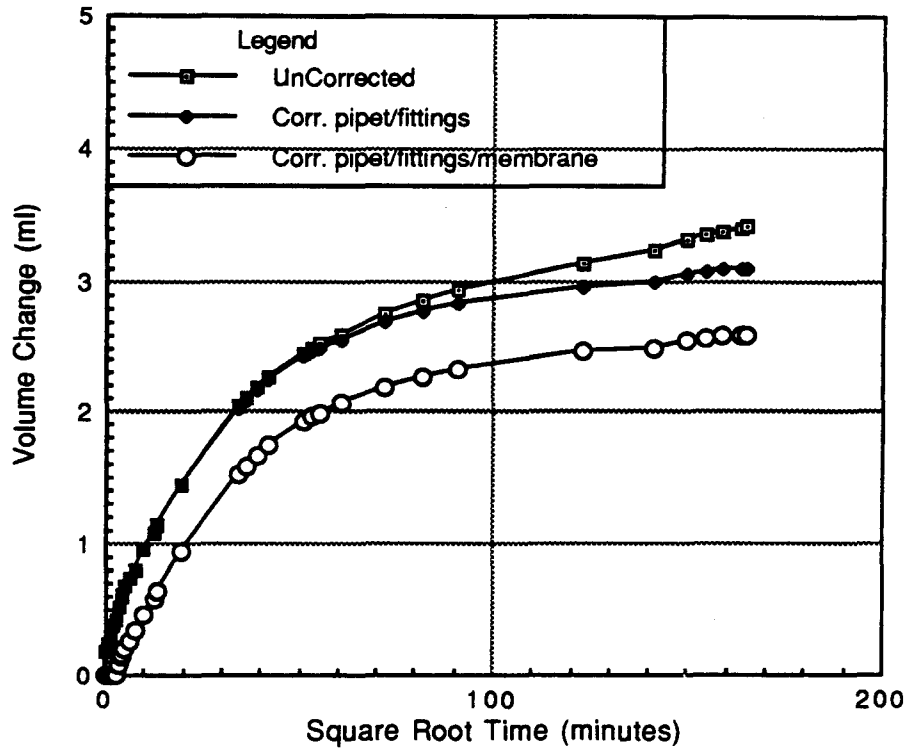

Fig. 6.23 Effects of Water Evaporation (Pipet & Fitting) and Membrane Leakage on the Measured Volume Change Response in Test CD13 (140 psi to 10 psi increment)

The filter paper time readings were used to correct (Fig. 6.23) the initial time-volume readings for CD13. Ideally, the corrections should be applied directly to the boundary conditions of the consolidation theory used to interpret the isotropic consolidation data. However, such investigations were not part of this contract. The filter paper swell shifts the experimental square root time-volume curve into a steeper initial slope, and a larger final volume change. These two effects tend to cancel out any error that would be obtained in the calculation of the coefficient of consolidation. However, if a more permeable filter paper (with the same compressibility) is used, the volume change would be nearly instantaneous and larger errors would be found in the calculated coefficient of consolidation.

We should note that the degrees of consolidation at failure were calculated on the basis of no corrections to the time-volume data

for these effects. Additionally, the theory used assumes that a "ramp" load is used to load the specimens to failure, while in fact the samples were subjected to periods of no loading during shutoff periods.

SUMMARY AND CONCLUSIONS

The following conclusions seem warranted based on the triaxial compression tests with rocks from the SSC site:

1. The cores of Eagleford shale contain fissures and weak horizontal planes, resulting in failure modes that are not in accord with Mohr-Coulomb assumptions.

2. Even small samples of the size used here, require very long periods of time to come to equilibrium during the swelling process. We were not able to wait for equilibrium to be established but we maintained constant pressure for extended times and the ΔV-log(t) curve showed no sign of transition from primary to secondary consolidation. The influence of filter paper swell and membrane/pipet leakage was measured, and seemed to explain at least part of the extended "primary" consolidation. The influence of gas and osmotic diffusive components were not addressed.

3. The time required for primary consolidation varies with the square of the sample size but secondary effects should not scale at all. If our observed ΔV-log(t) behavior is of a secondary type, then times will not be significantly longer for larger sample sizes than for the sizes used here. With larger samples, it might be possible to achieve more consistent behavior by having a random distribution of perfections in all samples.

4. Attempts to fit primary consolidation theory to volume change-time curves led to coefficients of consolidation that were among the lowest we have ever seen. The fitted

coefficients tended to decrease as the time duration of measurements increased. The range in coefficients of consolidation that we observed was generally from $3x10^{-3}$ sq.ft./day down to $1x10^{-4}$ sq.ft./day. For shallow clays, we generally expect coefficients of consolidation to be in the range of 1 sq.ft./day down to 0.001 sq.ft./day.

5. The material in the cores was stiff, with secant values of Young's modulus, at the 50% stress level, generally in the range of 6000 psi to 32,000 psi.

6. Values of "corrected" Poisson's ratio ranged from -0.22 to +0.02, -0.28 to -0.13, and -.034 to -0.11 for cell pressures 10 psi, 50 psi, and 100 psi, respectively. However, these values imply what we think are unlikely compressive lateral strains.

7. The shearing rates recommended in Phase 1 (1 day for 10 psi and 3 days for 50 psi and 100 psi) seem to give reasonable degrees of consolidation at failure. However, there may be important implications requiring further study in the shearing rates, as a result of an apparent viscosity effect observed in tests sheared at intermediate strain rates.

8. As a result of the apparently random distribution of surfaces of weakness in samples, the shearing strengths scattered widely at low cell pressures. When we used the "best" triaxial compression tests, and calculated stresses on the apparent failure planes, we found that the failure envelope would be defined using $\bar{\phi}$=21 degrees and $\bar{c}$=90 psi as an upper bound envelope and $\bar{\phi}$=25 degrees and $\bar{c}$=25 psi as an lower bound envelope.

9. Several experimental problems developed that are particularly relevant to material as incompressible as the Eagleford shale. One was leakage due to numerous sources (pipet, fittings, membrane, gas and osmotic diffusion). We were forced to use relatively heavy "commercial" membranes to retard leakage. No attempt was made to correct stress-strain curves for membrane stiffness. Consideration should be given to taking further steps to reduce leakage, e.g., using a cell fluid with the same osmotic pressure as the pore fluid of the samples or

switching to a cell fluid that is less likely to leak through the membranes.

10. The time required to shear a sample, under drained conditions, increases essentially with the square of the sample size, assuming that primary consolidation dominates. Nevertheless, there are advantages in testing larger samples when the material is fissured. Samples large enough to contain a random distribution of fissures are more likely to represent field conditions than are small samples where the existence, or lack thereof, of a fissure exerts a strong influence on behavior.

11. Interpreted moduli are too small if the machine deformations generated during shearing are not accounted for. The machine deformations should be estimated and used to correct the stress-strain data if the moduli are to be used in a constitutive model.

12. Moduli (in particular incremental values) are sensitive to the resolution of the data acquisition. Every effort should be made to reduce the uncertainty in the calibration and sensitivity of the sensors if moduli are needed.

SECTION 7

COMPARISON OF DATA ON ENGINEERING PROPERTIES OF THE EAGLEFORD SHALE MEASURED USING DIFFERENT TESTS

INTRODUCTION

Previous sections deliberately concentrated on a single test or test type, and avoided making more general comparisons. The more general comparisons are included in this section. This section will not contain a summary of data presented previously.

In this section, experimental problems will generally not be considered if these problems were discussed previously. The goal of this section is to try to develop an understanding of the measured properties. Tests with obvious problems, e.g., end failures, rough failure planes, gas diffusion into the pipet, etc. will tend to be de-emphasized

ATTERBERG LIMITS

The Atterberg limits were used as a means of estimating the uniformity of the cores among the different tests. The range in liquid limits was 67% to 79% for one-dimensional consolidation specimens, 66% to 89% for direct shear specimens, and 66% to 87% for triaxial compression specimens. The liquid limits of the one-dimensional consolidation samples were the lowest for 7 of the 8 cores containing the specimens (Table 7.1) . However, there was usually another specimen within the same core with a liquid limit

within 3%. The liquid limits for consolidation specimens in the borings B1597 and B1617 were significantly smaller (12% and 6%) than direct shear or triaxial specimens. Liquid limits of the direct shear specimens were the largest for six of the eight cores. However, in four of those six cores, another specimen within the same core with a liquid limit within 2%.

The locations of the specimens used in the various tests were selected to try to use uniform material for paired tests, e.g., for a one-dimensional consolidation test and a triaxial test on adjacent pieces of core. As a result, the consistency in the type test that had the minimum and maximum liquid limits may be not be due to material variability within the core.

It was noticed, on several occasions, that the samples used in the triaxial tests had a distinct organic odor when the tests were dismantled. No such odor was noticed for samples used in other tests. Clearly, any odoriferous material could escape readily in one-dimensional consolidation and direct shear tests but would tend to be trapped inside the membrane for triaxial tests.

The lengths of the test setups (from trimming time to breakdown) varied from 34 days to 56 days for one-dimensional consolidation, four to ten days (two outliers at 21 days) for direct shear, and 17 days to 61 days for triaxial compression. Thus, in most cases, the direct shear tests were performed in shorter periods of time than either the consolidation or triaxial tests. Our present inclination is to believe that some organic process occurs during the one-dimensional consolidation tests and to a lesser extent in the triaxial tests, causing the change in the Atterberg limits. Perhaps, the consolidation tests specimens were more susceptible to oxidation due to the long test period (gas could diffuse into the sample) and the small sample size. The triaxial specimens were larger, enclosed in a membrane, and surrounded by partially deaired (gas would flow into the cell) water. It would be interesting to know if such changes are actually occurring and, if so, are they also occurring in the cores during storage.

Boring	LL (%)	Test Length Days	Test ID
B1597	75	51	C12
	88	21	DS18
	87	28	CD24
B1619	67	46	C13
	66	21	DS17
	68	24	CD22
B1617	75	47	C14
	89	4	DS24
	81	26	CD23
B1637	71	44	C15
	87	10	DS21
	72	47	CD14
	77	61	CD18
	77	21	CD19
BC1	64	56	C16
	78	6	DS19
	76	17	CD11
	67	17	CD16
	66	16	CD17
B1697	79	34	C17
	82	6	DS22
	80	17	CD15
B1657	79	35	C18
	82	7	DS20
	86	22	CD12
BF1A	79	44	C19
	86	5	DS23
	83	24	CD13
	84	47	CD20
	80	25	CD21

Table 7.1 Liquid Limits by Boring

STRESS-STRAIN BEHAVIOR

Axial Stress-Strain

Stress-strain properties cannot be measured in direct shear tests. The axial strains in one-dimensional compression ranged from 4.6% to 6.5% at peak stress (180,000 psf), from 2.6% to 4.5% at one half the peak stress (87,000 psf), and -0.9% to -2.7% at the final stress (350 psf). The corrected axial strains (PIF phase) in triaxial compression tests, where the radial boundaries are subjected to constant stress, ranged from 1.8% to 2.7% at peak stress difference (28,000 psf to 68,000 psf stress difference) for specimens that did not have an end failure. The similarity in strains in one-dimensional consolidation can be attributed to the small lateral strains that developed during shearing in the triaxial tests.

It would not make much sense to compare the stress-strain curves directly, since the stress paths are different. The more logical method to compare the stress-strain response between tests would be to use a constitutive model. The model parameters would be determined from one (or more) set(s) of tests, then the response of tests executed experimentally at different stress paths would be compared to the predicted response obtained from the model. Such a comparison was not within the scope of the contract.

Stress-Void Ratio

Void Ratio Corrections. The use of the stress-volumetric strain response for the consolidation phases of the one-dimensional consolidation and isotropic triaxial consolidation seems to be a simple, logical method of comparing the tests. The e-log($\bar{\sigma}$) relationship from consolidation tests is a stress-strain relationship (Δe is strain defined using the height of solids), thus allowing comparison of e-log($\bar{\sigma}$) relationships for one-dimensional consolidation tests and for triaxial tests both during consolidation and during shear.

The problems of membrane and pipet arrangement leakage, osmotic and gas diffusion through the membranes makes it difficult to

determine reasonably accurate stress-strain [e-log($\bar{\sigma}$)] curves from the triaxial tests. Initial void ratios and volumes of solids were used from the original set-up data forms (see Task 2 data), and corrected the measured volume changes for membrane/pipet leakage (assuming a steady state leakage rate of 0.01 cc/day) and filter paper swell. To obtain a resolution of a change of void ratio equal to 0.001 (volume of solids equal to 50 cc), would require volume changes to be known to the nearest 0.050 cc. The triaxial tests were setup for periods extending from 15 days to 61 days, resulting in corrections to pipet readings from 0.15 cc to 0.61 cc.

A check on the validity of the corrections to pipet readings would be a comparison (Table 6.1) of measured and calculated final water contents for the triaxial specimens. Eleven of the fourteen triaxial tests did not have any gas diffusion into the pipet associated with the cell O-ring leak (the leak caused gas to bubble up through the cell fluid constantly during the test and should have influenced gas diffusion through the membrane).

Corrections to the pipet readings resulted in "good" estimates for 6 of the tests (CD12, CD13, CD15, CD18, CD20, CD23), 1 test with the calculated final water content greater than the measured value (CD11 at 10 psi), and 4 tests with the calculated final water content less than the measured value (CD17, CD19, CD21, CD24, all at 100 psi). The differences in calculated and measured final water contents are the result of differences in weights of water varying from 0.96 cc to 1.73 cc. Several reasons may contribute to the differences for the tests at 100 psi:

1. The specimens swelled during the setup and deairing process. However, the data for the consolidation stage from 140 psi to 100 psi suggest the swelling should be minimal for the first 15 minutes. We should note that we often "sprayed" the specimens at trimming time with a light mist of tap water to prevent significant drying. In the absense of spraying, the outside of the core would dry slightly, as trimming proceeded, and the specimens began to flake. The light mist would maintain a high humidity, but would be trimmed away as the trimming device was advanced. As a result the initial water contents in triaxial specimens may be elevated slightly. This should not effect the calculation of the final water content, since any small amount of sprayed water would be measured once the sample is trimmed.

2. The specimens swelled during tearing down of the tests, when the total stress was decreased from 100 psi to essentially 0 psi. The consolidation data from the 140 psi to 10 psi swell stages indicate that approximately 0.4 cc of water would be imbibed within the first 8 minutes, much of this being due to filter paper swell. We might expect more water to be imbibed at zero total stress because some fissile surfaces are likely to open.

3. The effects of diffusion of gas and osmotic gradients are not included in the corrections to the pipets. The fact that the comparisons between measured and calculated final water contents are "good" for some tests, and "bad" for others may be a result of neglecting the contributions of the diffusion of gas and osmotic gradients.

4. other unknown experimental errors.

Triaxial vs. One-Dimensional Consolidation. In the absence of information on the overall state of stress in the one-dimensional consolidation test, we will use the vertical effective stress in the diagrams. The mean effective stress will be used for triaxial tests. The choice of these definitions of stress clearly does not imply that the void ratio is solely a function of either the vertical effective stress nor the mean effective stress; the choice was based on the available data.

The resulting stress-void ratio curves are shown in Fig. 7.1 for the triaxial consolidation phases, and a typical (C13) one-dimensional consolidation test during first rebound and reloading. The range in void ratio for the triaxial consolidation phases at 100 psi is 0.017, 0.045 at 50 psi, and 0.030 at 10 psi. The differences in void ratios between the different samples at a given effective stress are small and may be real or may result from minor errors in specific gravity or other causes.

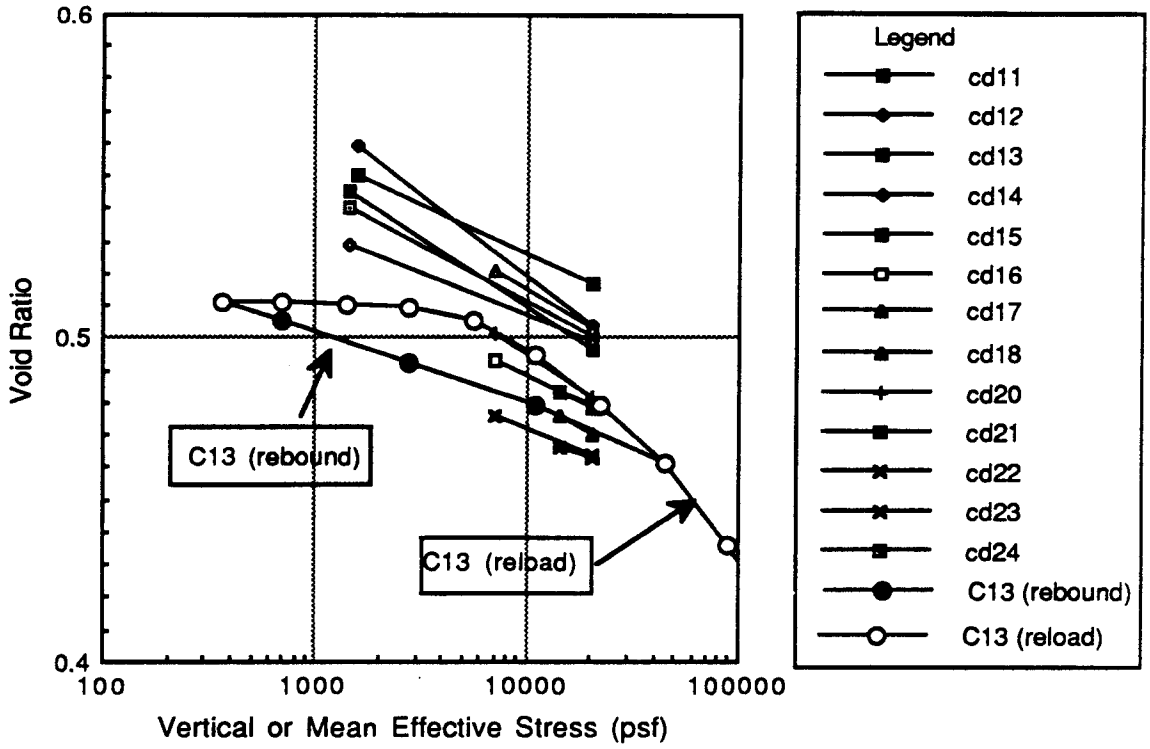

Fig. 7.1 Comparison of Rebound Stress-Strain Curves in Triaxial Compression with One Dimensional Compression Results on Eagleford Shale

Of more importance is the slope of the swelling curve. The range in the compression index for the first rebound for one-dimensional consolidation tests was 0.026 to 0.029 at 11,000 psf, and 0.019 to 0.023 at 2700 psf. The range in the swelling index (Table 7.2) for rebound from 20,160 psf (140 psi) for triaxial consolidation tests was 0.021 to 0.041 when rebounded to 14,400 psf (100 psi), 0.027 to 0.043 when rebounded to 7,200 psf (50 psi), and 0.026 to 0.050 when rebounded to 1,440 psf (10 psi). Some of the scatter, at a single cell pressure, in the triaxial swell curves is probably due to real differences in compressibility. The compression indices in triaxial compression did increase with liquid limit at a particular pressure except for three tests, CD 11 and CD15 at 10 psi, and CD17 at 100 psi. The anomalies may be due to errors associated with small volume changes (0.003 to 0.006 void ratio change at 100 psi), or errors in the measured liquid limits.

Test ID	Liquid Limit (%)	Field Eff. Stress (psi)	Initial Void Ratio	Consol. Pres. No. 1 (psi)	Corr. Void Ratio Press. 1	Final Consol. Pres. (psi)	Final Press. Corr. Void Ratio	Compr. Index
CD11	76	117	0.490	140	0.500	10	0.540	0.0349
CD12	86	92	0.502	140	0.504	10.9	0.559	0.0496
CD13	83	91	0.492	140	0.496	10	0.545	0.0428
CD14	72	116	0.487	141	0.499	10	0.529	0.0261
CD15	80	67	0.518	140	0.517	10.9	0.550	0.0298
CD16	67	118	0.464	141	0.478	50	0.493	0.0333
CD18	77	116	0.496	140	0.503	50	0.521	0.0403
CD20	84	91	0.481	140	0.482	50	0.501	0.0425
CD22	68	99	0.462	140	0.464	50	0.476	0.0268
CD17	66	118	0.454	140	0.470	100	0.476	0.0411
CD19	77	116	0.489	140	0.484	100	0.482	na
CD21	80	91	0.488	140	0.479	100	0.483	0.0274
CD23	81	114	0.458	140	0.463	100	0.466	0.0205
CD24	87	126	0.471	140	0.479	100	0.483	0.0274

Table 7.2 Summary of Triaxial Consolidation Stress-Void Ratio Data

Unfortunately, none of the samples were unloaded in steps to their final states due to lack of time, so it is difficult to draw conclusions on differences in the swell properites between isotropic and one-dimensional swelling. In general, the compression indices (noting the difference definitions) do appear to be in the same general range for one-dimensional and isotropic consolidation.

Most of the one-dimensional consolidation initial rebound curves are "concave" downward. The concave downward shape may be due to:

1. ring friction. The rings used in the consolidation tests were polished, greased, stainless steel but significant amounts of friction might still develop during rebound.

2. stress state. If the void ratio is mainly controlled by the mean stress, and K_o is considerably in excess of one for the one-dimensional rebound curve, then the stresses used with the one-dimensional curve should be increased proportionately. This effect is too small to be a sole explanation of the difference in slopes but it may be a contributing factor.

3. chemical changes. Significant effects caused by changes in chemistry seem unlikely because the first swell occurs within the first few days of the tests.

With only a small lateral strain, the triaxial and one-dimensional responses might be expected to be qualitatively similar. We should note that during the measurement of machine deformations, we measured up to 0.1 cc of water squeezed (1000 lb.) out of the end filter paper disks. The resulting error in measuring volume change during shear would eliminate accuracy in void ratio to 0.001.

Based on data in Fig. 7.1, it appears that the slopes of the semi-logarithmic stress-strain curves are essentially the same in one-dimensional and triaxial compression except in the low stress range where ring friction may be a problem in the one-dimensional tests.

COEFFICIENTS OF CONSOLIDATION

The coefficients of consolidation obtained from one-dimensional consolidation swelling stages were 3 to 670 (one was 2000) times larger than the coefficients of consolidation obtained from isotropic swell stages from triaxial tests. Based on earlier discussion and general experience, some of the following factors are involved:

1. The cores actually had a variation in material properties.

2. A range in coefficients can be obtained depending on where primary consolidation is assumed to end. For the one-dimensional consolidation tests, we generally began with root-time plotting and concluded that primary consolidation ended well before the final settlement reading. For triaxial consolidation, the ΔV-log(t) plots showed no evidence of the end of primary consolidation and we generally fit to the entire curve. The result is a tendency to obtain lower coefficients for the triaxial tests. Of course, if the triaxial volume change curves had indicated the end of primary at an earlier stage we would have fit to the early part of the curve.

3. In one-dimensional consolidation testing, secondary effects become increasingly important as the stress ratio decreases and as the consolidation time for the previous load increases.

4. For volume changes as small as those measured here, gas diffusion through the membranes, evaporation from the top of the pipet, and a number of other sources of error can become detectable. We attempted to quantify the effects of membrane/pipet leakage and filter paper swell, but did not apply those "corrections" to the data.

5. We have not made measurements to determine the influence of anisotropy on consolidation properties.

6. Some of the high values of the coefficient of consolidation could have resulted from the presence of undetected fissures or tiny seams of more pervious material that would have allowed more rapid internal drainage.

7. The initial void ratios and stress paths were different for the one-dimensional consolidation and triaxial swelling tests. The coefficients of consolidation (Fig. 7.2) for typical one-dimensional consolidation (C16) are much closer to the triaxial values if the same range in void ratio is used. The mean stresses (Fig. 7.3) in the isotropic consolidation tests varies over a much smaller range than one-dimensional consolidation.

8. The coefficient of consolidation varies directly with hydraulic conductivity and inversely with compressibility. We do not think the coefficients of consolidation obtained from the first rebound in one-dimensional consolidation produces reliable results because of opening of fissile surfaces and friction. We believe the reload coefficients of consolidation are the most reliable measurements in one-dimensional consolidation. In the low-stress range, the compressibilities (Fig. 7.1) differ markedly between the one-dimensional tests and the triaxial tests. This difference may be a factor in the observed differences in the coefficients of consolidation.

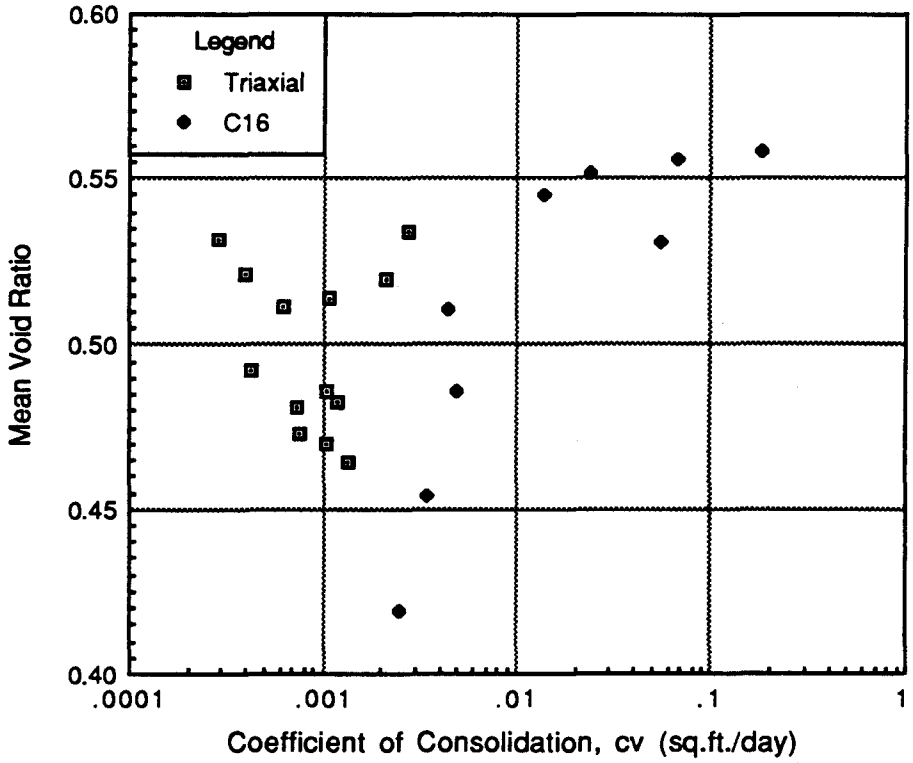

Fig. 7.2 Comparison of Coefficients of Consolidation for Triaxial Consolidation (CD11-24) and One-Dimensional Consolidation (C16 as typical)

9. The coefficient of consolidation calculated by fitting a primary consolidation theory to experimental data is too low because of secondary effects that occur during primary consolidation. If the secondary effects are larger in one-dimensional tests, as some expect, then coefficients should be larger than those we obtained in the one-dimensional tests. However, this effect would tend to increase the difference in coefficient of consolidation between one-dimensional and isotropic consolidation.

10. We suspect that the hydraulic conductivities are larger in the horizontal direction than vertically. The triaxial samples probably drain horizontally, preferably, and the one dimensional specimens clearly drain vertically. However, the horizontal effective stress may contribute to differences in the degree of fissile surface closure.

11. The lateral filter paper drains used in the triaxial tests are not freely draining, thus reducing the apparent coefficient of consolidation. An appropriate consolidation theory with non-

freely draining boundaries may be needed to assess the effects of the filter paper.

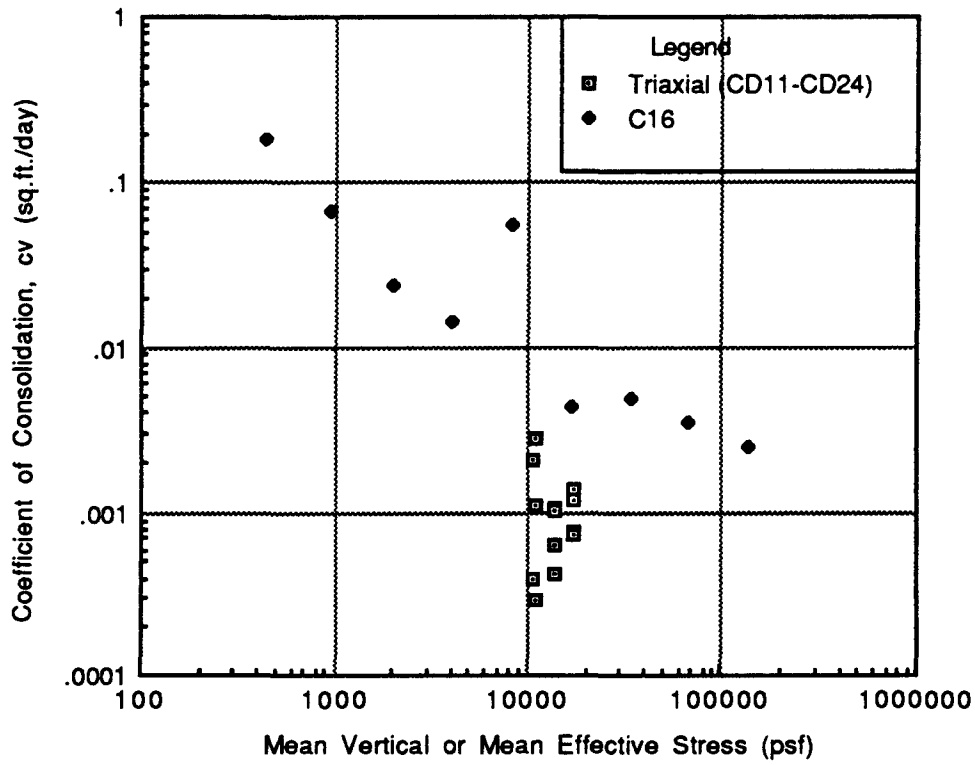

Fig. 7.3 Comparison of Coefficients of Consolidation for Triaxial and One-Dimensional Consolidation Tests

12. Membrane leakage due to pressure differences across the membrane and/or water chemistry difference between the specimen and cell water, add uncertainty to the volume-time data obtained in the triaxial tests.

We believe that a combination of these factors is influencing our results but that factors 1, 2, 4, 8, 11, and 13 in the above list are probably the most important.

FAILURE ENVELOPES FOR EAGLEFORD SHALE

A minor difficulty arises in trying to compare failure envelopes between direct shear and triaxial compression tests. Mohr's circles cannot be defined from direct shear tests so neither the Mohr-Coulomb nor modified Mohr-Coulomb diagrams can be used. One option is to plot a standard Mohr-Coulomb diagram with Mohr circles and pick off the normal stress and shearing stress at the intersection of each Mohr circle and the failure envelope. Problems develop in defining the tangent point when the data scatter widely.

We have decided to use the normal and shearing stresses calculated on the planes of maximum deformation (failure planes) in the triaxial tests and thus to use standard Coulomb diagrams for the comparisons. We will compare (Fig. 7.4) the triaxial results to

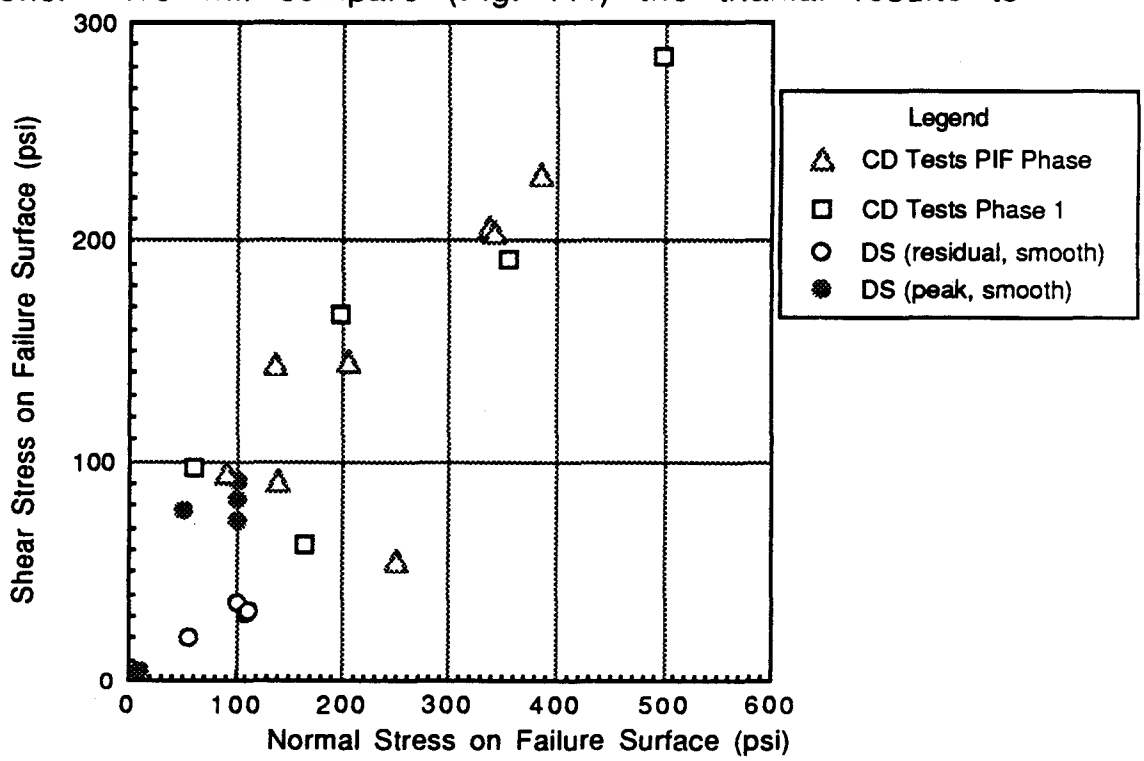

Fig. 7.4 Coulomb Diagram for Triaxial Compression Tests and Direct Shear Tests on Eagleford Shale using only "Good" Tests

direct shear data (peak and residual) for the samples that failed on

smooth planes. We could have computed the stresses on the triaxial failure planes after the shear plane developed to broaden the data base for the residual envelope. We chose not to, because of uncertainty in the piston friction and difficulty in determining the correct area (a function of the relative movement) of the failure planes sliding over each other.

Residual. The only triaxial test to be included in the cumulative residual Coulomb envelope is CD21, which failed at setup time on the small angle. The direct shear tests are DS9, DS21-DS24. The direct shear data are at a lower stress level the triaxial test (Fig. 7.5) because there was no increase in normal stress on the

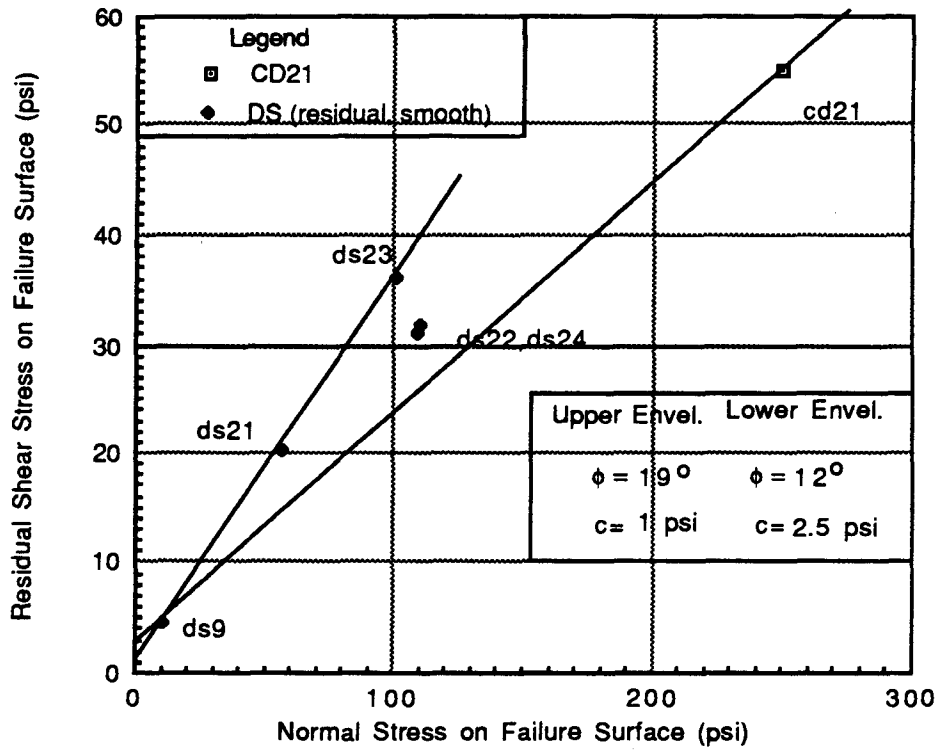

Fig. 7.5 Coulomb Diagram for Residual Stresses on the Failure Surface for Direct Shear and Triaxial Compression

failure surface during shear. The upper bound failure envelope has cohesion intercept of 1 psi and a slope ($\bar{\phi}$) of 19 degrees. The lower bound failure envelope has cohesion intercept of 2.5 psi and a slope ($\bar{\phi}$) of 12 degrees. In reality, the envelope may curve through the data points, but the insufficient number of data points does not

allow us to draw those conclusions. The range in the residual friction angles seem reasonable for a highly plastic material.

Peak. The triaxial tests that did not fail through the ends are to be included in the cumulative peak Coulomb envelope. The tests included are CD3, CD5, CD8, CD10, CD11, CD15, CD17, CD18, CD19, CD22, and CD23. The results from CD2 (probably a low degree of consolidation at failure), and CD21 are shown for convenience. The direct shear tests are DS21-DS24. Again, the direct shear data are at a lower stress level than most of the triaxial tests (Fig. 7.6) because there was no increase in normal stress on the failure surface during shear. The upper bound failure envelope has cohesion intercept of 90 psi (13,000 psf) and a slope ($\bar{\phi}$) of 21 degrees. The lower bound failure envelope has cohesion intercept of 26 psi (3700 psf) and a slope ($\bar{\phi}$) of 25 degrees. The range in the peak friction angles seem reasonable for a highly plastic material. The scatter in the Coulomb envelope decreases (as expected) as the normal stress on the failure surface increases. There is a relatively large range of normal stress (below 50 psi) which we currently do not have reliable shear strength data.

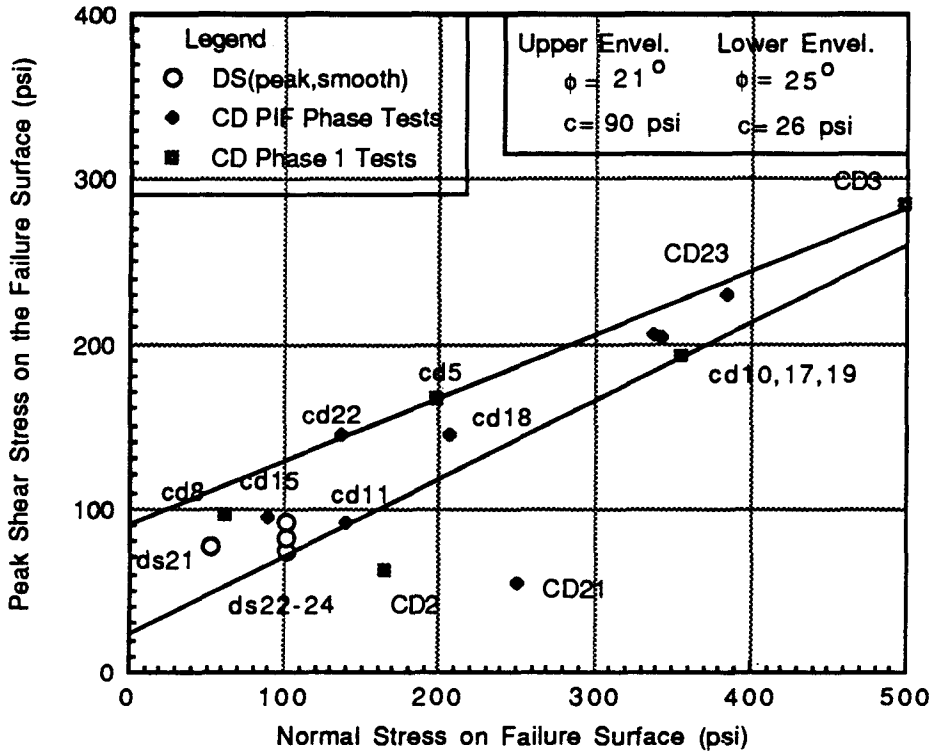

Fig. 7.6 Peak Coulomb Diagram for Triaxial Compression and Direct Shear Tests using Results from "Good" Tests